INVESTIGATIONS INTO THE CHEMISTRY OF DINUCLEAR COMPLEXES OF PALLADIUM, PLATINUM, AND GOLD

A Dissertation

by

ELHAM SADAT TABEI

Submitted to the Office of Graduate and Professional Studies of
Texas A&M University
in partial fulfillment of the requirements for the degree of

DOCTOR OF PHILOSOPHY

Chair of Committee,	François P. Gabbaï
Committee Members,	Marcetta Y. Darensbourg
	Donald J. Darensbourg
	Michael B. Hall
	Melissa A. Grunlan
Head of Department,	Simon W. North

August 2020

Major Subject: Chemistry

ABSTRACT

Over the past two decades, the chemistry of binuclear complexes containing a transition metal and a main group element from the 4th and 5th period has attracted a renewed interest prompted by the atypical transition metal-main group element interaction present at the core of these complexes. Special attention has been devoted to cases where the main group element behaves as a Lewis acid and the metal (M) as a Lewis base. According to the Covalent Bond Classification method, the main group element in these complexes acts as a Z-type ligand and draws density from the metal atom via a direct M→Z interaction. In addition to that being of fundamental interest, the presence of this interaction provides a vector for controlling the electron density of the metal atom, offering new opportunities in metal mediated catalysis. The presence of this interaction may also manifest in the atypical redox properties that these complexes sometimes display. Examples of such behavior include the susceptibility of some of these complexes to undergo light-driven reduction processes.

With the view of understanding the factors that control the strength of M→Z interactions, the first objective of this dissertation has been to computationally survey a series of model complexes containing Pt(0) as a metallobase and the Lewis acidic main group fluorides of group 13, 14, and 15. Using CO, CH_3CN, and CH_3NC as probe molecules, we have been able to confirm that Lewis acidity increases down a group. These studies also reveal the existence of an island of high Lewis acidity, including In(III), Ge(IV), Sn(IV), As(V), and Sb(V) fluorides. Drawing on the conclusion of this computational survey, it became the second objective of this dissertation to investigate the synthesis of complexes containing platinum as a metallobase and a germanium (IV) moiety as a Z-type ligand. These efforts have resulted in the characterization of a complex in which a Pt(II) center is held by two ancillary phosphine ligands in proximity to the Ge(IV) center. The structure, spectroscopic, and computed properties of this complex have confirmed the existence of a Pt(II)→Ge(IV) interaction. Owing to the presence of this interaction, the complex can be photoreduced cleanly in the presence of a sacrificial reducing agent to afford the corresponding Pt(I)-Ge(III) as a result of chlorine elimination. With the view to test the generality of these findings, the third objective of this dissertation has been to investigate the synthesis of related Pd-Ge complexes. In this case, we observed that the reductive process described above for platinum takes place thermally, without the need for UV irradiation, leading to the corresponding Pd(I)-Ge(III) complex. Finally, this dissertation also explores some aspects of the chemistry of bimetallic gold (I) and gold(II) complexes as carbophilic catalysts. The main conclusion from this study is that a positive correlation exists between the catalytic activity of these complexes and the oxidation state of the gold center.

DEDICATION

To the blessings in my life

Mom, Dad, Hamid and little Kosar

ACKNOWLEDGMENTS

I would like to express my gratitude to my advisor Prof. François P. Gabbaï, for the support and guidance of my research and Ph.D. study. Beyond the academic support, I'm appreciative of his caring and understanding.

I would also acknowledge my committee members, Prof. Marcetta Y. Darensbourg, Prof. Donald J. Darensbourg, Prof. Michael B. Hall, and Prof. Melissa A. Grunlan for their valuable time and insightful comments.

Thanks also go to my friends and colleagues in the Gabbaï group. Special thanks go to Dr. Haifeng Yang, Dr. Srobona Sen, and Dr. Menxy (Moncy) Yang for teaching me lab techniques and useful computational tips. I would like to especially thank Elishua Litle for his valuable time and efforts in proofreading my work.

Finally, thanks to my family, mother and father for their encouragement and my husband for his patience, love, and continual support.

CONTRIBUTORS AND FUNDING SOURCES

Contributors

This work was supervised by a dissertation committee consisting of Professor François P. Gabbaï (advisor), Professor Michael B. Hall, Professor Marcetta Y. Darensbourg, and Professor Donald J. Darensbourg of the Department of Chemistry and Professor Melissa A. Grunlan of the Department of Biomedical Engineering.

The software and computational resources for computational studies were supported by the Laboratory for Molecular Simulation at Texas A&M University. All other work conducted for the dissertation was completed by the student independently.

Funding Sources

This work was supported by the National Science Foundation (CHE-1566474), the Welch Foundation (Grant A-1423) and Texas A&M University (Arthur E. Martell Chair of Chemistry). The views expressed in this dissertation are those of the author and do not necessarily reflect those of the abovementioned funding agencies.

NOMENCLATURE

DMBD	2,3-dimethyl-1,3-butadiene
dcpm	bis(dicyclohexylphosphino)methane
DFT	Density Functional Theory
dppm	bis(diphenylphosphino)methane
dppp	$(Ph_2P)C_6H_4$
FIA	Fluoride ion affinity
GEI	Global Electrophilicity Index
HOMO	Highest occupied Molecular Orbital
LMCT	Ligand to Metal Charge Transfer
LUMO	Lowest Unoccupied Molecular Orbital
mtp	methylenethiophosphinate
NBO	Natural Bond Orbital
PT	diphenyltellurophene
tfepma	$MeN[P(OCH_2CF_3)_2]_2$
tht	tetrahydrothiophene

TABLE OF CONTENTS

Page

LIST OF FIGURES

LIST OF TABLES

Page

CHAPTER I

INTRODUCTION

1.1 Introduction to photochemistry

In 2018, the global carbon emissions reached an all-time high in the Earth's history. A report[1] released by a consortium of researchers known as the Global Carbon Project found that the global emissions in 2018, showed an increase of 2.7 percent from burning fossil fuels in comparison to 1.6 percent in 2017. It is projected that by the end of 2019, fossil-fuel related CO_2 emissions will reach 37.1 billion metric tons, and the total carbon dioxide concentrations in the atmosphere will reach 407 parts per million—about 45 percent higher than preindustrial levels.

With the increasing rate of carbon emission and subsequent role in climate change, there is a determination to replace fossil fuels with more sustainable energy sources and reduce carbon dioxide emissions. As an endless and appealing source of clean energy, solar energy is the best candidate. Research on utilizing and storing solar energy as a continual and clean source of energy is becoming increasingly important. For making the solar energy available for society to use on a large-scale, inexpensive storage mechanism with a high energy density is required. Chemical bonds are likely to have the highest energy density to serve the purpose of solar energy storage.[2]

1.1.1 Water splitting

In nature, collecting and storing solar energy in chemical bonds is accomplished by photosynthesis, a method that researchers are attempting to emulate to solve the solar energy challenge. Photo electrolysis of water using semiconductors as light absorbers and energy converters of solar energy in the simplest chemical bond, H_2, has been used.[3] Efficiently splitting water into usable hydrogen gas provides a clean fuel source whose only byproduct upon consumption is water. This transformation is based on a redox process that involves four protons and four electrons being removed from the water to produce oxygen and hydrogen (Figure 1).

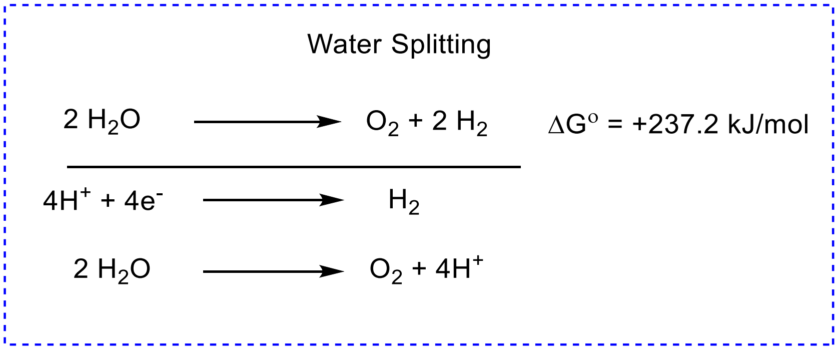

Figure 1. Water splitting reaction.

1.1.2 HX splitting

The formation of the H_2 can be achieved via an alternate mechanistically more straightforward synthetic route based on hydrohalic acid splitting (Figure 2).[4] The positive standard free energy values for the HX splitting reactions of HCl and HBr show that these reactions could also be store considerable amounts of energy.[5] The HX splitting process can meet the criteria of energy storage to the same extent as water splitting with a less complicated two-electron redox process, which makes the HX splitting an attractive target.[4]

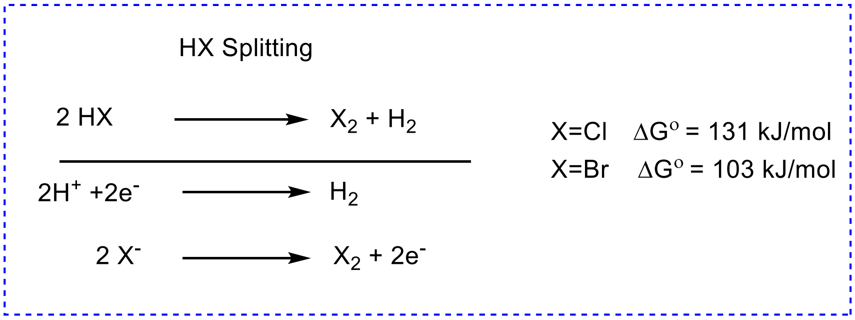

Figure 2. HX splitting reaction

An hypothetical HX splitting cycle, depicted in Figure 3, demonstrates the critical steps involved in photocatalysis.[5] In Step (i), oxidative addition of HX to the photocatalyst ([Cat]), results in a hydrido-halide intermediate. In Step (ii), a second HX addition forms a dihydrido-dihalide species, while in step (iii), H_2 reductively eliminates. Alternatively, if there is an M–H bond present in the intermediate, direct protonation by HX (iv) affords H_2 and the final $[Cat](X)_2$ intermediate. The consecutive steps (i)–(ii) are only possible in very reduced bimetallic catalysts. The acid-base pathway (iv) is the most probable path in monometallic catalysts or complexes with a less reducing resting state. Despite the mechanism of H_2 production, the final step (v) to close the cycle, comprises the thermodynamically challenging X_2 photo-elimination. As such, complexes that are reducing enough to reduce protons to, and in the meantime, are oxidizing enough to oxidize halides to halogen (X_2) are needed.

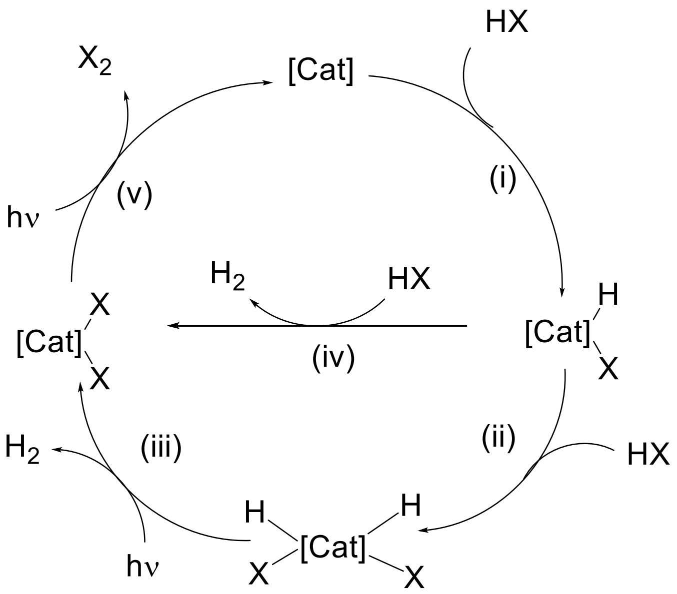

Figure 3. Hypothetical HX-splitting cycle supporting direct photon-to-fuel hydrogen photocatalysis.

Bimetallic mixed-valence complexes featuring the M-M bond, are potential photocatalysts. They can undergo the two-electron process of HX splitting.[5, 6] The Nocera group, who is actively involved in bimetallic photocatalysis, is attempting to develop hydrohalic acid splitting catalysts to generate solar fuel using bimetallic mixed-valence complexes of rhodium(Figure 4).[7-10]

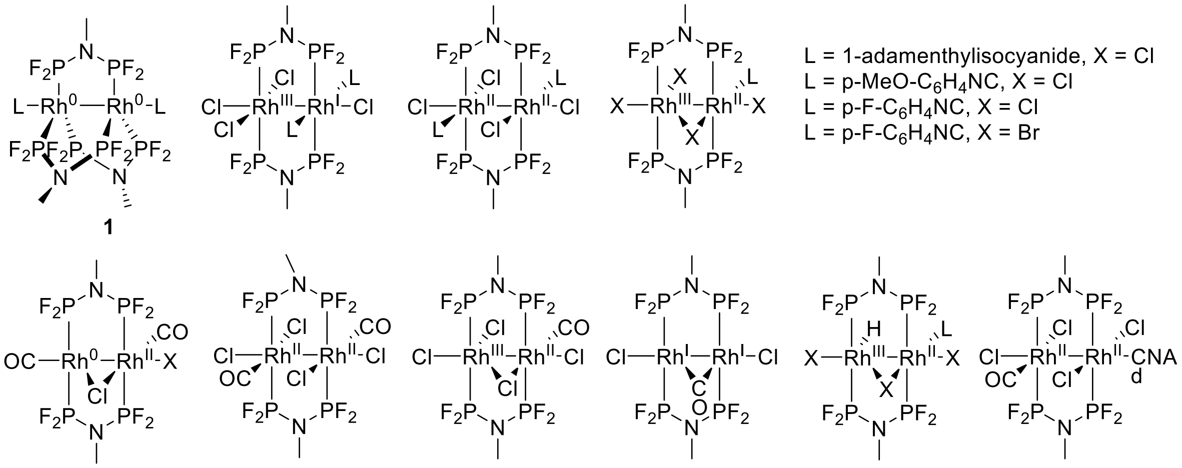

Figure 4. Bimetallic mixed-valence complexes of dirhodium with a metal-metal bond.

Complex **1** in Figure 4, featuring an Rh^0-Rh^0 core,[10] is one of the most promising homogenous catalytic systems used for the conversion of HX to H_2 and X_2. In this catalytic process, the electron rich Rh(0) center is susceptible to undergo oxidative addition of HCl. Upon irradiation in the presence of a radical chlorine trap, hydrogen is formed. The proposed mechanism for HX splitting using complex **1** as a catalyst is illustrated in Figure 5. This process consists of the oxidative addition of HCl to complex **1**, resulting in the dihalide-dihydride Rh^{II}-Rh^{II} complex **2**. Upon exposure to light, complex **2** eliminates H_2, which leads to the formation of the dihalide Rh^I-Rh^I complex **3**. Complex **3** disproportionate to form the dihalide Rh^0-Rh^{II} complex **4**. Ultimately, in the presence of light and a radical trap, this complex goes back to complex **1** via photoreduction. The mixed-valency at the rhodium metal centers is essential in that it ensures turnover of HX at the catalyst, allowing oxidative addition and reductive elimination to occur smoothly. The reaction's efficiency can be improved by modifying the catalyst's primary coordination sphere.

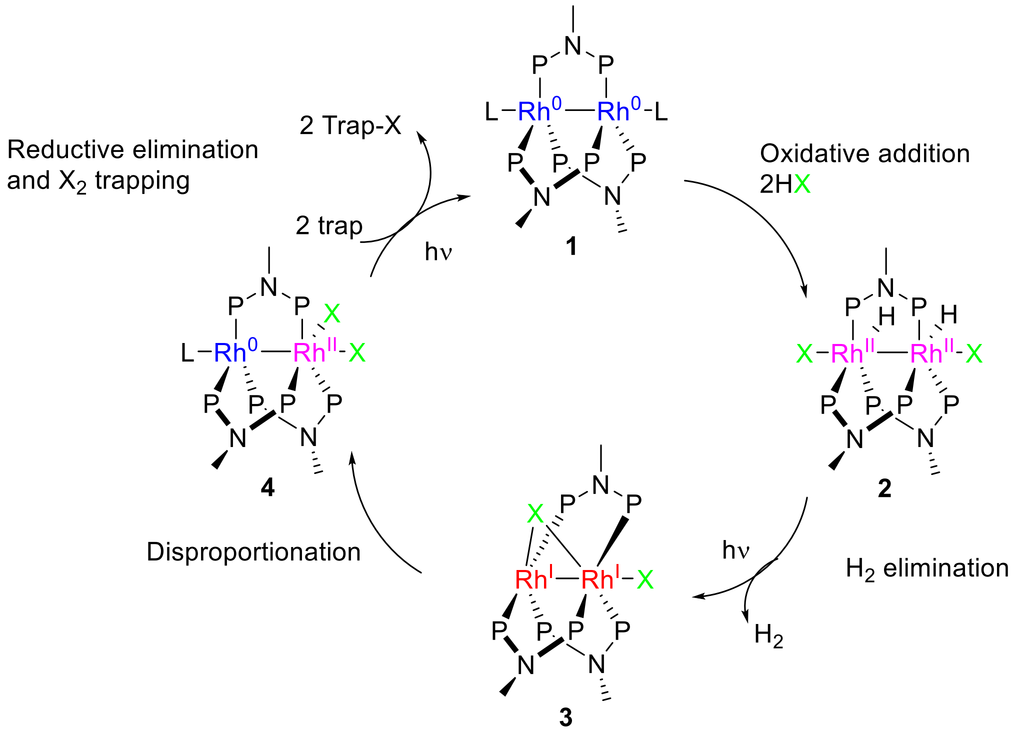

Figure 5. Proposed mechanism for HX splitting with complex **1**.

1.1.3 X_2 elimination driven by light

A critical step in the transition metal-catalyzed hydrohalic acid splitting process is the photoelimination of the halogen molecule from a dihalide complex.[11] The overall efficiency of the HX splitting process hinges on the activation of strong M-X bonds and the reductive elimination of halogen,[12] a process that is uncommon and thermodynamically unfavorable.[13] Even if the energy barrier for this reaction is overcome by irradiation, trapping the halogen becomes critical due to the reversibility of the reaction.[7, 8, 14, 15]

1.1.3.1 X_2 elimination from late transition metals

The photoreductive elimination of halogens from transition metal complexes is not favorable thermodynamically and involves the activation of strong M-X bonds. However, despite the stability of M-X bonds, the accessible low lying M-X σ^* orbital can be populated upon electronic excitation[6] leading to the weakening of the M-X bond and resulting in the homolytic splitting making transition metals (M) suitable for elimination of halogens.

Systems featuring more oxidizing metal centers, compared to the dirhodium complexes, are more efficient in the elimination of X_2.[5] To pursue this, several classes of metal-metal bonded bimetallic species have been designed and reported by Nocera,[14, 16-18] that maintain the electronic structure that drives the photoelimination chemistry of the original dirhodium complexes.

Complex $[Pt^{III}Au^{II}(dppm)_2(Ph)Cl_2](PF_6)$ (dppm = bis(diphenylphosphino)methane) (**5**,Figure 6) undergoes halogen photoelimination to regenerate the $Pt^{II}Au^{I}$ precursor with a quantum yield of 5.7% when in the presence of high concentration of 2,3-dimethyl-1,3-butadiene (DMBD) as a halogen trap.[14] The observed quantum yield shows an almost ten-fold increase compared to the isoelectronic d^9-d^7 $Rh_2^{0,\ II}$ complexes.[8] Furthermore, the homobimetallic d^7–d^7 complex $Pt_2^{III,\ III}(tfepma)_2Cl_6$ (tfepma = $MeN[P(OCH_2CF_3)_2]_2$), complex **6**, shows a higher solution quantum yields of 38%.[18] This complex provided the the first documented example of a Cl_2 photoelimination in the solid state.

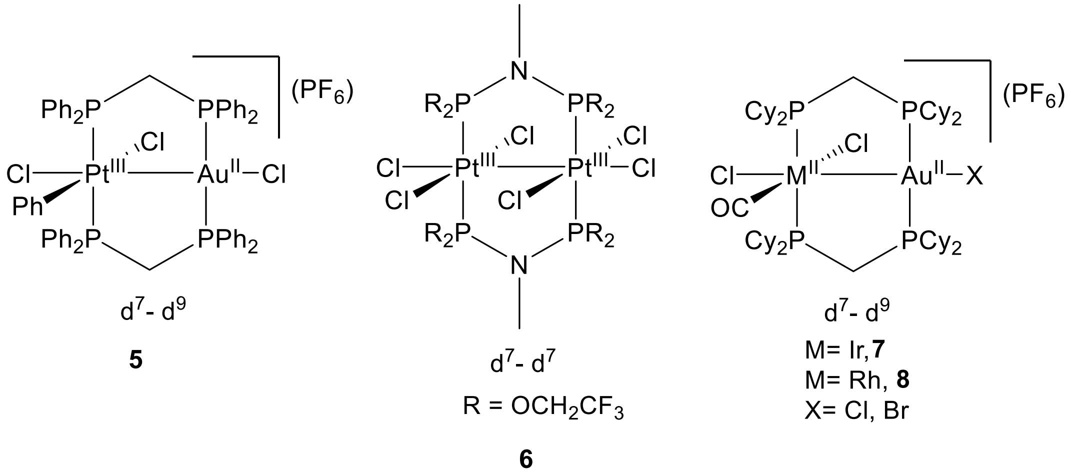

Figure 6. Bimetallic transition metal complexes undergo X_2 elimination.

Heterobimetallic complexes of $[M^{II}Au^{II(}dcpm)_2(CO)X_2]PF_6$ (M = Ir,**7**; Rh,**8** X = Cl, Br, dcpm = bis(dicyclohexylphosphino)methane) effectively eliminate halogen in the presence of DMBD, with quantum yields of ca. 10% for M = Ir, X = Br and 18% for M = Rh, X = Br.

Monomeric gold complexes of type $Au^{III}(PR_3)X_3$ (**9**) as well as bimetallic complexes of the type $Au_2{}^{I,\ III}[\mu CH_2(R_2P)_2]X_4$, (**10)** and $Au_2{}^{III,\ III}[\mu\text{-}CH_2(R_2P)_2]X_6$ (R) Ph, Cy, X) Cl-, Br-)(**11)**tend to undergo facile photoelimination of halogen (Figure 7). The bimetallic gold complexes, which lack a formal metal-metal interaction, reveal that a metal-metal bond is not a prerequisite for smooth halogen elimination. LMCT excitation is the driving force behind the M-X bond activation and halogen elimination in this series of Au^{III} complexes. Photochemistry at the Au^{III} centers consists of the two-electron photoelimination of X_2 from a monomeric centers and the four-electron photoelimination of two equivalent of X_2 from bimetallic centers. Reported quantum yields for these complexes are between 10% and 20%. Surprisingly, these systems provide rare examples of trap-free halogen photoelimination.[12]

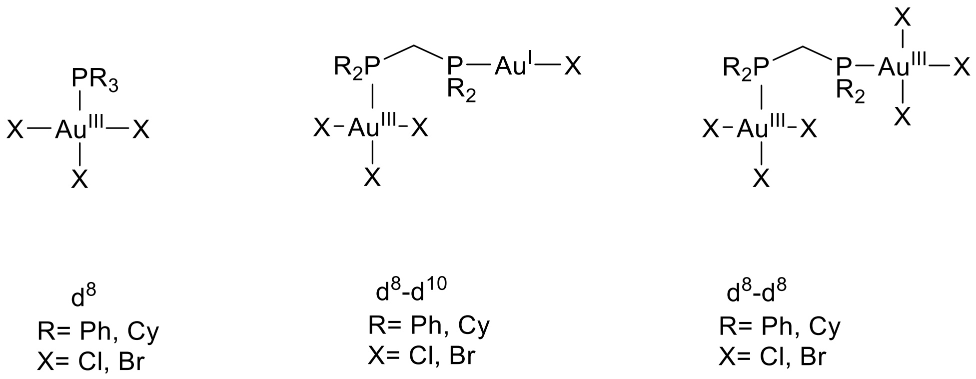

9 **10** **11**

Figure 7. Au complexes with the potential of eliminating X_2.

Sharp *et al* reported series of mononuclear Pt(IV) complexes in the form of $Pt(PEt_3)_2RX_3$ (X= Cl, Br) (**12**) capable of undergoing reductive photoelimination of halogens in the presence of the UV light (Figure 8).[11, 19] Complexes where X= Cl had a maximum quantum yield of 58% while for the complexes with X=Br the reported quantum yield is in the range of < 1% to 59% except for $Pt(PEt_3)_2(Br)_3R$ (R = *o*-$(CF_3)C_6H_4$) that eliminates bromine with a very high quantum yield of 82%. [11]

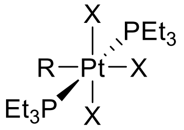

12

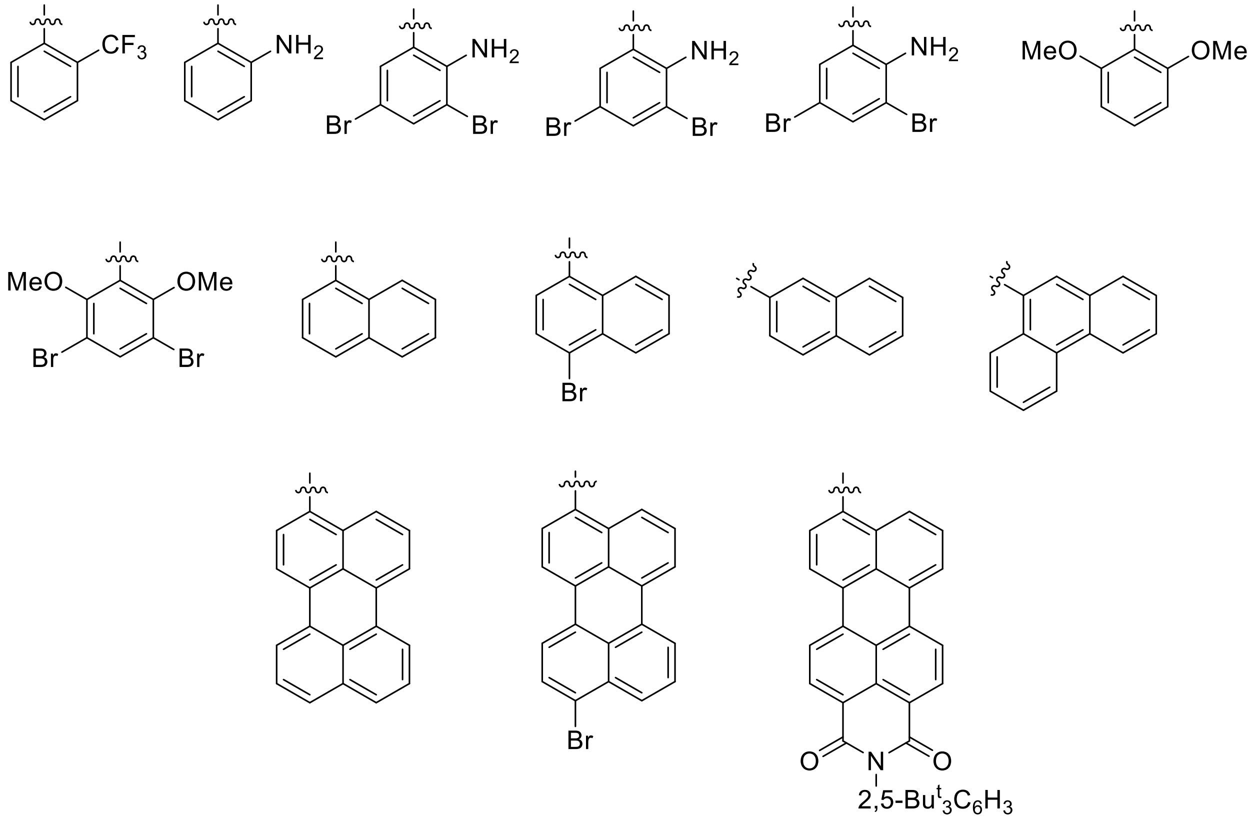

Figure 8. Series of $Pt(PEt_3)_2RX_3$ (X=Cl, Br) complexes capable of undergoing photoreductive elimination.

All complexes discussed in this section, contain metals from group 10 or group 11. All group 10 and 11 complexes show higher quantum yields than group 9 complexes. By designing compounds with the minimal amount of structural rearrangement upon photoelimination, it is possible to improve quantum yields and increase the likelihood of X_2 elimination in the absence of a trap.[5]

1.1.3.2 X_2 elimination from main group compounds

Many main group elements due to their ability to undergo a two-electron redox process are appealing candidates for halogen elimination. However, examples of halogen elimination reactions involving main group elements are rare, with only a handful of compounds able to support this process. Research in this area remains limited to compounds of tellurium[20-23] and antimony.[24]

Compound **13** in Figure 9 was reported by Seferos.[23] The Te atom of this derivative is incorporated within the π-conjugated scaffold of a tellurophene and can exist in the +II or +IV oxidation state. When in the +IV oxidation state, these compounds can be photoreduced with a quantum yield of just 0.19% for X = Br. Variation of the halide or increasing the concentration of the halogen trap does little to improve the quantum yield. Density Functional Theory (DFT) calculations carried out on this system, suggests that the nature of the HOMO-LUMO transition is the source of the low quantum yield. The excited state is delocalized across the entire molecule instead of having a Te-X antibonding character.[23] The reactivity and the photochemistry of the halogenated 2,5-diphenyltellurophene **14** have been explored.[22] In the presence of an organic halogen trap, the photodehalogenation reaction occurs with a quantum yield of 16.9% for X=Br, 1.6% for X= Cl, and 2.3% for X = F. Chlorine and fluorine photoreductive elimination in the presence of the organic halogen trap is accompanied by decomposition reactions. However, a significant improvement has been achieved in trapping fluorine by using water as a trap, and no sign of decomposition was observed.

In the other contributions by Seferos, a series of compounds, including **15** and **16**, have been designed. The lowest energy excited state of these compounds is localized on the tellurophene and features significant Te-X antibonding character.[22] When electron-withdrawing substituents are present, these systems become efficient platforms for the photoelimination of halogens with quantum yields that are comparable to those of transition metal complexes.[17, 18] The 2,5-bis(pentaflourophenyl)tellurophene **16** eliminates Br_2 with a quantum yield of 42%, while reductive photoelimination of chlorine is more challenging than bromine leading to lower quantum yields due to the high Te-Cl bond energy.

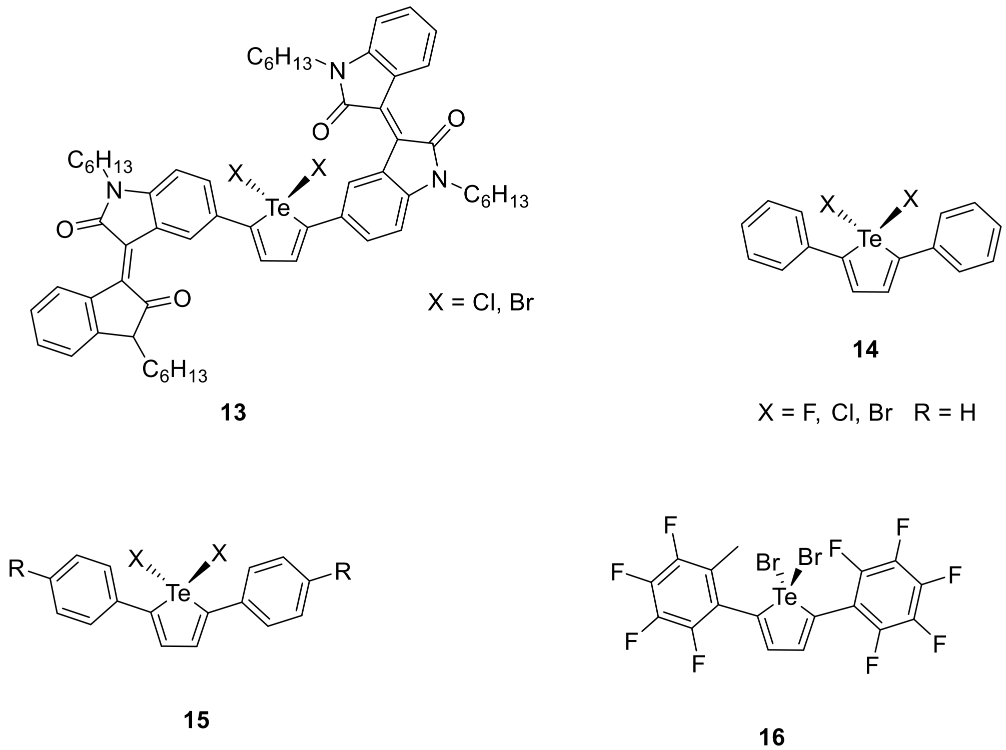

X = Cl, Br

13

14

X = F, Cl, Br   R = H

15

16

X = Br   R = NEt_2, OtBu, tBu, CN, CF_3, NO_2, NO_2-NBu_2

Figure 9. Tellurophene platforms undergo two-electron redox halogen elimination.

Another system solely using main group elements to carry out X_2 elimination was recently reported by Nocera.[24] This system, which is based on a $Sb^{V}X_2$ corrole unit undergoes smooth conversion into the Sb^{III} corrole derivative when irradiated in the presence of halogen traps (Figure 10). In the absence of a trap, the halogen atoms react with the corrole ring, pointing to the vulnerability of this compound and the importance of a trap. The $Sb^{V}Br_2$ corrole, compound **18**, has a higher photoreductive elimination quantum yield (0.88%) when compared to the $Sb^{V}Cl_2$ corrole, compound **17** (0.17%).

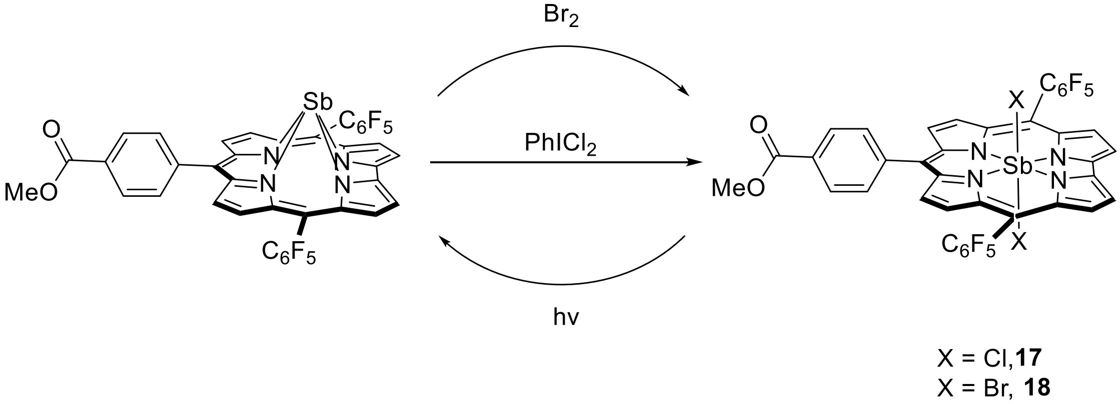

Figure 10. Halogen photo elimination from Sb^{V} dihalide corroles.

1.1.3.3 X_2 elimination from late transition metal-main group complexes

Most platforms suitable for the photoreductive elimination of halogens identified to date contain a late transition metal or main group elements, yet there are a few that contain both. In these complexes, the main group element can act as an electron buffer, and the elimination process would only involve M-X bond breaking. As such, the Gabbaï group[25] reported a novel redox-active main group/transition metal platform of heterobimetallic $[ClTe^{III}Pt^{III}Cl_3(o\text{-dppp})_2]$ (o-dppp = o-$(Ph_2P)C_6H_4$, complex **19** in Figure 11). The complex features a hypervalent four-coordinate tellurium atom and an octahedral platinum center. Density Functional Theory (DFT) and Natural Bond Orbital (NBO) calculations show the presence of Pt→Te interaction. This dinuclear platform can undergo photoreductive elimination of Cl_2 upon irradiation by UV light and in the presence of a radical trap such as 2,3-dimethyl-1,3-butadiene (DMBD). Complex **19** showed a quantum yield of 4.4%, mimicking the behavior of transition metal-only analogues. A unique facet of this platform originates from the capacity of the tellurium atom to buffer the electron density of the redox-active platinum center. These buffering properties are made possible by the ability of the tetravalent tellurium center to switch between a regular eight-electron and a hypervalent configuration.

Other main group-transition metal species that support the photoreductive elimination of halogens include $[Cl_2Sb^{IV}Pt^{III}Cl_3(o\text{-dppp})_2]$ (**20**),[26] and $[Cl_3Sb^{V}Pd^{II}Cl_2(o\text{-dppp})_2]$ (**21**)[27] which have been investigated by the Gabbaï group (Figure 19). Antimony can undergo facile III/V redox chemistry; also, the tri- or pentavalent antimony offers a higher degree of electronic control, making antimony a suitable ligand for the reductive elimination of halogens. The Sb-Pt platform (**19**) shows a high photoevolution quantum yield of $\phi = 13.8$ % at a DMBD concentration of 4.4 M. This is due to the destabilization of the oxidized complex by five electron-withdrawing chlorine ligands. This Sb-Pt platform also undergoes photoreduction in the solid state.

Photoreductive dehalogenation reactions occur in many transition metal complexes, but such reactivity with palladium complexes is rare.[28-30] In the platinum analog,[26] the antimony center acts as a spectator in the dehalogenation reaction. At the same time, results for the palladium complex **21**,[27] show that the photoreductive elimination occurs at the antimony center. Overall, the process involves a one-electron reduction of both antimony and palladium centers. This process results in the formation of a σ-bond between Sb and Pd. Complex **21** features a Lewis acidic trichlorostiborane moiety positioned in the ligand backbone. Upon irradiation with UV light, the complex undergoes a clean photoreductive chlorine elimination reaction to yield $[Cl_2Sb^{IV}Pd^{I}Cl(o\text{-dppp})_2]$, which features a covalent Sb− Pd bond.

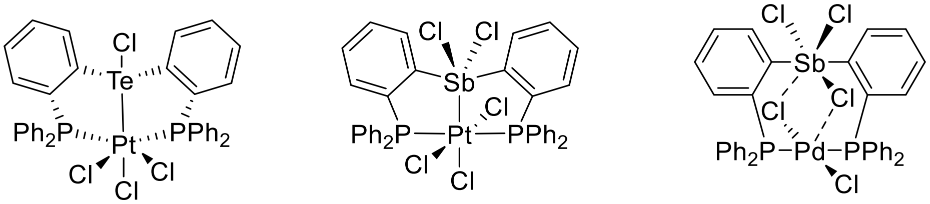

19 $\Phi = 4.4\%$

20 $\Phi = 13.8\%$

21 $\Phi = 0.55\%$

Figure 11. Transition metal/main group complexes undergoing halogen elimination

1.2 Introduction to germanium containing complexes

1.2.1 Germanium containing pincer complexes

Pincer type ligands with the general formula of LEL (L = P, N, S; E = C, N, main group elements of groups 13, 14, and 15) are an essential class of compounds. They can provide a decent balance of reactivity and stability to the transition metal complexes in which they are incorporated.[31] As illustrated in Figure 12, the central atom of the pincer ligand (E) can be modified a Z-type, an X type or an L-type ligand which may later engage in cooperative metal/ligand interactions. The PCP- and the NCN-type ligands are the most common pincer ligands being extensively studied.[32, 33] Their complexes usually have high thermal stability due to their tridentate structure which imposes rigidity, and on the other hand, the anionic X-type moiety will induce reactivity.[34]

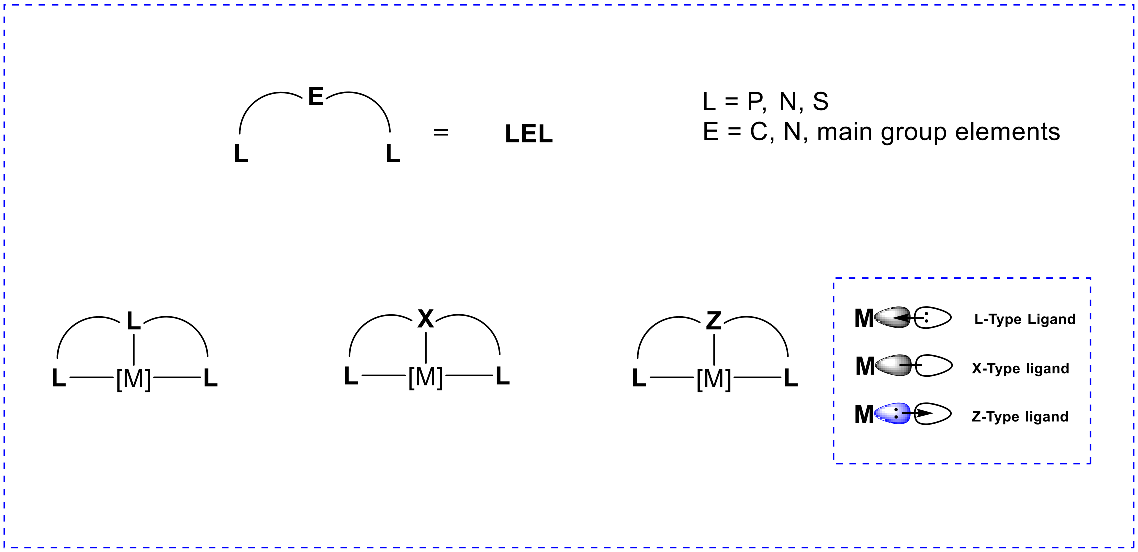

Figure 12. General scheme of pincer ligands and their corresponding transition metal complexes.

The chemistry of heavier group 14 compounds as a pincer ligand has been less explored except for the silicon-containing pincers.[34] Their transition metal complexes have been utilized in many organic transformations as recently reviewed by Takaya and Iwasawa.[34] Transition metal complexes of PSiP type pincer ligands with the σ-silyl bond show high potential for new paths of catalytic reactivity involving challenging bond activation reactions.[35] The strong electron-donating character of silyl ligands give these complexes their outstanding reactivity.[35] Replacing the silyl group with the germyl and the stanyl groups could provide a variety of molecular structure and electron distribution, which may lead to significant differences in reactivity.[35] Surprisingly the chemistry of germanium and tin and their potential application have been less developed. Reports on the germanium containing complexes are dominated by cases where the germanium is terminally bound to the transition metal.[36-40] Pincer type ligands containing a central germanium atom are a new development. Despite the limited germanium containing pincer complexes, they have displayed interesting attributes in catalysis that differ from those of the silicon analogs.[41]

1.2.1.1 Germylene containing pincer complexes

Heavier tetrylene ligands can act as potent electron donor ligands. Developing novel pincer tetrylene ligands and their use in catalytic transformations when combined with transition metals is an ongoing subject of interest.[42-47] The first PGeP pincer ligand Ge(NHCH$_2$P^{t}Bu$_2$)$_2$C$_6$H$_4$, compound **22**, was reported by Cabeza (Figure 13).[48]

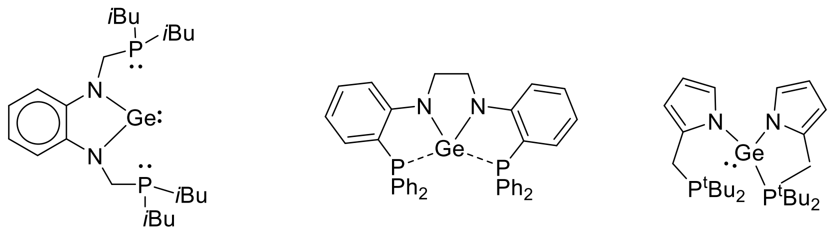

22 **23** **24**

Figure 13. Examples of recent pincer ligands containing germylene as a donor group.

The reaction of compound **22** with a few transition metal fragments containing Co^0, Rh^I, Pd^{II}, Pt^{II}, Ni^{II} center has been targeted.[48, 49] Compounds **23**[50] and **24**[51] are recent developments in the chemistry of PGeP germylene pincer ligands. Reactivity studies suggest that the germanium atom can increase its coordination number through an insertion process that affords bridging germylene as in compound **29** or monohapto chloridogermyl pincer ligands such as in compounds **25-28** (See Figure 14).[48]

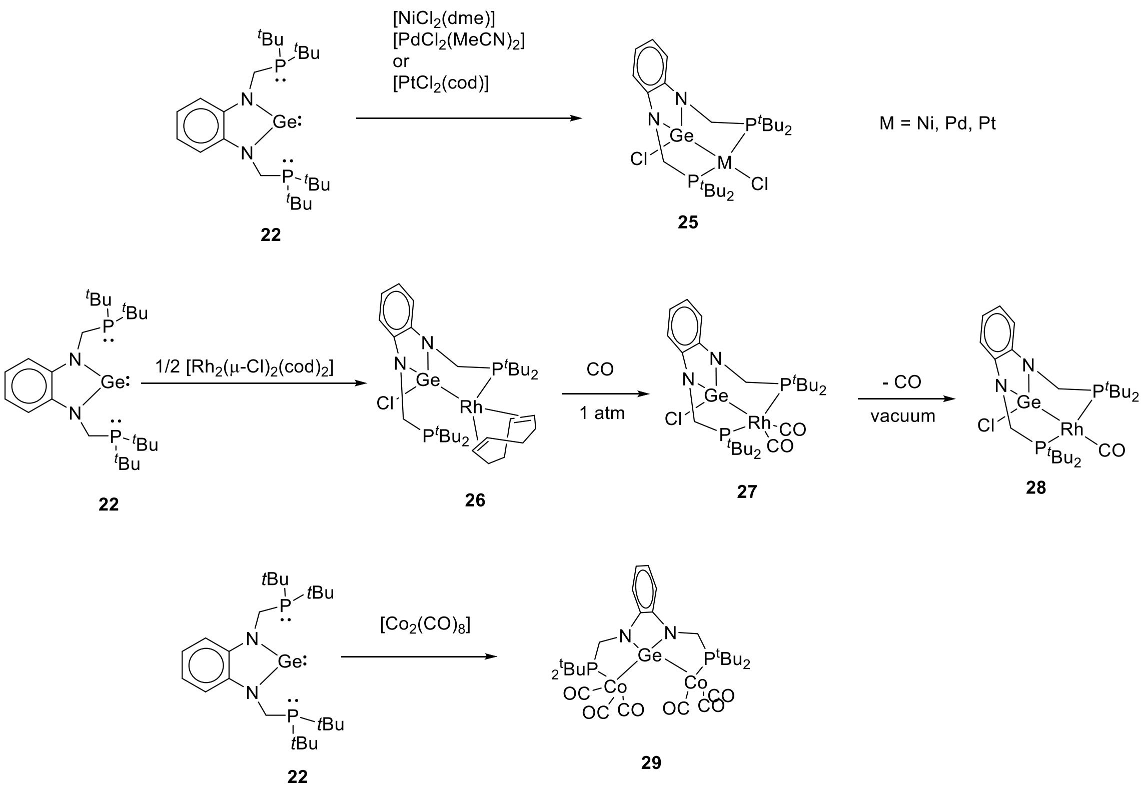

Figure 14. The N-hetrocyclicgermaylene $Ge(NHCH_2P^tBu_2)_2C_6H_4$, compound **22**, and its related transition metal complexes.

The reactivity of group 10 complexes of compound **25**, as shown in Figure 15, have been studied towards nucleophilic reagents. The reactivity results indicate that the germanium atom is the center of reaction in these complexes.[49]

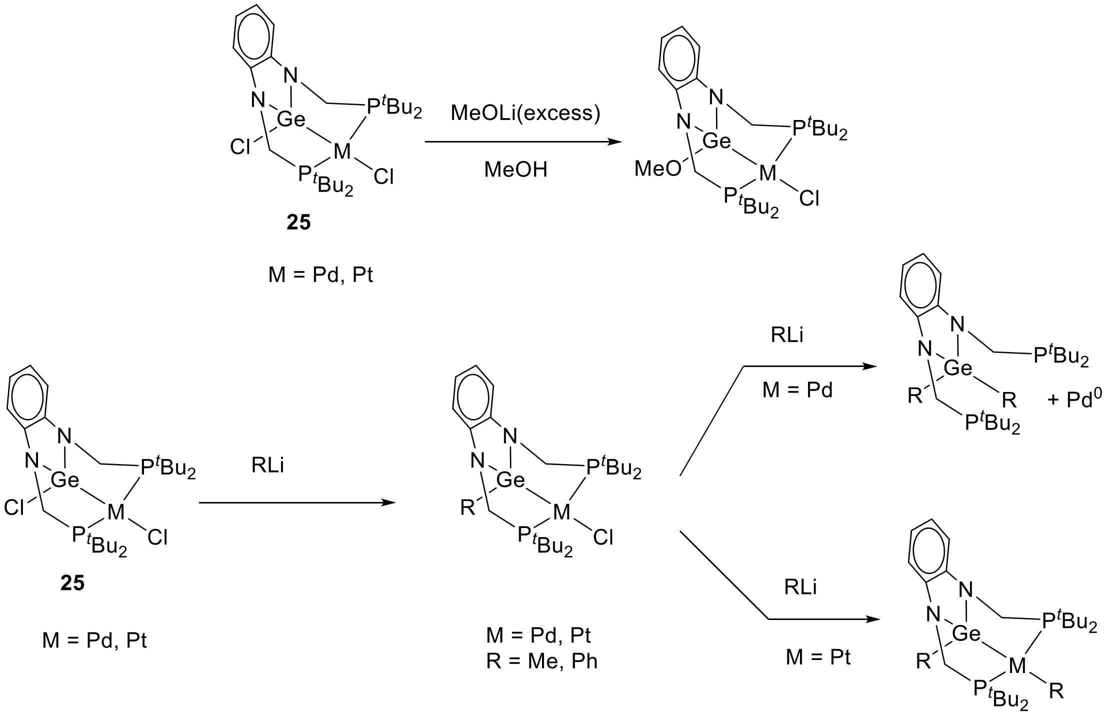

Figure 15. The reactivity of compound **25** towards nucleophilic reagents.

1.2.1.2 Germyl containing pincer complexes

Tridentate PGeP-pincer type ligands being synthesized from diphosphogermane[35, 52-55] are valuable germanium containing pincer ligand systems (Figure 16). This class of ligands has been successfully used as organometallic catalysts.[54, 55] Tridentate pincer complexes of divalent group 10 metals are expected to be active catalysts for molecular transformation since similar PCP–palladium(II) complexes have been widely utilized in synthetic organic chemistry.[31] Palladium complexes of PGeP germyl pincer ligands have been used as catalysts in the hydrocarboxylation of allenes and alkenes (Figure 17). [54, 56] The reactions of the pincer ligands **30** and **31** with $[PdCl(C_3H_5)]_2$ leads to the formation of palladium complexes **32** and **33**, which, upon halide abstraction with AgOTf, yield **[32]OTf** and **[33]OTf** as active catalysts, respectively ((a) and (b) in Figure 17). Complex **[32]OTf** also shows catalytic reactivity in aldol reactions (Figure 18).[55]

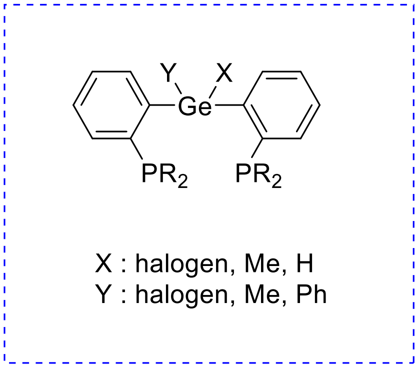

Figure 16. Tridentate PGeP germyl type pincer ligands.

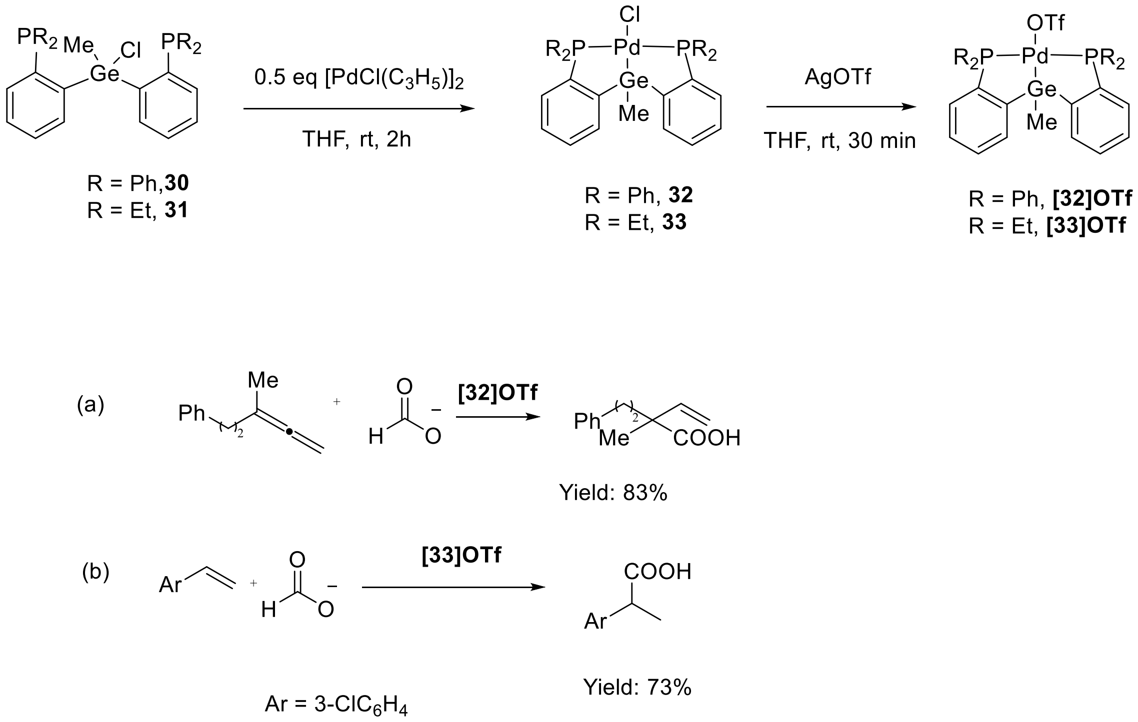

Figure 17. PGeP-pincer Pd complexes as an active catalyst in the hydrocarboxylation of allenes (a), and alkenes (b) with formate salt.

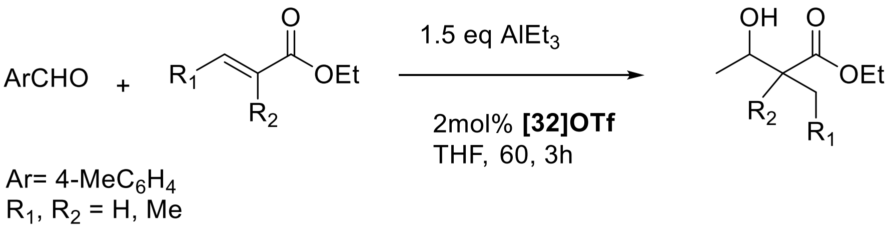

Figure 18. Aldol addition reaction catalyzed by **[32]OTf**.

Iwasawa has reported the reaction of the PGeP germyl ligand **34** with $Pd(PPh_3)_4$ which forms the mononuclear η^2-(Ge–H)-palladium complex **35**.[57] This complex is the first example of a mononuclear group 10 metal complex bearing a coordinated Ge–H σ-bond, which can further be used in the hydrometalation of ethylene (Figure 19).

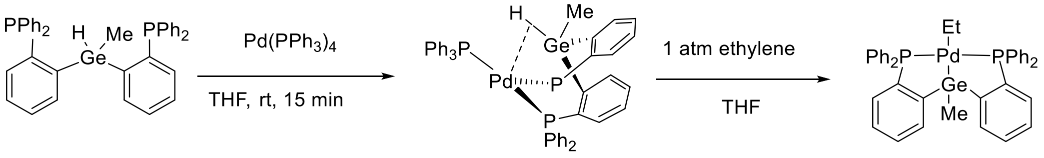

34

35

Figure 19. Synthesis and isolation of the η^2-(Ge–H)Pd^0 complex **35** used in hydrometallation of ethylene.

Germyl pincer ligands have been studied for their mode of bond activation. The Ge–X bond activation in the rhodium and the iridium complexes bearing the $\{o\text{-}(Ph_2P)C_6H_4\}_2GeX_2$ (X = F, Cl, and Me) ligand have been addressed by Nakazawa[35, 52, 53] as illustrated in Figure 20.

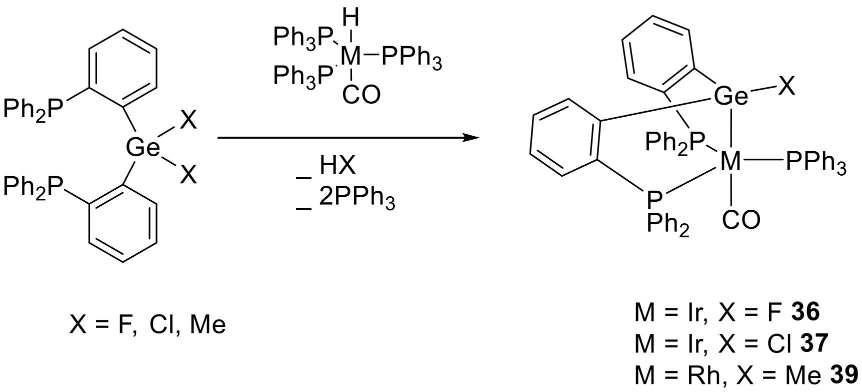

Figure 20. The Ge-X bond activation with the iridium complex.

The iridium complexes **36** and **37** have been studied for their mode of Ge−X bond activation.[52, 53] Complex **36** is the first example of a complex where Ge−F bond activation by a transition metal center occurs. In this complex σ-bond metathesis (**A** in Figure 21) between the Ge−F and Ir−H σ-bonds takes place. DFT calculations for this complex suggests a strong dative Ir→Ge interaction. The Ir→Ge interaction weakens the σ-bond, which leads to the coupling between the fluorine on germanium and the hydrogen on iridium, making the Ge−F bond activation facile. However, DFT calculations for complex **37** indicates a different mode of activation. The Ge–Cl σ-bond is cleaved through an S_N2-type pathway (**B** in Figure 21). This complex, along with its silicon analog, provide the first evidence for transition metal-mediated E–Cl activation (E = Si, Ge) via an S_N2-type reaction.

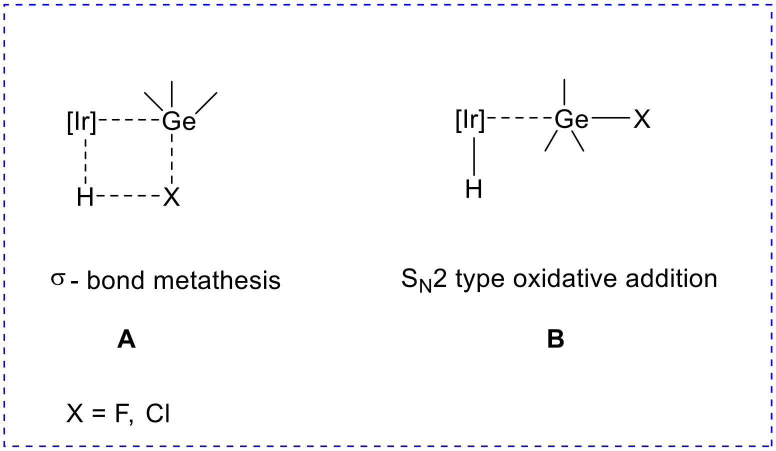

Figure 21.The possible pathways for Ge–X σ-bond cleavage by an iridium hydride complex.

Utilizing (o-$(Ph_2P)C_6H_4)_2GeFPh$, compound **40**, as a ligand, leads to an unexpected selectivity for Ge−F over Ge−C_{Ph} σ bond activation (Figure 22). DFT calculations favors metathesis mechanisms with inverse electron flow. The transfer of electron density from iridium to germanium weakens the Ge−F bond and results in HF formation. Comparison of the germanium containing complex **41** and the silicon-containing complex **42**, reveals that the electron flow is stronger in the germanium containing complex, which explains the unexpected selectivity of Ge−F over Ge−C_{Ph} bond activation.

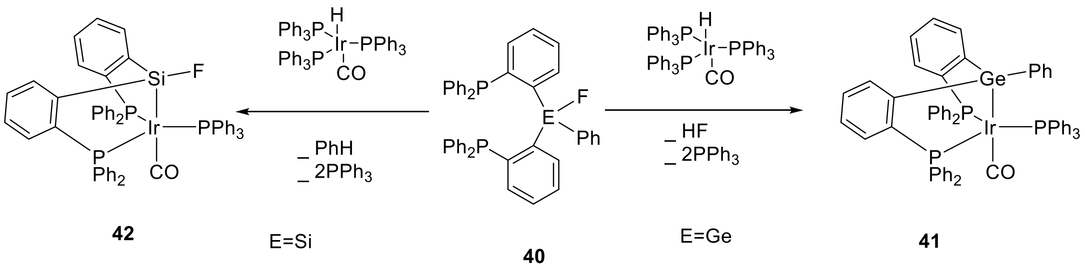

42 **40** **41**

Figure 22. E–F bond activation *vs.* E–C_{Ph} bond activation in the germanium and silicon-containing iridium complexes.

1.2.2 Germanium containing tripodal complexes

Another crucial group of ligands containing heavy group 14 elements are those with a tripodal framework. The ligands with the following general formula of [{*o*-(Ph_2P)C_6H_4}$_3$GeX] (X= F, **43**, X = H, **44** in Figure 23) have been coordinated to transition metal fragments.[35, 58-60]

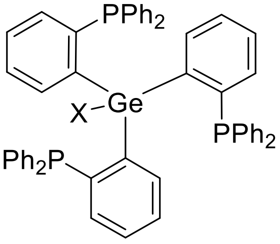

X = F, **43**
X = H, **44**

Figure 23.Tripodal framework with the general formula of [{*o*-(Ph_2P)C_6H_4}$_3$GeX] (X = F, **43**, X = H, **44**).

Nakazawa[61] exploited the σ-donating ability of group 11 metals (Cu, Ag, and Au) to access complexes of type **45-47** starting from **43** (Figure 24). Experimental and theoretical results offer a systematic evaluation of the σ-donating ability of the group 11 metals and σ-acceptor ability of the group 14 elements.

Figure 24. The reaction of compound **43** with group 11 metals.

Compound **44** has been coordinated to transition metal fragments containing Pt^0, Pt^{II}, Ru^{II}, and Ir^I center. In all cases, the reactions lead to germyl complexes formed either by elimination reactions or by insertion of the low valent transition metal in the Ge-H bond (Figure 25).

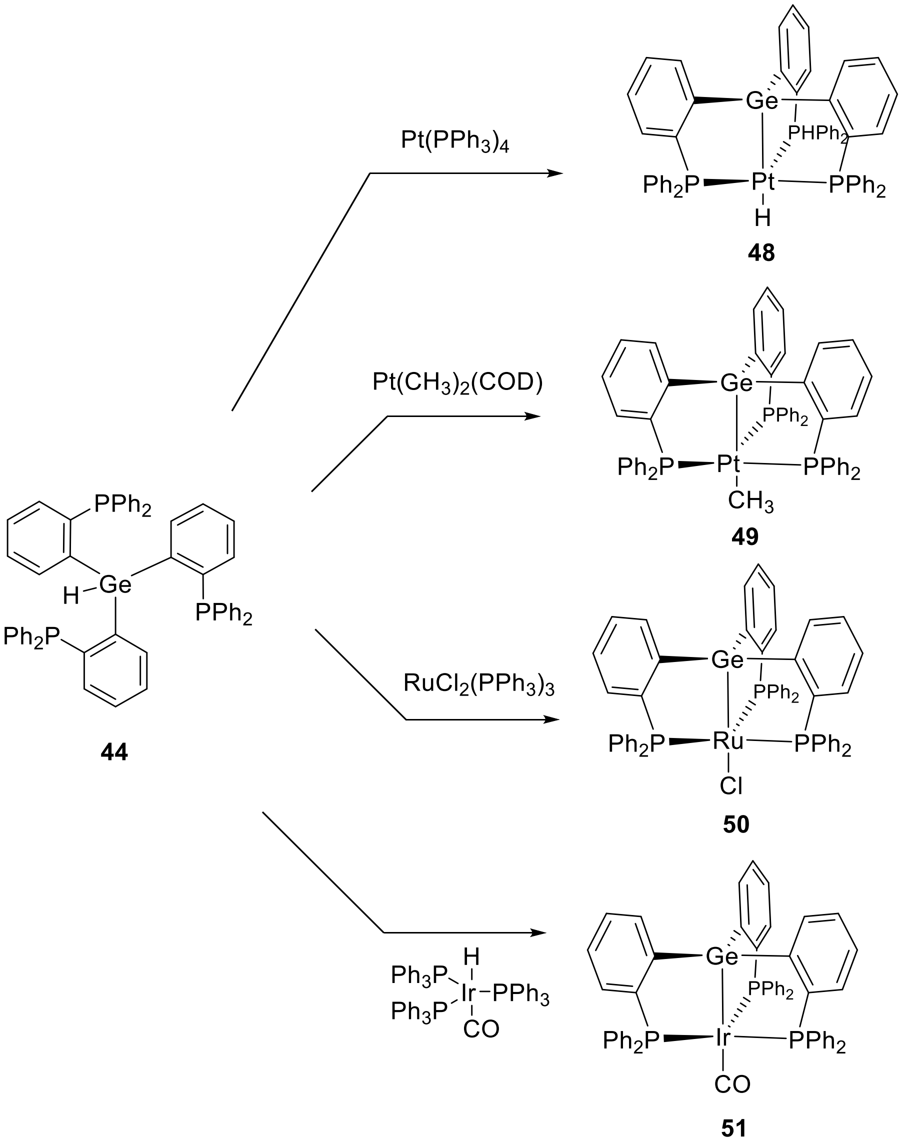

Figure 25. The reaction of compound **44** with transition metal fragments.

Altogether, this section shows that germanium complexes of Pd, Ir, Rh, and Ru have been explored and studied in bond activation and catalysis. Germanium-containing platinum and gold complexes are understudied suggesting the existence of a vast field for new discoveries.[41]

CHAPTER II

PROBING LEWIS ACIDITY OF MAIN GROUP FLUORIDES OF GROUPS 13, 14, AND 15 USING REPORTER FRAGMENTS

2.1 Introduction

Tuning the Lewis acidity of transition metal catalysts by tailoring the secondary coordination sphere has become an active research area for catalytically active organometallic complexes. Transition metals can be classified as both Lewis acids and Lewis bases. The electropositive nature of transition metals more commonly leads to coordination complexes that exhibit a certain degree of Lewis acidity at the metal center. Traditionally, transition metal basicity is limited to metal-to-ligand π-back donation. However, in the presence of electrophilic substrates, transition metals can also behave as an electron-pair donor. As such, being able to design Lewis acidic ligands positioned to interact with the transition metal catalyst could lead to electron donation from the metal center to the Lewis acidic ligand.

2.1.1 Transition metal Lewis basicity

Transition metal ligands are commonly composed of single-electron donors or two-electron donors, where the electropositive metal usually is considered a Lewis acid. While less prevalent, Lewis basic metals in low oxidation states can serve as electron donors to ligands.[62] The first examples were reported by Hieber with metal carbonyl hydrides where metal carbonyl anions can do nucleophilic displacement on inorganic and organohalides;[63-65] then later by Wilkinson who studied the protonation of cyclopentadienyl metal complexes.[66, 67] The notion of transition metal basicity was expanded by the discovery of complexes in which the metal centers can serve as electron donors toward Lewis acids such as BF_3, BH_3, O_2, and SO_2.[62]

Transition metal Lewis basicity can be manifested by the formation of an adduct between the metal as a Lewis base and a Lewis acid resulting in a dative bond. In many of these complexes, a main group acceptor acts as Z-type ligands.[68-74]

2.1.2 Z-type ligands

According to the classification[75, 76] of covalent bonds in transition metal complexes, there are three types of ligands: L-type ligands, which are two electron σ-donor ligands; X-type ligands which are referred to as one-electron donor; and Lewis acidic two-electron σ-acceptor ligands that are classified as Z-type ligands. Z-type ligands can interact with the metal center as a supported (connected via the backbone of a chelating ligand) or unsupported (simple coordination as an independent Lewis acid) ligands. Complexes with supported and unsupported metal→Z-type ligands interaction are shown in Figure 26.

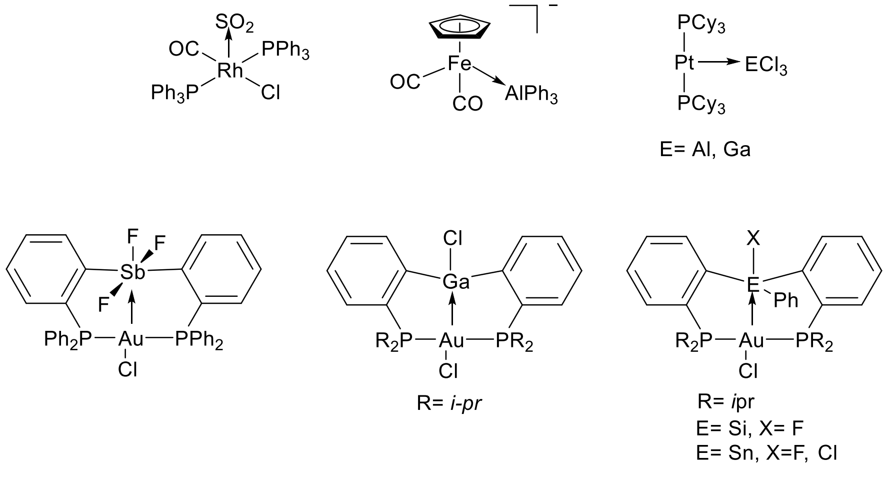

Figure 26. Examples of complexes with unsupported and supported M→Z interactions.

2.1.2.1 Nature of the M→Z interaction

Incorporating Z-type ligands in proximity of a metal can force this metal to behave as a Lewis base. The interaction between a transition metal and a Lewis acidic Z-type ligand is the reverse of the more common transition metal L-type ligand interaction, where the metal is the electron-pair donor. In an M→Z interaction, the transition metal is engaged in a covalent donor-acceptor interaction. This M→Z interaction is classified as a covalent donor-acceptor interaction described as a 2-center 2-electron interaction between an occupied metal d orbital and a vacant p orbital or low lying σ^* orbital on the Lewis acid.[74] More complicated 3-center 4-electron interactions will occur when a σ donor ligand such as Cl is in a *trans* position.[74] A simplified illustration of the possible orbital interactions is shown in Figure 27.

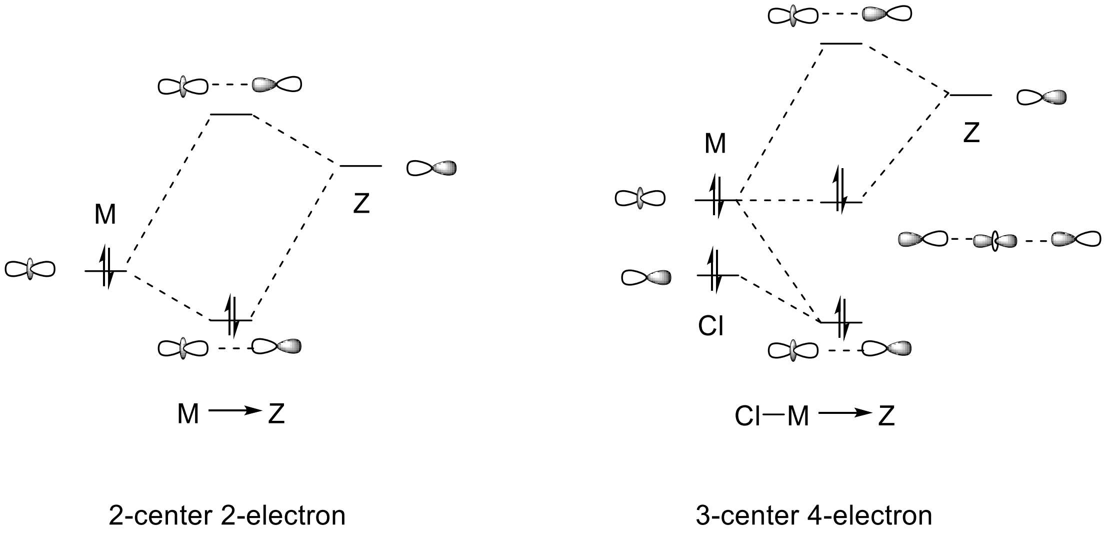

Figure 27. Simplified orbital interaction diagrams for M→Z and Cl–M→Z.

2.1.2.2 Characteristics of M→Z interactions

As the number and variety of transition metal complexes featuring Z-type ligand are increasing, more information about the nature of the M→Z interaction has been gained. In 2011 Bourissou[74] summarized the achievements around the concept of M→Z interaction, as well as the influence of the coordination of Lewis acids on the properties of metal fragments both geometrically and electronically. It was determined that the M–Z distance must be significantly shorter than the sum of the van der Waals radii of the two interacting elements. The M→Z interaction is typically parameterized by r = M–Z distance/sum of the covalent radii of M and Z. Somewhat arbitrarily, an M→Z interaction is judged to be present when $r < 1.25$.[74]

X-ray diffraction data have shown how Z-type ligands are affected by coordination to a metal (Figure 28). Group 13 Lewis acids $E^{13}R_3$ (E^{13} = B, Al, Ga, In), show a change in geometry from trigonal planar to tetrahedral when a metal is coordinating. Similarly, when SO_2 coordinates as a σ-acceptor ligand the geometry will change from bent to pyramidal, while heavier group 14 Lewis acids will change geometry from tetrahedral to trigonal bipyramidal upon coordination.[74]

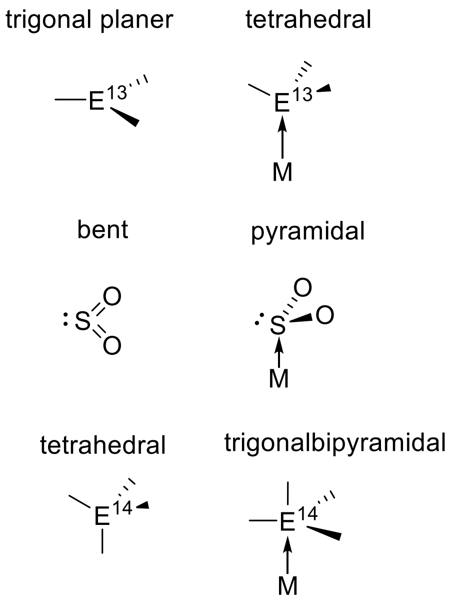

Figure 28. Schematic geometry changes upon the coordination of Lewis acids to transition metals.

In the case of NMR active σ- acceptor nuclei, such as ^{11}B, ^{29}Si, and ^{119}Sn, NMR spectroscopy data will provide useful information. In these complexes, NMR resonances are shifted upfield when their coordination number increases.[74]

Theoretical calculations, such as DFT calculation, can accurately describe M→Z interactions. Kohn–Sham molecular orbitals and also NBO analysis will provide more information about the bonding situation. Orbitals of each fragment involved and also the extent of charge transfer from the metal to the Lewis acid ligand can be estimated.

2.1.3 Quantification of Lewis acidity

Lewis acid-base interactions can be used for fine-tuning molecular designs and for imparting unique reactivities. However, quantification of the Lewis acidity is challenging due to the ambiguity of how the strength of a Lewis acid is defined. Several methods have been developed to quantify the Lewis acidity, such as the Gutmann–Beckett method, [77, 78]and the Childs method.[79]

IR band shifts[80] and Fluoride Ion Affinities (FIA) can also be used.[81-83] However, there is no universal scale.

The study of periodic trends shows that the Lewis acidity of p-block elements varies as the group is descended. The irregular trend is observed within group 13, while the stability of the water–EX_3 (EX_3 = group 13 trihalide) adducts have been computed. Results indicate that aluminum and indium are the most Lewis acidic elements, followed by gallium and then boron.[84] However, in the case of tetravalent group 14 elements, a more progressive increase in Lewis acidity is observed.[85] The magnitude of an M→Z interaction could be varied by changing the nature of the atom acting as Z-type ligand.

2.1.4 Reporter ligands

IR spectroscopy is a classical analytical technique used to study and identify diagnostic vibration frequencies for the elucidation of structural characteristics in the studied molecules. Moreover, it has been used as a tool in the study of metal basicity in which the unique vibration frequencies of the reporter moieties can be studied. Using IR spectroscopy, it would be possible to monitor the degree of charge transfer upon the binding of a σ-acceptor moiety. Carbon monoxide (CO) is one of the candidates to have been frequently used as a reporter moiety. The CO stretching frequency, ν(C≡O), is influenced by the electron density of the metal center. CO will bind to metals via σ donation. Back donation from the metal to the empty antibonding orbitals of CO will further strengthen the interaction. The magnitude of the back donation will affect the C≡O bond order and the C≡O stretching frequency. Stronger back-bonding will result in a reduction of the bond order, which will lead to a decrease in ν(C≡O). Weaker back bonding leads to a stronger C≡O bond and a higher stretching frequency, which implies that the magnitude of ν(C≡O) is a reflection of the electron density on the metal center.[86] Furthermore, acetonitrile also can act as an IR probe due to its high symmetry and the exposed frequency of the C≡N stretching mode, *ν*(C≡N). Usually, *ν*(C≡N) is shifted to higher frequencies upon binding of a Lewis acid.[87]

2.2 Research objectives

The study of M→Z bonding is drawing interest because depleting the electron density of transition metals via such an interaction could be used to tune the electrophilicity of the metal. The [Pt(PCy$_3$)$_2$] complex has received a significant amount of attention[88] because of its propensity to form M→Z interactions. The Lewis basic properties of [Pt(PCy$_3$)$_2$] as a Lewis base have been extensively studied by Braunschweig,[73, 88-105] among others. The reactivity of Pt(PCy$_3$)$_2$ as a Lewis base has been tested with various main group Lewis acids, including BeCl$_2$[100], BX$_3$[101, 103], AlX$_3$[99], GaX$_3$[102], BiCl$_3$[98], InX$_3$[89], SbF$_3$[91], and AsF$_3$.[105] The nature of the products of these reactions vary; either by forming simple adducts of type **A** or through oxidative addition leading to products of type **B**, as shown in Figure 29.

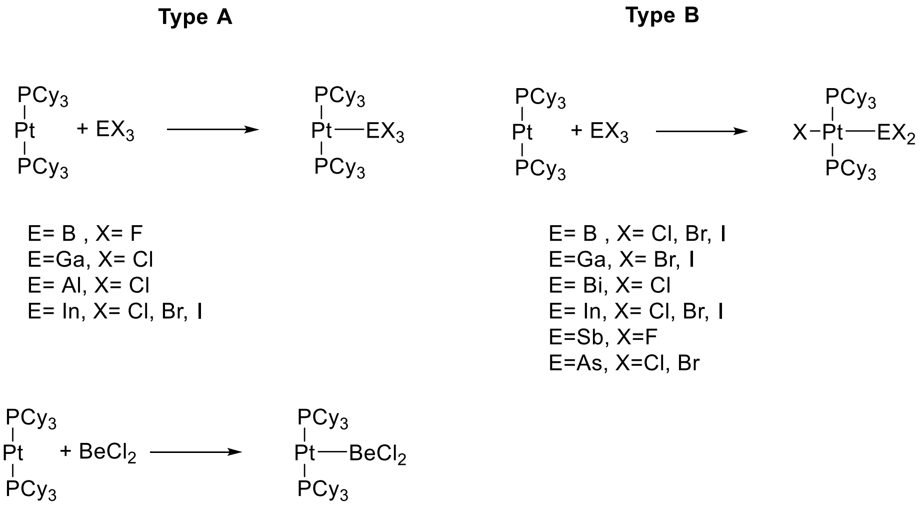

Figure 29. Transition metal Lewis base interaction with main group Lewis acids.

Inspired by the results above, it was imperative to understand and elucidate the factors that control the strength of the M→Z interactions. Therefore, the objective was to probe the Lewis acidity of group 13, 14, and 15 fluorides with $Pt(PMe_3)_2$ (referred to as [Pt]) as a Lewis base. It was further decided to use CO, CH_3CN, and CH_3NC as reporter fragments. [Pt] was used as a Lewis base and allowed to bind *in silico* to different Lewis acidic main group fluorides of general formula EF_x (E= main group elements of groups 13, 14 and 15, x= 3, 4, and 5). Main group fluorides were used to disfavor oxidative addition reactions. The [Pt]-EF_x adducts were further allowed to interact with the reporter fragments mentioned above (Figure 30 (b)).

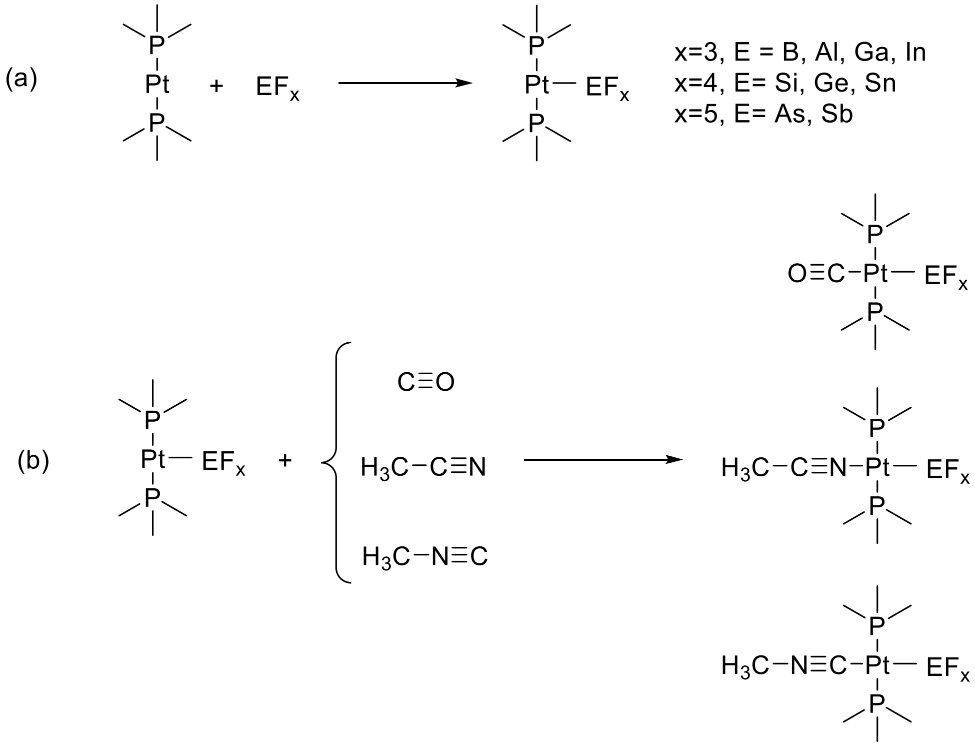

Figure 30. (a) Scheme of adduct formation between $Pt(PMe_3)_2$ and groups 13, 14, and 15 fluorides as Lewis acids. (b) Interaction of the Lewis acid-Lewis base adducts with reporter fragments.

The geometries of the [Pt]–EF$_x$ complexes were optimized using DFT methods with the BP86 functional. Frequency calculations were performed on the optimized geometries to confirm that a minimum had been reached. Interactions between the reporter moieties and the optimized structures of the [Pt]–EF$_x$ complexes were studied by calculating the stretching frequencies of the CO, CH_3CN, and CH_3NC ligands. We hoped that a comparison of the changes in stretching frequencies of the reporter fragments would provide a better understanding of the strength of the main group fluorides as Lewis acids. Furthermore, the enthalpy of the reaction between the [Pt]-EF$_x$ complexes and the reporter moieties was calculated, and the trend was compared with the pattern obtained from stretching frequencies.

2.3 Results and discussions

Density Functional Theory (DFT) structural optimizations were performed using the Gaussian 09 suite of programs[106] with effective core potentials on all heavy atoms (functional: BP86;[107, 108] mixed basis set: Al, As, B, Ga, Ge, In, Sb, Si, Sn, Pt: cc–pVTZ–PP;[109] P: 6–311g+(d,p);[110, 111] C, H, F, N, O: 6–31g[112]). Frequency calculations were also performed on the optimized geometries, showing no imaginary frequencies unless otherwise stated. All the optimizations were performed in the gas phase.

2.3.1 Group 13 Lewis acids

The structures of the adducts between [Pt] and the group 13 Lewis acids have been optimized, and the frequency calculations showed no negative frequencies. The optimized structures are shown in Figure 31, and the structural information is summarized in Table 1.

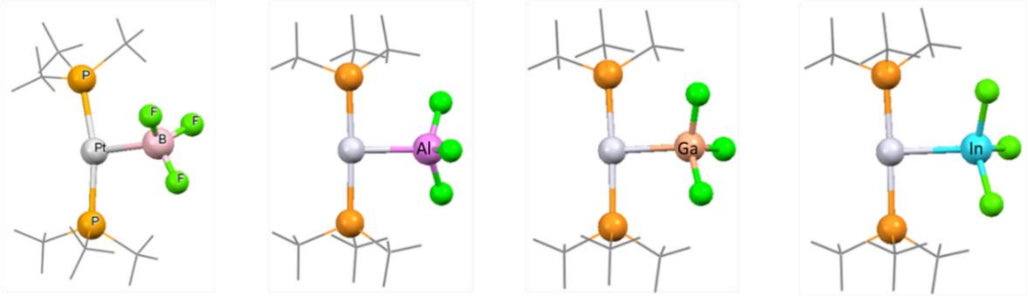

Figure 31. Optimized structures of group 13 Lewis acid - Lewis base adducts.

In this series, the Pt-E bond distance increases going down the group as expected from an increase in the covalent radius of the group 13 elements. All structures have a T-shaped geometry around the platinum center, with the P-Pt-P angles pseudo linear. The BF_3 adduct shows a more acute P-Pt-P angle of 173.56°. The average ∠Pt-E-F and ∠F-E-F angles show that the geometry around E is rearranged from planar in the free form to a tetrahedral geometry after binding. The calculated r ratio values are measured to be in the range of $0.95 < r < 1.01$, which is consistent with the presence of M→Z donor-acceptor interaction.

Table 1. Optimized structural data for group 13 Lewis acid-Lewis base adducts.

	Pt-E (Å)	∠P-Pt-P (°)	∠Pt-E-F(°)	∠F-E-F (°)	*r* ratio
[Pt]-BF_3	2.23	173.56	105.87	112.81	1.01
[Pt]-AlF_3	2.44	177.08	106.97	111.85	0.95
[Pt]-GaF_3	2.45	177.36	107.90	111.00	0.95
[Pt]-InF_3	2.62	177.65	107.17	111.68	0.94

The group 13 Lewis acid-base adducts were allowed to interact in silico with CO, CH_3CN, and CH_3NC to probe the electron density on the platinum center. The changes in the C≡O, C≡N, and N≡C frequencies in these complexes probe the extent of electron depletion at the metal center. As a result, it will be possible to estimate the strength of the Lewis acid-transition metal Lewis base adduct. Figure 32, Figure 34, and Figure 35 illustrate the optimized structures of the group 13 Lewis acid-base adducts after complexation with CO, CH_3CN, and CH_3NC.

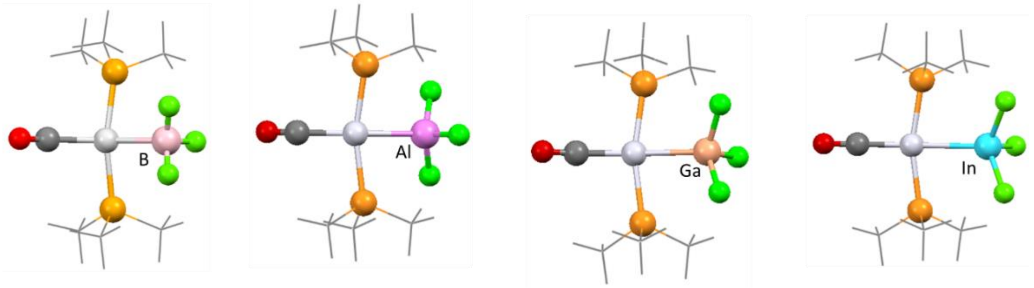

Figure 32. Optimized structure of CO-[Pt]-EF_3 complexes.

Table 2. Optimized structural data for CO-[Pt]-EF_3 complexes.

	ν (C≡O) (cm^{-1})	C≡O (Å)	Pt-CO (Å)	∠P-Pt-P (°)	Pt-E (Å)	ΔH (Kcal/mol)
CO-[Pt]-BF_3	1797.28	1.198	1.98	165.28	2.28	-22.47
CO-[Pt]-AlF_3	1832.99	1.194	1.96	164.16	2.55	-24.78
CO-[Pt]-GaF_3	1865.43	1.190	1.93	165.00	2.54	-29.04
CO-[Pt]-InF_3	1891.50	1.187	1.91	164.01	2.72	-31.65

Structural results for CO-[Pt]EF$_3$ complexes are summarized in Table 2, showing that the ν(C≡O) increases going down the group. The C≡O bond distance, along with the Pt-CO bond distance, are both decreasing going down the group. This bond shortening indicates that σ-donation is increasing while π back-donation is decreasing. This interpretation is supported by the increase noted in ν(C≡O). Furthermore, the ΔH of the reaction of [Pt]EF$_3$ with CO in silico was calculated, and it was observed that going down the group, the compound becomes more stable, agreeing with the changes in ν(C≡O).

Like CO, acetonitrile has been used as an IR probe in many studies,[113-116] but unlike CO, acetonitrile is not prone to accept back-bonding. Its molecular orbital shows that the π^* orbital for CH$_3$CN is less exposed. Figure 33 illustrates the LUMO frontier orbitals of CO, CH$_3$CN, and CH$_3$NC.

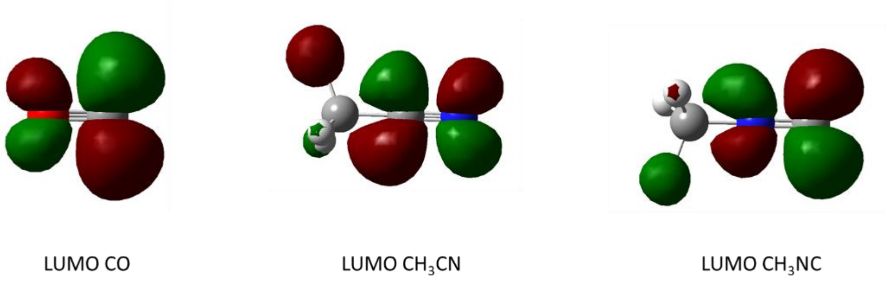

Figure 33. CO, CH$_3$CN, and CH$_3$NC frontier LUMO orbitals.

It is noteworthy that acetonitrile been used as a donor ligand in several experimental and theoretical studies on Lewis acid-base interactions.[115-117] The change of ν(C≡N) after binding compared to the free form was attributed to the strength of the Lewis acid. As Lewis acidity increases, the Δ ν(C≡N) becomes more significant.

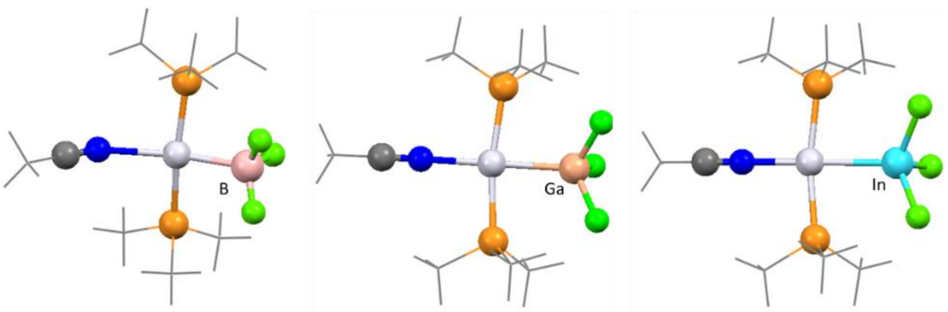

Figure 34. Optimized structure of CH_3CN-[Pt]-EF_3.

The structures of complexes of general formula CH_3CN-[Pt]-EF_3 have been optimized. However, CH_3CN-[Pt]-AlF_3 did not meet the convergence criteria. Frequency calculation for other complexes showed no negative frequency. The resulting optimized structures are illustrated in Figure 34, and the structural data are compiled in Table 3. The data show that going down the group, the *ν*(C≡N) increases. The C≡N bond distance did not change, which could be related to its intrinsic tendency to be less involved in back bonding. However, Pt-CN bond distance shortens, indicating stronger σ-donation. The same is seen for the CO adducts, and the ΔH of the reaction of [Pt]-EF_3 with CH_3CN becomes more negative, descending the group.

Table 3. Optimized structural data for CH_3CN-[Pt]-EF_3 complexes.

	ν(C≡N) (cm^{-1})	C≡N (Å)	Pt-CN (Å)	∠P-Pt-P (°)	Pt-E (Å)	ΔH (Kcal/mol)
CH_3CN-[Pt]-BF_3	2190.12	1.187	2.23	169.85	2.19	-1.27
CH_3CN-[Pt]-GaF_3	2214.68	1.183	2.14	169.39	2.47	-9.12
CH_3CN-[Pt]-InF_3	2215.09	1.183	2.10	167.91	2.65	-12.04

The [Pt]-EF_3 adducts of group 13 were reacted with methylisonitrile as a comparison to CO and CH_3CN. The results for the methylisonitrile complexes show similar trends in the values of *ν*(N≡C), the Pt-NC bond distance, the Pt-E bond distance, and ΔH. Overall, the observed trends have been consistent for the CO and CH_3CN containing complexes. The optimized structures are shown in Figure 35, and the structural information is summarized in Table 4

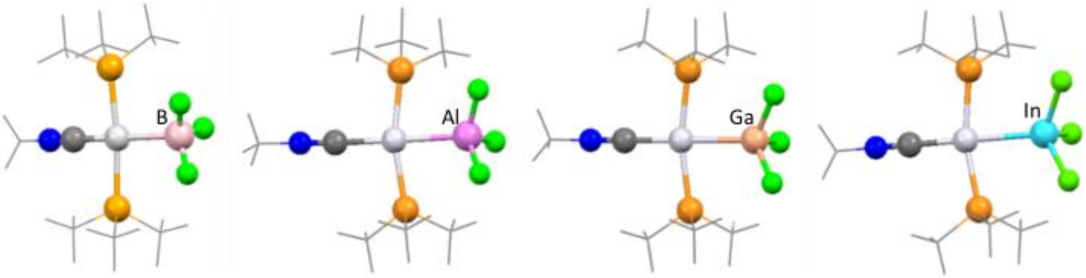

Figure 35. Optimized structure of CH_3NC-[Pt]-EF_3.

Table 4. Optimized structural data for CH_3NC-[Pt]-EF_3 complexes.

	ν (N≡C) (cm^{-1})	N≡C (Å)	Pt-NC (Å)	∠P-Pt-P (°)	Pt-E (Å)	ΔH (Kcal/mol)
CH_3NC-[Pt]-BF_3	2071.64	1.205	2.03	164.23	2.26	-16.95
CH_3NC-[Pt]-AlF_3	2107.15	1.200	2.01	164.63	2.56	-21.56
CH_3NC-[Pt]-GaF_3	2129.67	1.197	1.98	165.48	2.53	-28.22
CH_3NC-[Pt]-InF_3	2136.38	1.197	1.96	164.27	2.69	-31.91

Results from the interaction of reporter moieties with the Lewis acid-base adducts of group 13 obtained in the current study lead to the conclusion that the Lewis acidity increases in the following order: BF_3 < AlF_3 < GaF_3 < InF_3. Results from three reporter fragments show that the stretching frequency increases going down the group. However, the trend obtained here differs from the usually reported trend[117-121] for the Lewis acidity of group 13 elements.

Timoshkin performed extensive studies[117-120] on group 13 trihalides as a Lewis acid to derive a trend of Lewis acidity. In one study, complexes of group 13 metal halides with pyridine type ligands (pyridine, pyrazine, and 4,4´bipyridine) have been investigated. The 1:1 molecular complex appears to have the strongest donor-acceptor bond. The acceptor ability of Lewis acids in the subjected complexes decreases in the series $AlCl_3$ > $AlBr_3$ > $GaCl_3$ > $GaBr_3$ > GaI_3.[122] In a separate investigation, an extensive theoretical study was performed on structurally characterized MX_3 complexes (M = Al, Ga; X = Cl, Br, I) as Lewis acids and nitrogen-, phosphorus-, arsenic-, and oxygen-containing donor ligands as Lewis base, to obtain the Lewis acidity trends for aluminum and gallium halides. The pattern of Al > Ga, Cl≈Br > I was observed for Lewis acidity.[119] In another report, the theoretical dissociation energies of the donor-acceptor complexes of type MX_3-D (M: Al, Ga, In; X: F, Cl, Br, I; D: YH_3, PX_3, X^-; Y: N, P, As) were used as a comparison mean. The trend of Al > Ga <In, F > Cl > Br > I was observed for all investigated complexes.[118] Nitriles and isonitriles complexes of group 13 derivatives also showed a tendency of donor-acceptor interaction. The acceptor ability of MX_3 (M: Al, Ga, In; X: Cl, H, CH_3) varied in the following order Al > Ga ≤ In, Cl > H > CH_3.[117] In all these studies the trend seen for Lewis acidity of group 13 halides follows the order B < Al > Ga < In. The anomaly observed in the pattern might arise from the d-block contraction seen for the period four elements, which is the result of the poor shielding of the nuclear charge by d-orbitals' electrons. This poor shielding leads to the smaller radius for Ga^{3+} than expected, resulting in gallium being more electronegative than Aluminum. It will justify the irregularity seen in the Lewis acidity of group 13 elements.

Nevertheless, complexes based on ‘double-decker’ ligands reported by Lu[123, 124] which a group 13 element (E) (E = Al, Ga, In) is accommodated in the lower deck and a transition metal ion (M) (M = Ni, Co) coordinated at the upper deck provide a platform with the M→E interaction with an increase in Lewis acidity in the order Al < Ga < In, the same order observed in the current study.

Results from the current study that uses a transition metal as a base show the following order B < Al< Ga < In for the Lewis acidity of group 13 fluorides. The observed trend is different from B < Ga< Al < In with the irregularity in increasing Lewis acidity descending the group. However, the observed trend is in agreement with those reported by Lu[123, 124] showing the order of B < Al < Ga < In. Overall, for group 13 elements, the absolute and the relative Lewis acidity depends on the nature of the Lewis base, which is chosen as a bonding partner for the donor-acceptor complex.

2.3.2 Group 14 Lewis acids

Heavier Group 14 elements known to readily form hypervalent compounds through donor-acceptor interactions with organic Lewis bases,[74, 125] leading to an increase in their coordination number from four to five or six. SiF_4, GeF_4, and SnF_4 already exhibit Lewis acidity toward F^- to produce SiF_6^{2-}, GeF_6^{2-}, and SnF_6^{2-}, respectively. This concept can be extended to the interaction of saturated group 14 compounds as σ acceptor ligands with electron rich transition metals as bases.[74]

Heavier group 14 fluorides have been explored as Lewis acids in this study, and their Lewis acidity was probed indirectly using reporter fragments. The structure of the adducts formed between the platinum complex as a metallobase and the Lewis acids of interest were optimized, and frequency calculation confirms all are local minima. The optimized structures are shown in Figure 36, and structural data are summarized in Table 5.

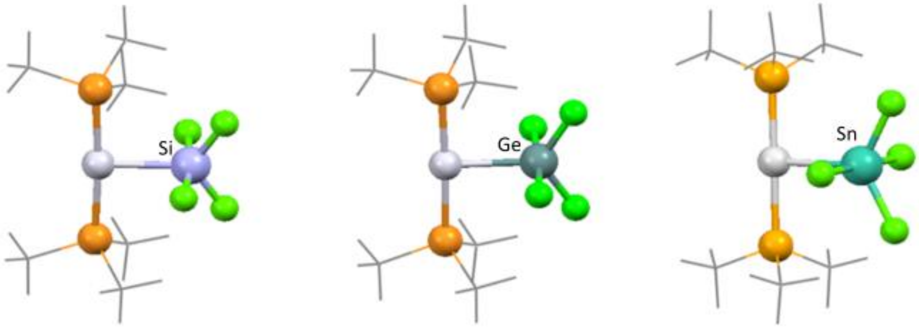

Figure 36. Optimized structures of group 14 Lewis acid-Lewis base adduct.

Optimized structures show the Pt-E (E = Si, Ge, and Sn) bond distance increases going down the group, which agrees with the increase in the covalent radius going down the group. The geometry around the platinum center is T-shaped, with the ∠P-Pt-P angle being close to linear. The averaged ∠Pt-E-F_{eq} and ∠Pt-E-F_{ax} bond angles are close to 120° and 90°, as well as, ∠F_{eq}-E-F_{eq} and ∠F_{ax}-E-F_{eq} bond angles, which leads to a trigonal bipyramidal geometry around E with the platinum center located in an equatorial position. The calculated r ratio values are measured to be in the range of $0.94 < r < 0.97$, which indicates the presence of a donor-acceptor M→Z interaction.

Table 5. Optimized structural data for [Pt]-EF_4 complexes

	Pt-E (Å)	∠P-Pt-P (°)	∠Pt-E-F (°)	∠F-E-F (°)	*r* ratio
[Pt]-SiF_4	2.39	175.87	122.10 85.45	115.82(eq-eq) 92.53(ax-eq)	0.97
[Pt]-GeF_4	2.42	177.27	121.16 87.71	117.68(eq-eq) 91.19(ax-eq)	0.95
[Pt]-SnF_4	2.58	177.28	117.72 89.16	124.58(eq-eq) 90.40(ax-eq)	0.94

The platinum group 14 Lewis acid adducts were reacted with probe fragments. Optimized structures and frequency calculations show that they are all at their local minima except for CO-[Pt]-SiF_4, which showed a negative frequency at -35.99. The optimized structures are shown in Figure 37, Figure 38, and Figure 39. The structural information also is summarized in Table 6, Table 7, and Table 8.

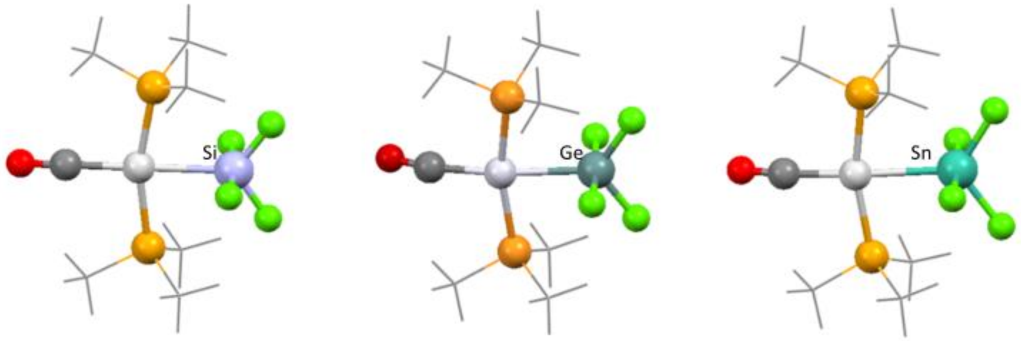

Figure 37. Optimized structure of CO-[Pt]-EF_4 complexes.

The results show that ν(C≡O) increases for Ge containing complex compare to the Sn containing complex. Furthermore, the ΔH of the reaction of [Pt]-EF_4 with CO was calculated, and it was observed that going down the group, the compound becomes more stable, agreeing with the changes in ν(C≡O).

Table 6. Optimized structural data for CO-[Pt]-EF_4 complexes.

	ν (C≡O) (cm^{-1})	C≡O (Å)	Pt-CO (Å)	∠P-Pt-P (°)	Pt-E (Å)	ΔH (Kcal/mol)
CO-[Pt]-GeF_4	1885.53	1.189	1.91	165.65	2.51	-32.66
CO-[Pt]-SnF_4	1899.16	1.187	1.90	164.55	2.69	-34.21

The structures of complexes of general formula CH_3CN-[Pt]-EF_4 have been optimized, and frequency calculation showed no negative frequency. The optimized structures are illustrated in Figure 38, and the structural data are compiled in Table 7.

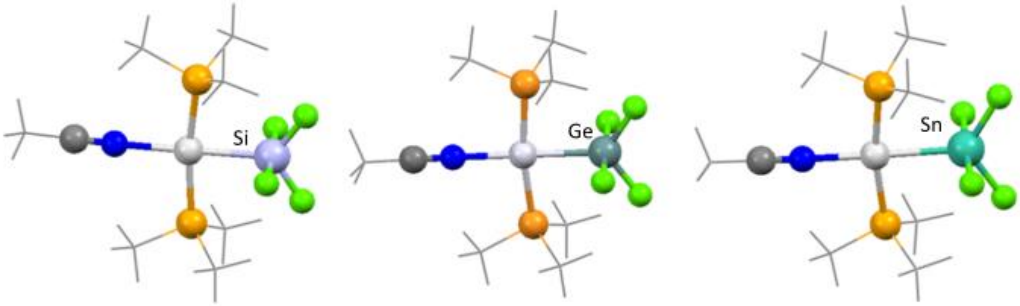

Figure 38. Optimized structure of CH_3CN-[Pt]-EF_4 complexes.

The same trend was observed for the CH_3CN adducts as with CO; ν(C≡N) increasing going down the group. The enthalpy of reaction of the adduct with CH_3CN becomes a more negative value.

Table 7. Optimized structural data for CH_3CN-[Pt]-EF_4 complexes

	ν (C≡N) (cm^{-1})	C≡N (Å)	Pt-CN (Å)	∠P-Pt-P (°)	Pt-E (Å)	ΔH (Kcal/mol)
CH_3CN-[Pt]-SiF_4	2213.11	1.183	2.15	171.12	2.41	-7.75
CH_3CN-[Pt]-GeF_4	2220.31	1.182	2.09	170.81	2.45	-13.24
CH_3CN-[Pt]-SnF_4	2222.03	1.182	2.09	169.54	2.62	-14.82

Transition metal base-Lewis acid adducts of group 14 were also reacted with methylisonitrile. Results for the methylisonitrile complexes show similar trends for *ν*(N≡C), the Pt-NC bond distance, the Pt-E bond distance, and the ΔH values. Overall, the observed trends are consistent for the CO and CH_3CN containing complexes. The optimized structures are shown in Figure 39, and the structural information is summarized in Table 8.

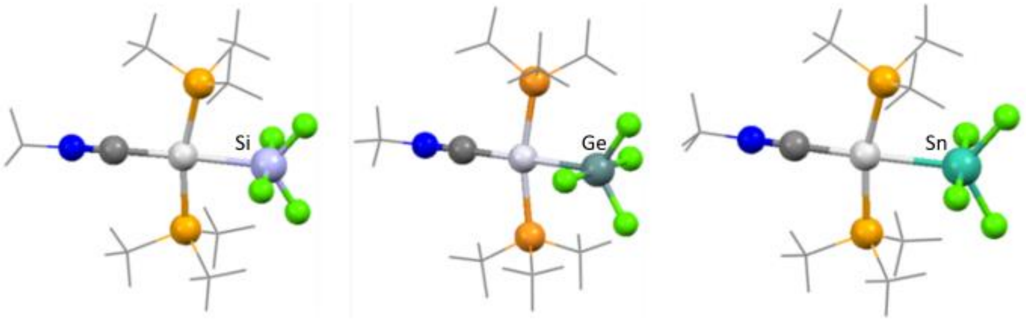

Figure 39. Optimized structure of CH_3NC-[Pt]-EF_4 complexes.

Table 8. Optimized structural data for CH_3NC-[Pt]-EF_4 complexes.

	ν(N≡C) (cm^{-1})	N≡C (Å)	Pt-NC (Å)	∠P-Pt-P (°)	Pt-E (Å)	ΔH (Kcal/mol)
CH_3NC-[Pt]-SiF_4	2124.33	1.198	1.99	166.45	2.47	-25.32
CH_3NC-[Pt]-GeF_4	2139.66	1.197	1.97	166.26	2.50	-32.16
CH_3NC-[Pt]-SnF_4	2144.54	1.196	1.96	165.7	2.67	-35.06

Lewis acidity trend for Group 14 Lewis acids obtained from the above results follows the trend $SiF_4 < GeF_4 < SnF_4$. This trend is in agreement with the literature data.[85, 120] Theoretical study by Timoshkin[120] on the donor-acceptor complexes of silicon, germanium and tin tetrahalides with nitrogen-containing donors, $MX_4 \cdot nL$ (M=Si, Ge, and Sn; X =F, Cl, Br; L=NH_3, Py, 2,2′bipy, 1,10-phen) in the gas phase, show that the stability of complexes decreases in the order of Sn > Ge > Si; F > Cl > Br. The same report concluded, the promising candidates for stable gas-phase complexes of group 14 halides are complexes of tin tetrahalides with rigid bidentate donor ligands, such as 1,10-phenanthroline.[120] Group 14 tetrahalides, although being quite strong Lewis acids, their apparent acidity is ‘shadowed’ by the reorganization effects of the complex formation.[120]

2.3.3 Group 15 Lewis acids

SbF_5 has been known as a strong Lewis acid among group 15 halides for a long time, as reflected by its high fluoride ion affinity.[87] Upon accepting F^-, the geometry around Sb will change from trigonal bipyramidal to octahedral in SbF_6^-.

The structure of group 15 Lewis acid adducts with [Pt] as a metallobase have been optimized, and the frequency calculations showed no negative frequency. Optimized structures of the adducts are shown in Figure 40., and the structural data are summarized in Table 9.

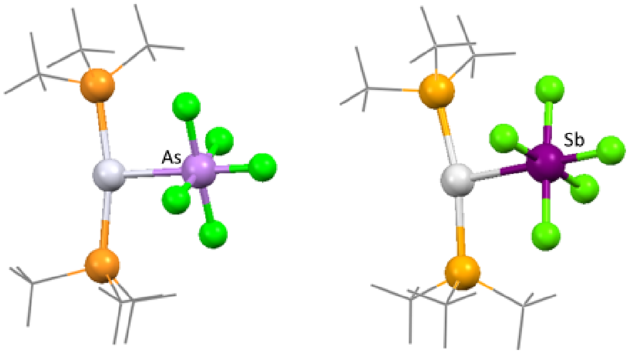

Figure 40. Optimized structures of group 15 Lewis acid-Lewis base adduct.

For these two compounds, the Pt-E bond distance is longer for E = Sb as expected from the larger covalent radius of Sb. The two structures have distorted T-shaped geometry around the platinum center, with the ∠P-Pt-P being more acute compared to groups 13 and 14 Lewis acids. The average ∠Pt-E-F and ∠F-E-F bond angles are close to 90°, confirming an octahedral geometry around the main group element. The calculated *r* ratio values are determined to be 0.96 and 0.94, which indicates the presence of an M→Z interaction.

Table 9. Optimized structural data for [Pt]-EF_5 complexes

	Pt-E (Å)	∠P-Pt-P (°)	∠Pt-E-F (°)	∠F-E-F (°)	*r* ratio
[Pt]-AsF_5	2.46	166.88	90.67	90.01	0.96
[Pt]-SbF_5	2.60	168.18	88.40	90.05	0.94

These group 15 Lewis acid-Lewis base adducts were reacted with CO, CH_3CN, and CH_3NC as a reporter fragment. The optimized structures and frequency calculations showed they are local minima due to the absence of negative frequencies. The optimized structures are shown in Figure 41, Figure 42, and Figure 43. The structural data are summarized in Table 10, Table 11, and Table 12.

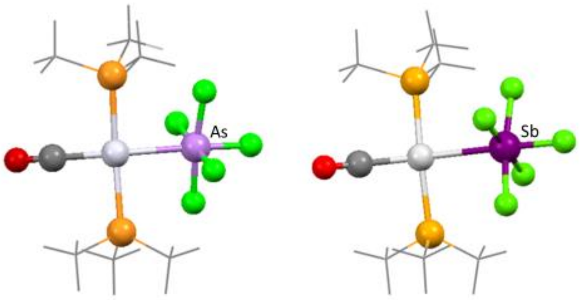

Figure 41. Optimized structure of CO-[Pt]-EF_5 complexes.

For this series, it was observed that ν(C≡O), ν(C≡N), and ν(N≡C) are stronger for the related Sb containing complexes compare to the As analog. Furthermore, the enthalpy of the reaction of the reporter fragment with the adduct moiety is more negative for the Sb-containing complexes. The change in the ν(C≡O) in the corresponding complexes are more drastic compared to the change in ν(C≡N), and ν(N≡C). This difference could be due to the stronger back-bonding on CO ligand compared to the nitriles and isonitriles.

Table 10. Optimized structural data for CO-[Pt]-EF_5 complexes.

	ν(C≡O) (cm^{-1})	C≡O (Å)	Pt-CO (Å)	∠P-Pt-P (°)	Pt-E (Å)	ΔH (Kcal/mol)
CO-[Pt]-AsF_5	1873.78	1.190	1.92	171.38	2.55	-30.07
CO-[Pt]-SbF_5	1885.82	1.188	1.91	172.14	2.71	-30.64

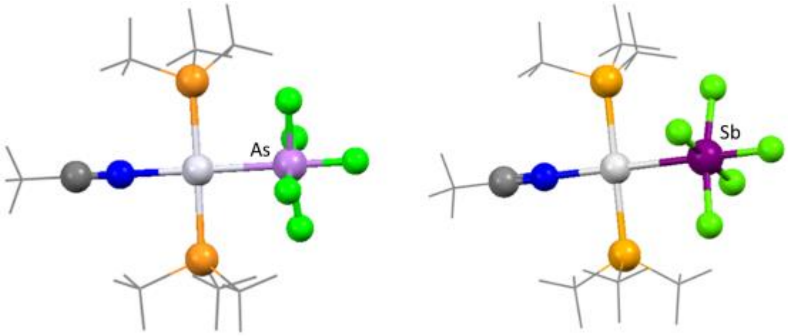

Figure 42. Optimized structural data for CH_3CN-[Pt]-EF_5 complexes.

Table 11. Optimized structural data for CH_3CN-[Pt]-EF_5 complexes.

	ν(C≡N) (cm^{-1})	C≡N (Å)	Pt-CN (Å)	∠P-Pt-P (°)	Pt-E (Å)	ΔH (Kcal/mol)
CH_3CN-[Pt]-AsF_5	2226.25	1.182	2.08	178.65	2.45	-11.33
CH_3CN-[Pt]-SbF_5	2228.78	1.181	2.08	179.60	2.64	-12.09

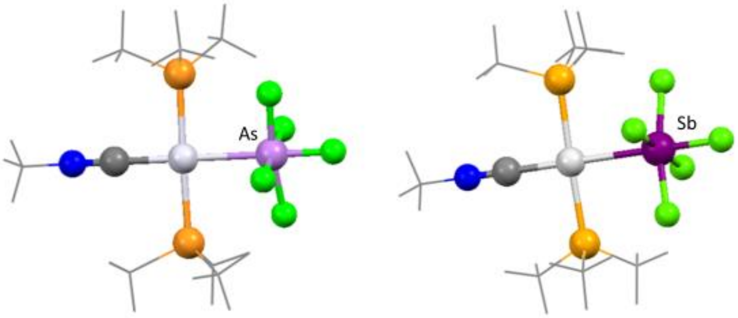

Figure 43. Optimized structural data for CH_3NC-[Pt]-EF_5 complexes.

Table 12. Optimized structural data for CH_3NC-[Pt]-EF_5 complexes.

	ν (N≡C) (cm^{-1})	N≡C (Å)	Pt-NC (Å)	∠P-Pt-P (°)	Pt-E (Å)	ΔH (Kcal/mol)
CH_3NC-[Pt]-AsF_5	2151.31	1.195	1.96	177.86	2.54	-30.15
CH_3NC-[Pt]-SbF_5	2153.56	1.194	1.96	179.46	2.70	-31.87

The trend of Lewis acidity obtained for this series shows that SbF_5 is more acidic than AsF_5, which agrees with literature data using GEI (Global Electrophilicity Index)[126] or FIA (Fluoride ion affinity)[81-83] methods among other reports supporting the order $SbF_5 > AsF_5 > PF_5$ for the Lewis acidity of group 15 pentafluorides.

2.4 Conclusion

Efforts in this chapter were aimed at assessing the strength of main group fluorides as Z-type ligands toward platinum(0) using reporter fragments positioned trans from the Z-ligand. The fragments used included CO, CH_3CN, and CH_3NC. The computed energies of ν(C≡O), ν(C≡N), and ν(N≡C) and the enthalpy associated with the coordination of the reporter ligand have been correlated to the Lewis acidity of main group fluorides as Lewis acids. As mentioned above, the stretching frequencies of the reporter ligand reflect the electron density on the metal center. Stronger Z-type ligands will make the Pt center more electron-poor, leading to stronger coordination of the reporter ligand and an increase in the corresponding stretching frequencies. The trend of Lewis acidity for each reporter fragment, as well as the ΔH trend, is summarized as below.

Table 13. The corresponding stretching frequencies and the ΔH trend. for CO as the reporter ligand.

EF_X	**BF_3**	**AlF_3**	**GaF_3**	**InF_3**	**GeF_4**	**SnF_4**	**AsF_5**	**SbF_5**
***v*(C≡O) (cm^{-1})**	1797.28	1832.99	1865.43	1891.50	1885.53	1899.16	1873.78	1885.82
ΔH (Kcal/mol)	-22.475	-24.783	-29.043	-31.645	-32.661	-34.205	-30.068	-30.643

Table 14. The corresponding stretching frequencies and the ΔH trend. For CH_3CN as the reporter ligand.

EF_X	**BF_3**	**GaF_3**	**InF_3**	**SiF_4**	**GeF_4**	**SnF_4**	**AsF_5**	**SbF_5**
***v*(C≡N) (cm^{-1})**	2190.12	2214.68	2215.09	2213.11	2220.31	2222.03	2226.25	2228.78
ΔH (Kcal/mol)	-1.268	-9.117	-12.042	-7.7484	-13.235	-14.82	-11.332	-12.091

Table 15. The corresponding stretching frequencies and the ΔH trend. For CH_3NC as the reporter ligand.

EF_X	**BF_3**	**AlF_3**	**GaF_3**	**InF_3**	**SiF_4**	**GeF_4**	**SnF_4**	**AsF_5**	**SbF_5**
***v*(C≡N) (cm^{-1})**	2071.64	2107.15	2129.67	2136.38	2124.33	2139.66	2144.54	2151.31	2153.56
ΔH (Kcal/mol)	-16.949	-21.557	-28.217	-31.913	-25.315	-32.155	-35.059	-30.149	-31.873

The data obtained in this study reveal that going down the group, the Lewis acidity increases. In(III), Ge(IV), Sn(IV), As(V), and Sb(V) fluorides appear to be the most Lewis acidic. The higher Lewis acidity of these main group fluorides is also reflected by the more negative enthalpy associated to the coordination of the ligand when these main group fluoride act as the Z-type ligand.

CHAPTER III

PHOTOSTIMULATED CL$_2$ REDUCTIVE ELIMINATION FROM A GE-PT COMPLEX

3.1 Introduction

Late transition metal complexes that support the photoreductive elimination of an X$_2$ equivalent (X = halogen) have attracted a great deal of recent interest due to their relevance to solar energy storage approaches based on light-driven HX splitting reactions.[4, 9, 127-132] Realizing that this area of research might be limited by a restricted set of elements that support these photoreduction reactions,[12, 16-18, 133-138] several groups including ours have started to survey derivatives that contain main group elements amenable to two-electron redox chemistry. The best-studied systems are tellurophenedihalides of type PT-R (PT = diphenyltellurophene, compound **16** in Figure 44) with electron-withdrawing substituents which were shown by Seferos to undergo clean photolysis into the parent tellurophenes.[139] More recently, antimony has also merged as a suitable element for this type of transformation. Our group reported that complex **21**[140] undergoes a clean photoreductive chlorine elimination reaction which produces [$Cl_2Sb^{IV}Pd^{I}Cl(o\text{-dppp})_2$], thus suggesting that antimony can support the photoreductive elimination of chlorine.[140] Nocera[24] confirmed this possibility by describing antimony(V) corrole dihalide, complexes **17** and **18**, which can also be reduced into the corresponding antimony(III) corrole by irradiation.

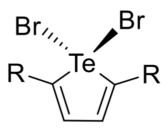

16

R= C_6F_5
Φ = 42.4%

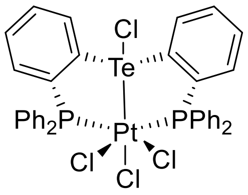

19

Φ = 4.4%

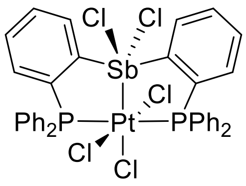

20

Φ = 13.8%

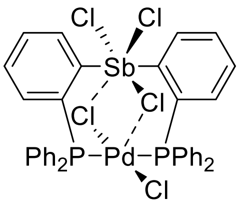

21

Φ = 0.55%

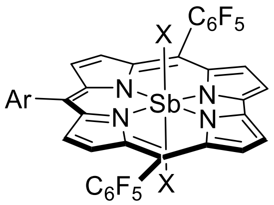

Ar= methyl benzoat

X= Cl, **17**
X= Br, **18**

Φ_{Cl} = 1.6%
Φ_{Br} = 0.32%

Figure 44. Reported molecular platforms for chlorine photoreductive elimination involving main group elements.

3.2 Research objectives

With the view of broadening the type of elements that support this photoreductive chemistry, we have now made the hypothesis that group 14 elements with accessible II/IV oxidation states may also be prone to photoreduction via halogen evolution. In this work, we disclose our efforts to incorporate germanium in redox-active late transition metal complexes.

3.3 Results and discussion

As an entry point, we decided to coordinate the known (o-(Ph_2P)C_6H_4)$_2$$GeCl_2$ ligand, compound **52** to divalent platinum. Reaction of this ligand with (Me_2S)$_2$$PtCl_2$ in CH_2Cl_2 afforded [$Cl_2GePtCl_2$(o-dppp)$_2$] (complex **53**, o-dppp = o-(Ph_2P)C_6H_4) as an air-stable complex (Figure 45).

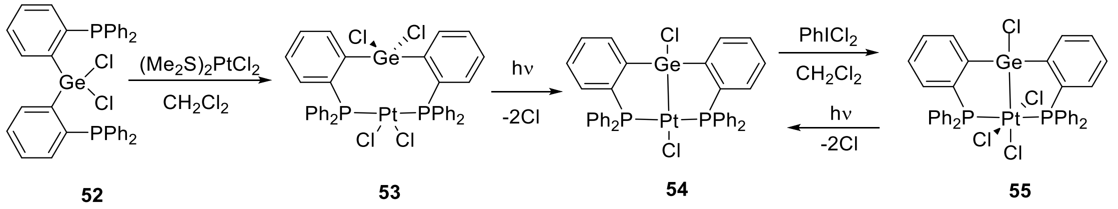

Figure 45. Synthesis pathway for complexes **53-55**

This new complex has been characterized by NMR spectroscopy and X-ray diffraction. Complex **53** displays a broad ^{31}P NMR resonance at $\delta = 21.7$ ppm flanked by platinum satellites (J_{Pt-P}=3522 Hz). Comparison of this coupling constant with that of *cis*-[(Ph_3P)$_2$$PtCl_2$] ($J_{Pt-P}$=3673 Hz) and *trans*-[($Ph_3P$)$_2$$PtCl_2$] ($J_{Pt-P}$ = 2630 Hz)[141] suggested the *cis*-coordination of the two phosphino arms of the ligand to the platinum center of complex **53**. A single crystal diffraction study further confirmed this conclusion (Figure 46). A salient feature of this structure is the ∠Pt-Ge-Cl1 angle which approaches linearity. Hence, despite the long Ge-Pt distance of 3.3135 (8) Å, the platinum atom appears positioned to engage the germanium center by donation of a dz^2 lone pair into the σ* orbital of the Ge−Cl1 bond. In agreement with this view, we note that the Ge−Cl1 bond (2.1890(19) Å) is distinctly longer than the Ge−Cl2 (2.1492(18) Å). The σ-accepting properties of halogermanes have been previously documented in the case of coinage metal complex in which a fluorogermane moiety acts as the acceptor.[142-145]

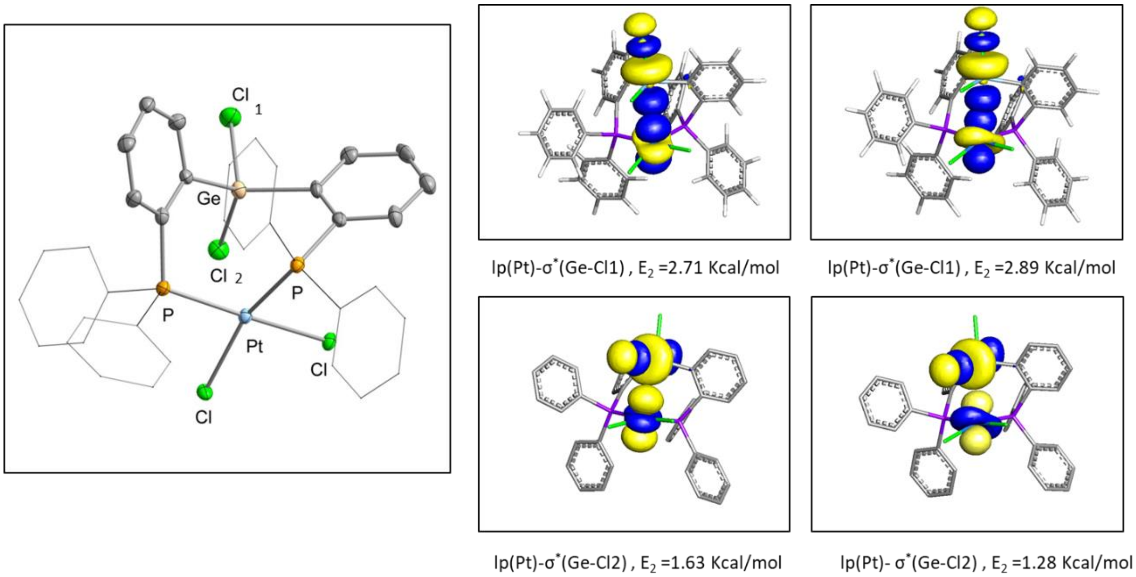

lp(Pt)-σ*(Ge-Cl1) , E₂ =2.71 Kcal/mol lp(Pt)-σ*(Ge-Cl1) , E₂ =2.89 Kcal/mol

lp(Pt)-σ*(Ge-Cl2) , E₂ =1.63 Kcal/mol lp(Pt)- σ*(Ge-Cl2) , E₂ =1.28 Kcal/mol

Figure 46. Left: X-ray crystallographic geometry of complex **53**. Thermal ellipsoids are drawn at the 50% probability level. Phenyl groups are drawn in wireframe. Hydrogen atoms are omitted for clarity. Right: NBO plot of lp(Pt)-σ^*(Ge-Cl1) , E^2 =2.71 Kcal/mol and 2.89 Kcal/mol (top) and lp(Pt)-σ^*(Ge-Cl2), E^2 =1.63 Kcal/mol and 1.28 Kcal/mol (bottom).

Although this complex is thermally stable, we observed that it is light sensitive. Indeed, irradiation of this complex with UV light results in the slow disappearance of the ^{31}P NMR resonance of complex **53** and the emergence of a new product complex **54** characterized by resonance at δ = 58 ppm ($J_{\text{Pt-P}}$= 2885 Hz). When carried out in CH_2Cl_2, this reaction was accompanied by the formation of unidentified species. The addition of 2,3-dimethyl-1,3-butadiene (DMBD) or SMe_2 as a halogen trap led to a cleaner transformation and the preponderant formation of complex **54**. We also noted the intermediate appearance of complex **55** detected at δ = 37 ppm in the ^{31}P NMR spectrum. The intensity of this intermediate resonance remained low throughout the photolysis to ultimately vanish when the starting material, complex **53**, was entirely consumed.

Speculating that complex **54** was the result of light-induced elimination of a Cl_2 equivalent, we decided to attempt its synthesis using an independent route. To this end, the ligand (*o*-$(Ph_2P)C_6H_4)_2GeCl_2$, compound **52**, was allowed to react in THF with *trans*-$[(Ph_3P)_2Pt(C_2H_4)]$. This reaction proceeded quickly to afford compound **54**, as indicated by ^{31}P NMR spectroscopy.

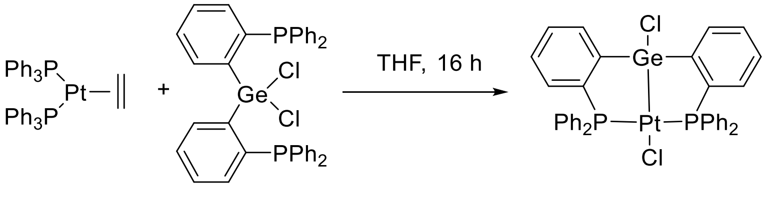

52 **54**

Figure 47. Independent synthetic path for complex **54**.

A single-crystal X-ray diffraction analysis (*vide infra*) confirmed the structure of complex **54** as a divalent platinum-chlorogermyl complex, thus demonstrating that complex **53** is indeed a viable platform for the light-induced chlorine evolution. It is also worth pointing out that the generation of complex **54** is a rare example of light assisted reductive bond formation between the main group element and a transition metal atom. The Ge-Pt bond distance of 2.3338(4) Å in complex **54** is comparable to that found in [GePtCl(*o*-dppp)$_3$] (2.3545(2)Å), a complex recently described by Braun.[60] At the difference of this complex where the platinum is in a trigonal bipyramidal geometry, the transition metal center in complex **54** adopts a square planar geometry as expected for a metal with a d^8 electronic configuration. The Pt-Cl (2.3882(9) Å) and Ge-Cl (2.2107(10) Å) are also notably longer than the corresponding linkages in complex **53** (av. Pt-Cl = 2.37; av. Ge-Cl = 2.17), in agreement with the more reduced nature of the dinuclear core of complex **54**.

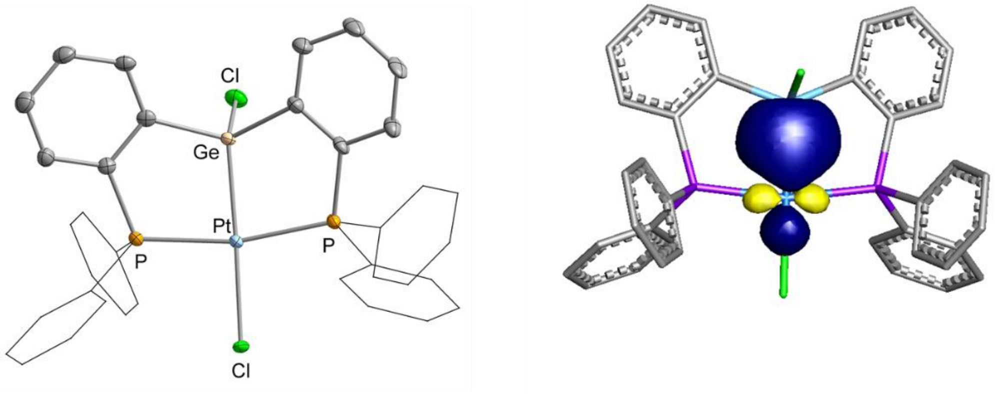

Figure 48. Solid state structure of **54**. Thermal ellipsoids are drawn at the 50% probability level. Phenyl groups are drawn in wireframe. Hydrogen atoms are omitted for clarity. Selected bonds and angles: Ge−Pt: 2.3338(4) Å, Ge−Cl: 2.2107(10) Å, Pt−Cl: 2.3882(9) Å; ∠Ge−Pt−Cl, 177.524(27)°; ∠Cl−Ge−Pt, 118.445(30).

Given that recyclability is an essential requirement of light-driven catalytic schemes, we became eager to test whether complex **54** could be re-oxidized into complex **53**. We first attempted to carry out this oxidation using HCl. When carried out in THF under an inert atmosphere, no sign of oxidation was detected, which led us to consider the use of $PhICl_2$. The addition of this reagent to a solution of complex **54** in CH_2Cl_2 did not afford the expected complex **53**. Instead, the reaction was accompanied by the appearance of a signal at 37.4 ppm, a chemical shift corresponding to the intermediate complex **55** observed during the photolysis of complex **53**. Complex **55** could be readily isolated from this reaction as an air-stable solid. Single crystal X-ray diffraction shows that complex **55** is a structural isomer of complex **53**, with the platinum atom in a tetravalent state and σ-bonded to the chlorogermyl ligand. In agreement with the more oxidized nature of the complex, the Ge-Cl (2.169(5) Å) in complex **55** is distinctly shorter than in complex **53** (2.2107(10) Å). The σ-donating properties of the germyl ligand lead to a relative elongation of the Pt-Cl4 (2.446(5)Å *vs.* 2.300(4) Å for Pt−Cl2 and 2.346 (4) Å for Pt−Cl3) involving the chlorine atom trans from the germyl ligand.

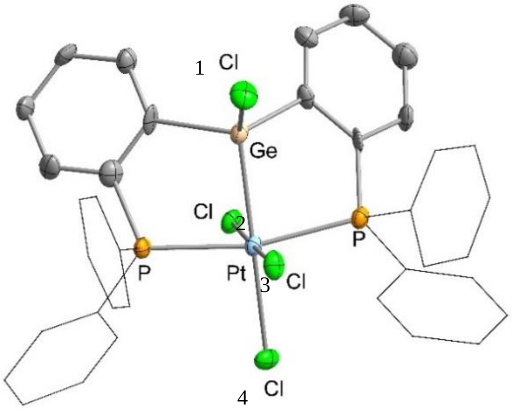

Figure 49. Solid state structure of complex **55**. Thermal ellipsoids are drawn at the 50% probability level. Phenyl groups are drawn in wireframe. Hydrogen atoms are omitted for clarity. Bonds and angles: Ge−Pt: 2.396 (2) Å, Ge−Cl1: 2.169(5) Å , Pt−Cl2: 2.300(4) Å, Pt−Cl3: 2.346 (4)Å, Pt−Cl4: 2.446(5)Å; ∠Ge−Pt−Cl, 174.366(127)°; ∠Cl−Ge−Pt, 116.443(178).

Complex **55** possesses a tetravalent platinum trichloride moiety analogous to that found in complexes **20** and **21**, which readily eliminate chlorine when irradiated in the presence of a trap such as DMBD. Given its potential to eliminate chlorine, complex **55** was subjected to irradiation in the presence of SMe_2 as a trap, and the resulting product was confirmed by ^{31}PNMR to be the reduced form, mainly complex **54**.

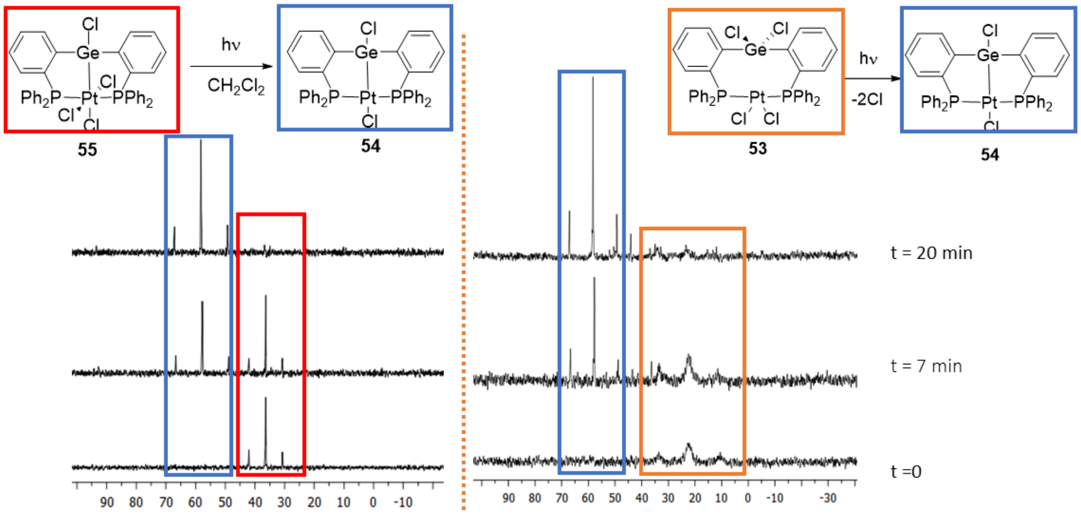

Figure 50. Comparison of photoreaction progress of compound **53** and **55**.

Complexes **53-55** were also characterized by UV-Vis spectroscopy. Complex **54** has a λ_{max} = 277 nm, and the maximum absorbance for complex **55** will appear at λ_{max} = 300 and λ_{max} = 345 nm, while complex **53** does not show any notable absorbance features below 300 nm.

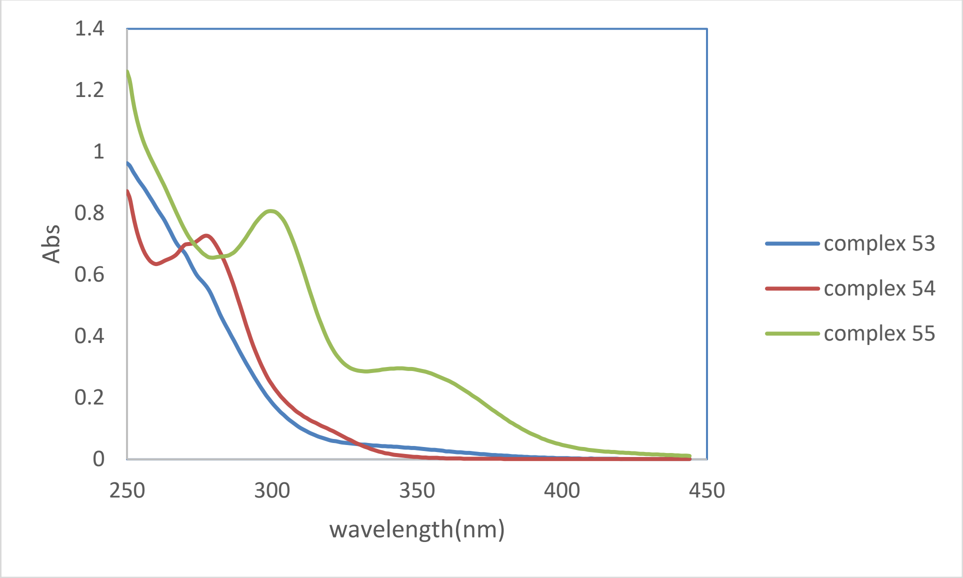

Figure 51. Absorbance spectra of complexes **53-55** in CH_2Cl_2.

In the process of HCl splitting to produce Cl_2 and H_2, the reversibility of the process is of great importance. The systems studied by our group on main group/ transition metal complexes, oxidation of the reduced form by HCl have not been detected. It was observed that complex **54** in this study tends to react with a trace of HCl impurity in the benchtop NMR solvent $CDCl_3$. By using distilled $CDCl_3$, the oxidized form had not been detected. This leads to further investigation of the oxidation process by HCl. A series of experiments were performed to shine more light on the matter. The ^{31}P NMR spectra of complex **54** have been followed in both $CDCl_3$ and THF. Concentrated HCl was added to a THF solution of complex **54** in the presence and absence of oxygen. The results are summarized in Figure 52.

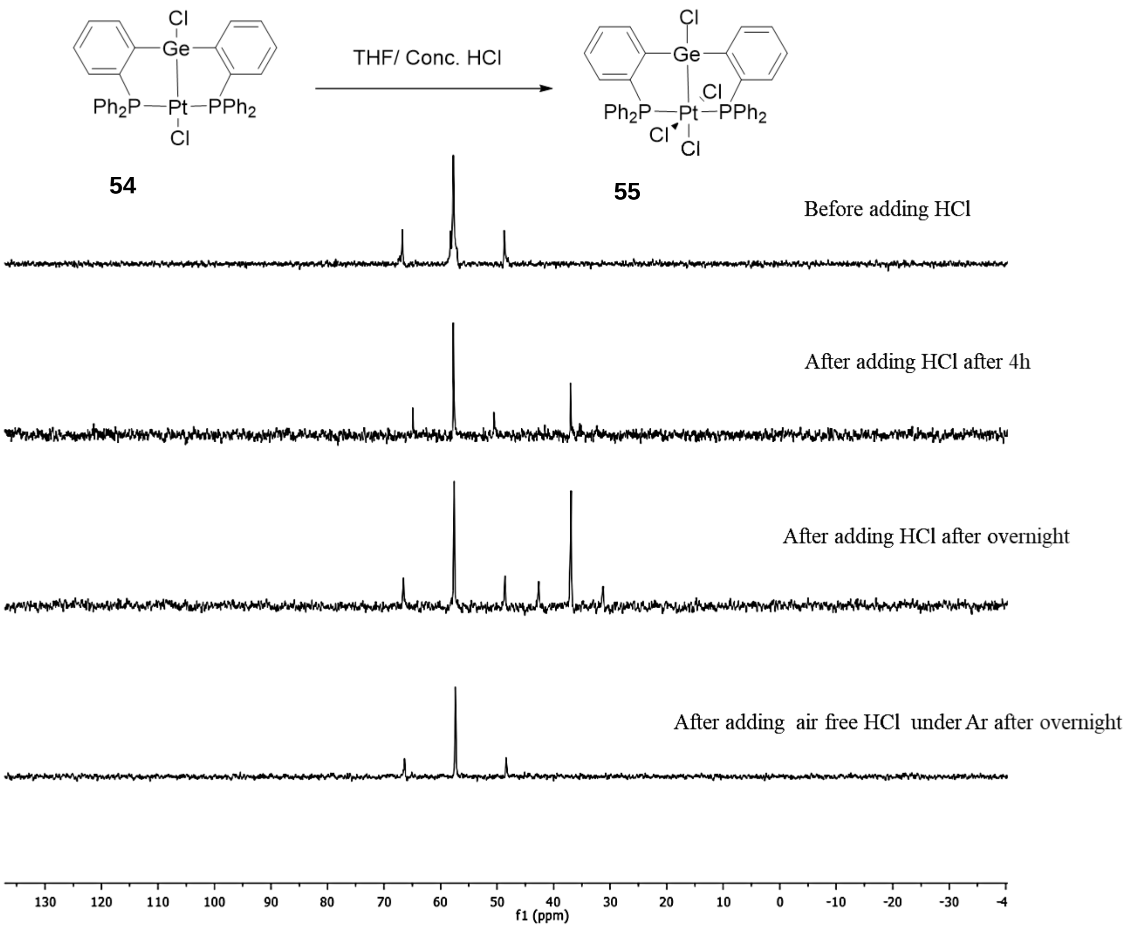

Figure 52. The reaction of complex **54** with concentrated HCl in THF with and without the presence of oxygen.

In pure THF, by adding concentrated HCl, a resonance at 36 ppm is detected, indicating the presence of **55**. However, under argon, this oxidation product is not observed. Furthermore, bubbling oxygen in the THF solution increases the rate of the oxidation reaction. Figure 53 shows a proposed mechanism for the oxygen assisted oxidation of the platinum center.

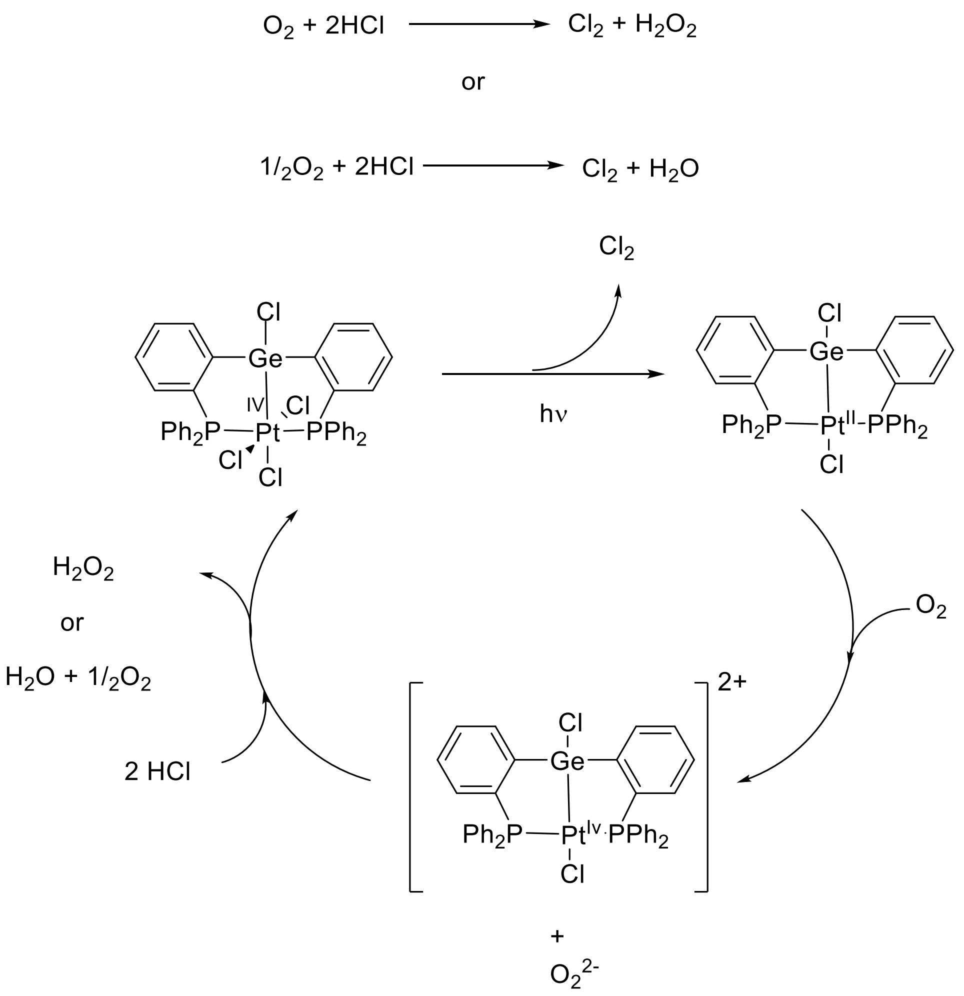

Figure 53. A proposed mechanism for the oxygen assisted oxidation of the platinum center by HCl.

3.4 Conclusion

In this research, germanium-containing complexes have been investigated. A Pt(II) complex, complex **53**, with Lewis acidic Ge(IV) in its ligand backbone showed that despite long Ge–Pt distances, the platinum is positioned in a direction to be engaged in a weak donation from the platinum lone pair to the σ^* of Ge–Cl bond. This interaction will make the complex susceptible to photoreduction of chlorine in the presence of the sacrificial reducing agent, which leads to production of Pt(I)–Ge(III) complex, complex **54**.

3.5 Experimental

Materials and methods. All chemicals were purchased from commercial sources and were used without any further purification. The solvents were purified by distillation. $Cl_2Pt(SMe_2)$[146], *o*-$(Ph_2P)C_6H_4)_2GeCl_2$[52], and $PhICl_2$[147] were prepared by following previously published procedures. The photochemical experiments were carried out using a Nikon Microscope 100W mercury lamp connected with Nikon HBO 100W power supply (Model 78591). During photolysis, the reaction sample was placed in front of a cooling fan (SA-317, SLM Instruments) such that the temperature was maintained at 30°C. UV-vis spectra were recorded in a Shimadzu UV-2501PC spectrophotometer. NMR spectra were recorded on a Varian Unity Inova 500 FT NMR spectrometer or Varian Inova 400 MHz or Bruker 400 MHz. Chemical shifts (δ) are given in ppm and are calibrated against residual solvent signals for ^1H and ^{13}C and an external H_3PO_4 (85%) standard (assigned as 0 ppm) for ^{31}P. Elemental analysis were performed in Atlantic Microlab, Inc., Norcross, GA.

Computational Details. Density functional theory (DFT) structural optimizations were performed using Gaussian 09 suite[106] of programs with effective core potentials on all heavy atoms (functional: BP86;[107, 108] mixed basis set: Ge/Pt: cc–pVTZ–PP;[109] P/Cl: 6–311g+(d,p);[110, 111] C, H: 6–31g.[112] Frequency calculations were also performed on the optimized geometries, showing no imaginary frequencies. The optimized structures were subjected to an NBO analysis, using the NBO 6.0 program.[148] The resulting NBOs and Natural Localized Molecular Orbitals (NLMOs) were visualized and plotted using the Jimp 2 program.[149, 150]

[$Cl_2GePtCl_2$(*o*-dppp)$_2$], 53

To a solution of *o*-$(Ph_2P)C_6H_4)_2GeCl_2$, compound **52**, (365.6 mg, 0.55 mmol) in CH_2Cl_2 (4 ml) was added $PtCl_2(SMe_2)_2$ (214.2 mg, 0.55 mmol) and the mixture was stirred for 2h. The solvent was removed under vacuum, washed with ether and hexane and dried under vacuum. Yield: 505.3 mg (98.2%). Single crystals were obtained by slow diffusion of hexanes into a $CDCl_3$ solution of **53**. Elemental analysis for $C_{36}H_{28}Cl_4P_2GePt$ with one mole of CH_2Cl_2, $C_{37}H_{30}Cl_6P_2GePt$: Calcd: C, 43.70; H, 2.97; Found: C, 43.46; H, 2.96. ^{1}H NMR (400.20; $CDCl_3$): 8.59 (br d, 2H), 8.20-6.30 (m, 26H), ^{13}C{^{1}H} NMR (125.76 MHz; $CDCl_3$): 143.0 (m), 136.5 (d, *J* = 13.3), 132.8 (br s), 131.4 (d, *J* = 8.8), 131.2 (s), 128.6-126.8 (m). Not all expected peaks were. ^{31}P {^{1}H} NMR (161.70 MHz; $CDCl_3$): 21.7 ppm (s, $J_{Pt\text{-}P}$: 3522 Hz).

[ClGePtCl (*o*-dppp)$_2$], 54

Complex **54** could be prepared from chemical and photochemical pathway.

Photochemical pathway: To a solution of [$Cl_2GePtCl_2$(*o*-dppp)$_2$], complex **53** (100 mg, 0.11 mmol) in CH_2Cl_2 (3ml) was added SMe_2(0.35ml, 4.75mmol) as a radical trap. The solution was irradiated overnight with a 100-Watt Hg lamp. The solvent was removed, and the residue was washed with methanol to remove the decomposition side products. The remaining solid was dissolved in THF, filtered and dried under vacuum (50 mg, 54.1%).

Chemical pathway: To a solution of *o*-(Ph_2P)C_6H_4)$_2$$GeCl_2$, compound **52**, (44.5 mg, 0.067 mmol) in THF (10 ml) was added a solution of ethylenebis(triphenylphosphine)platinum(0) (50 mg, 0.067 mmol) in THF. The mixture was stirred for 20h. The solvent was evaporated. The product was recrystallized by diffusion of hexanes into a THF solution of the compound.

Single crystals suitable for X-ray measurement were obtained by slow diffusion of hexanes into a CH_2Cl_2 solution of the compound that also contained a few drops of benzene.

^{1}H NMR (400.20 MHz; $CDCl_3$): 8.27 (d, 2H, *o*– P(Ge)C_6H_4, $^3J_{H\text{–}H}$ = 7.6 Hz), 7.77–7.67 (m, 4H), 7.63-7.36 (m, 22H). ^{13}C{^{1}H} NMR (125.66 MHz; $CDCl_3$): 152.6 (t, *J* = 25.1), 140.0 (t, *J* = 31.9), 134.1 (t, *J* = 6.7), 133.7 (t, *J* = 7.0), 133.5 (t, *J* = 4.0), 132.6 (t, *J* = 10.3), 131.5 (s), 130.9 (s), 130.7

, 128.8(t, J = 5.3), 128.4 (t, J = 5.6), 128.2 (t, J = 5.4). $^{31}P\{^1H\}$ NMR (202.16 MHz; $CDCl_3$): 57.8 (s, $J_{Pt–P}$ = 2885.0 Hz).

Elemental analysis for $C_{36}H_{28}Cl_2P_2GePt$ with one mole of THF, $C_{40}H_{36}Cl_2P_2GeOPt$: Calcd: C, 51.48; H, 3.89; Found: C, 51.1; H, 3.87.

[ClGePtCl$_3$ (*o*-dppp)$_2$], 55

To a solution of [ClGePtCl (*o*-dppp)$_2$], complex **54**, (32.3 mg, 0.038 mmol) in CH_2Cl_2 (2 ml) was added $PhICl_2$ (12.4 mg, 0.045 mmol) and the mixture was stirred for 30 minutes. The solvent was removed and washed with Et_2O and crystallized from a CH_2Cl_2 solution layered with hexanes. (30.2 mg, 86.5% yield). Single crystals for X-ray measurement were obtained by solvent diffusion of hexane in CH_2Cl_2. Elemental analysis for $C_{36}H_{28}Cl_4P_2GePt$: Calcd: C, 45.26; H, 3.01; Found: C, 44.80; H, 2.75. ^1H NMR (499.7 MHz; $CDCl_3$): 8.30 (d, 2H, *o*– P(Ge)C_6H_4, $^3J_{H–H}$ = 7.36 Hz), 8.13–8.20 (m, 4H), 7.71 (t, 2H, $^3J_{H–H}$ = 7.36 Hz, $^3J_{H–P}$ = 3.99 Hz), 7.47–7.60 (m, 10H), 7.30-7.40 (m, 10H).$^{13}C\{^1H\}$ NMR (125.66 MHz; $CDCl_3$): 136.6 (t, J = 5.6), 134.7 (t, J = 3.9), 134.1 (t, J = 5.1), 132.8 (t, J = 9.7), 132.2 (s), 131.9 (s), 131.5 (s), 130.9 (t, J = 4.5), 128.3 (t, J = 5.6), 127.7 (t, J = 5.6), 124.6 (s). $^{31}P\{^1H\}$ NMR (161.7 MHz; $CDCl_3$): 37.4 (s, $^1J_{Pt–P}$ = 1845.8 Hz).

Crystallographic Measurements. All reflections were measured at 110(2) K using a Bruker APEX-II CCD area detector diffractometer with Mo-Kα radiation (λ = 0.71073 Å). A specimen of suitable size and quality was selected and mounted onto a nylon loop/glass wool. The semi-empirical method SADABS was applied for absorption correction. The structures were solved by direct methods, which successfully located most of the none-hydrogen atoms. Subsequent refinement on F^2 using the SHELXTL/PC package (version 6.1)[151] and Olex2[152] allowed the location of the remaining non-hydrogen atoms. All H-atoms were geometrically placed and refined using a standard riding model.

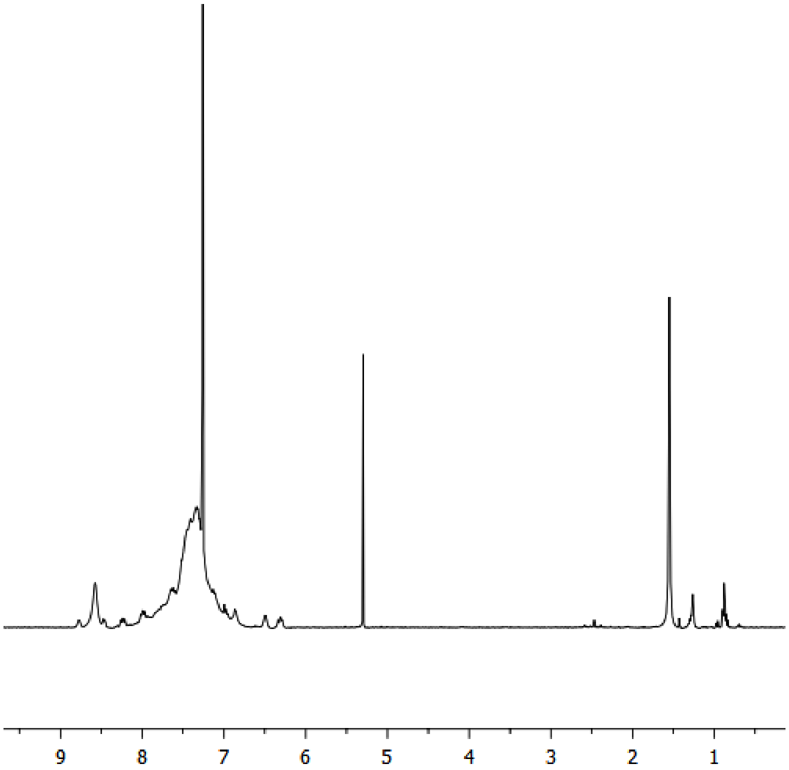

Figure 54. ^{1}H NMR of [$Cl_2GePtCl_2$(*o*-dppp)$_2$], complex **53**.

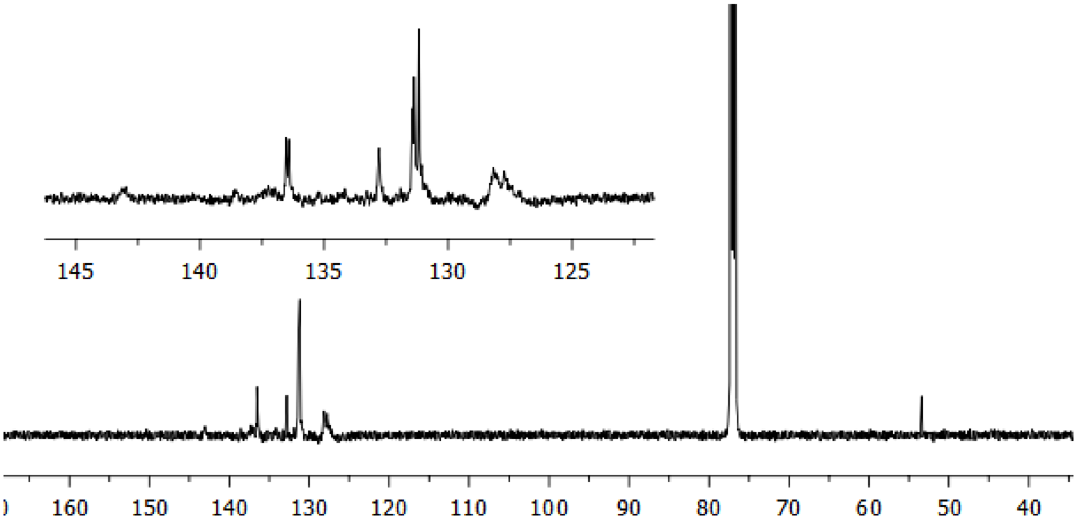

Figure 55. ^{13}C NMR of [$Cl_2GePtCl_2$(*o*-dppp)$_2$], complex **53**.

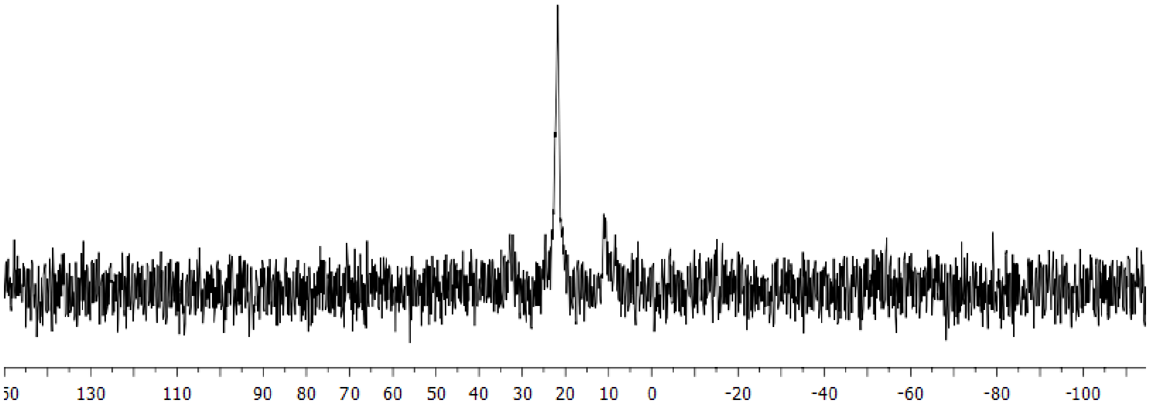

Figure 56. ^{31}P NMR of [$Cl_2GePtCl_2$(*o*-dppp)$_2$], complex **53**.

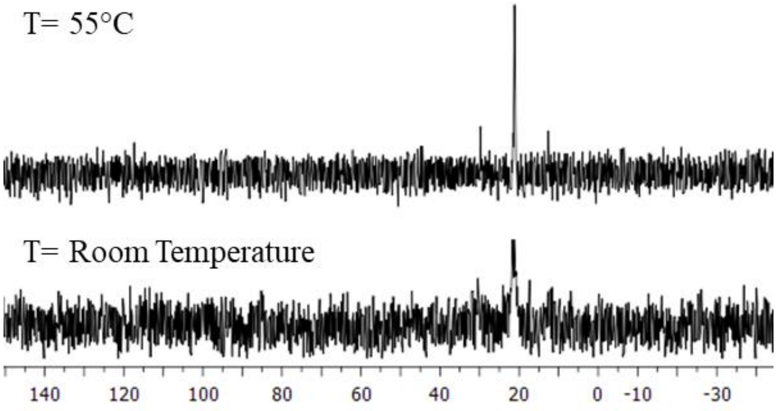

Figure 57. ^{31}P NMR of complex **53** at room temperature and 55°C.

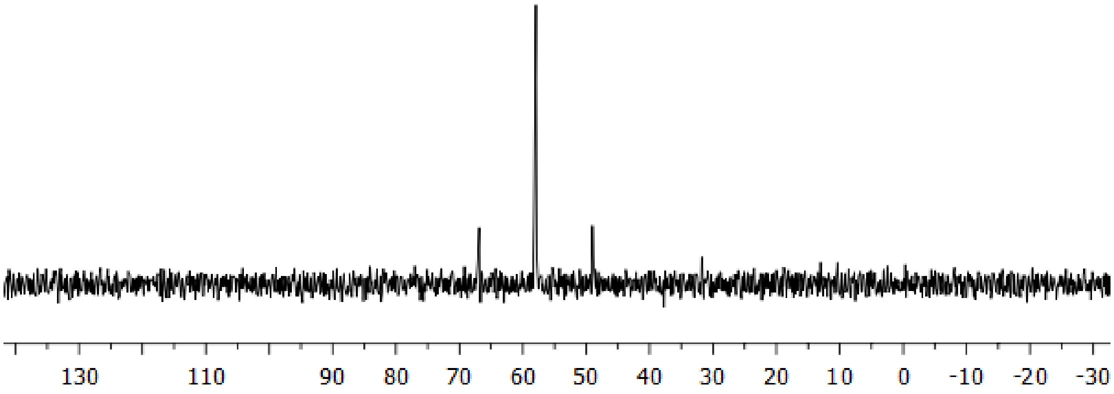

Figure 58. ^{31}PNMR of [ClGePtCl (*o*-dppp)$_2$], complex **54**.

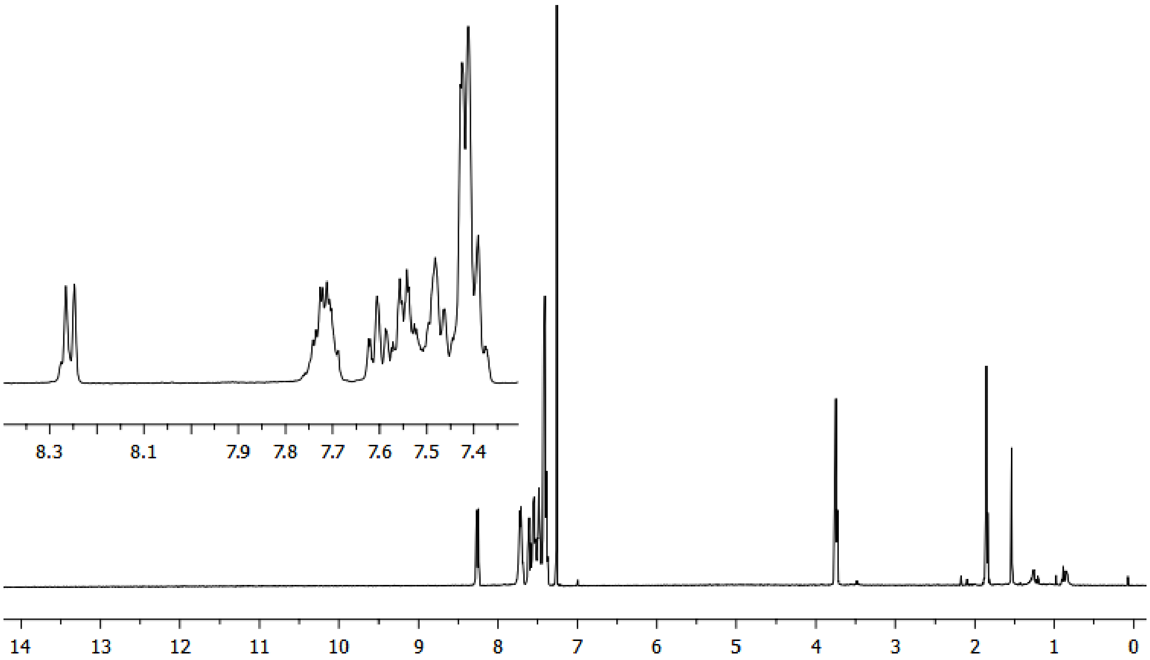

Figure 59. ^{1}H NMR of [ClGePtCl (*o*-dppp)$_2$], complex **54**.

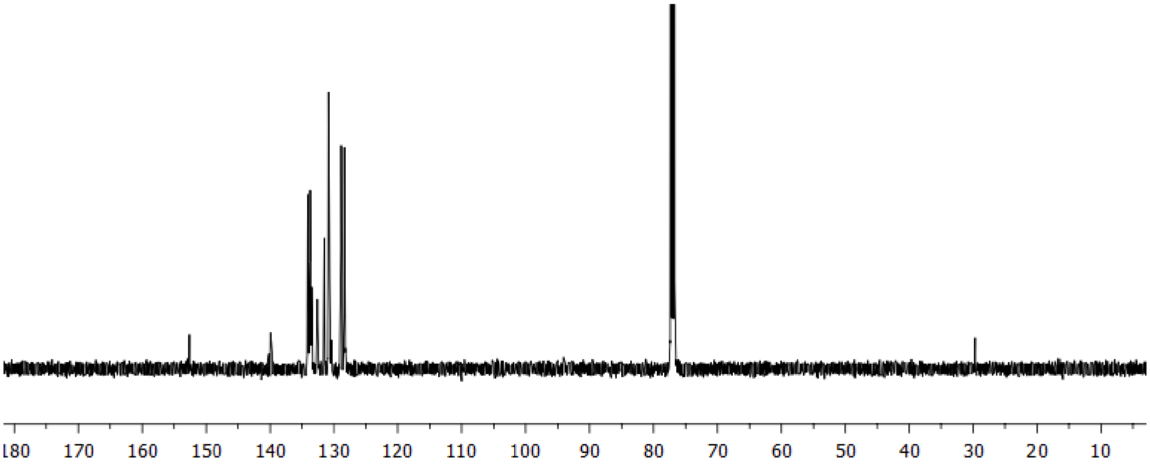

Figure 60. ^{13}C NMR of [ClGePtCl (*o*-dppp)$_2$], complex **54**.

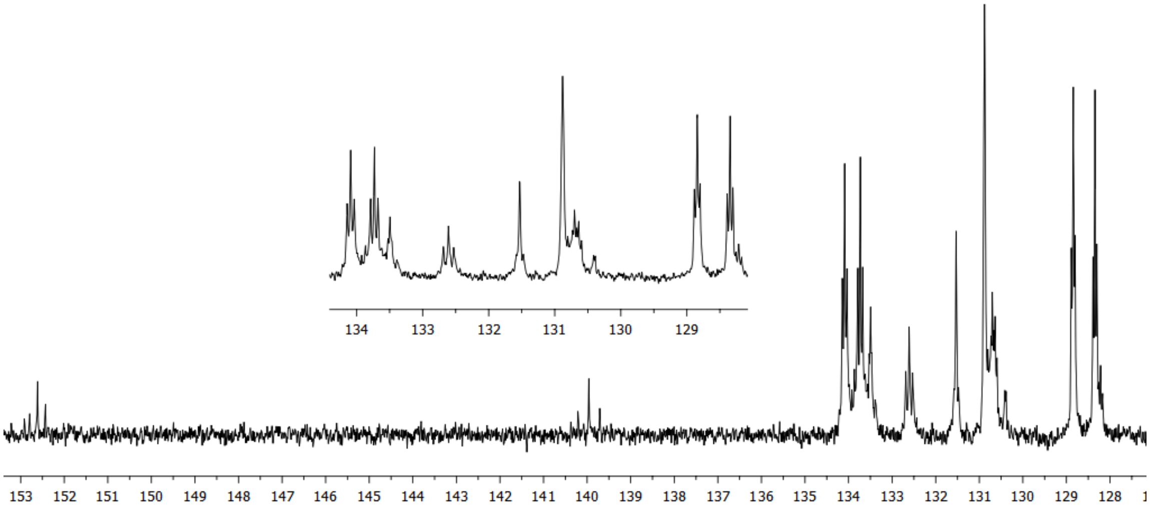

Figure 61. ^{13}C NMR of [ClGePtCl (*o*-dppp)$_2$], complex **54**.

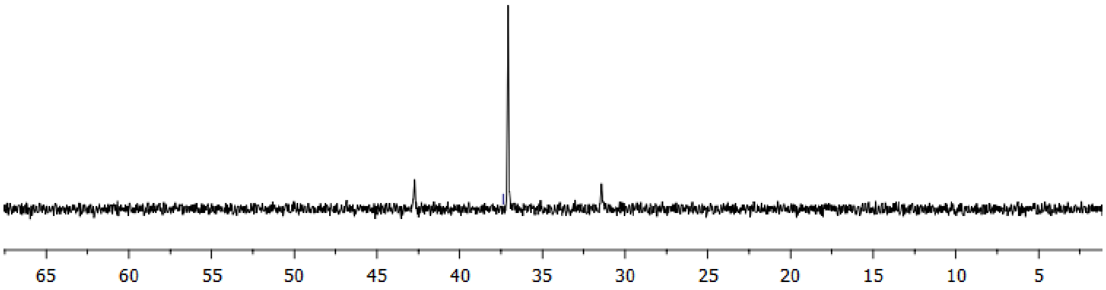

Figure 62. ^{31}P NMR of [ClGePtCl$_3$ (*o*-dppp)$_2$], complex **55** in CDCl$_3$.

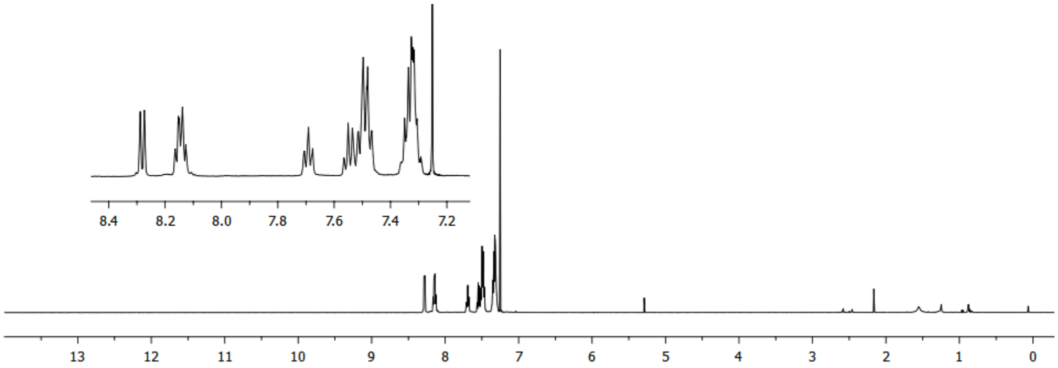

Figure 63. ^{1}H NMR of [ClGePtCl$_3$ (*o*-dppp)$_2$], complex **55** in CDCl$_3$.

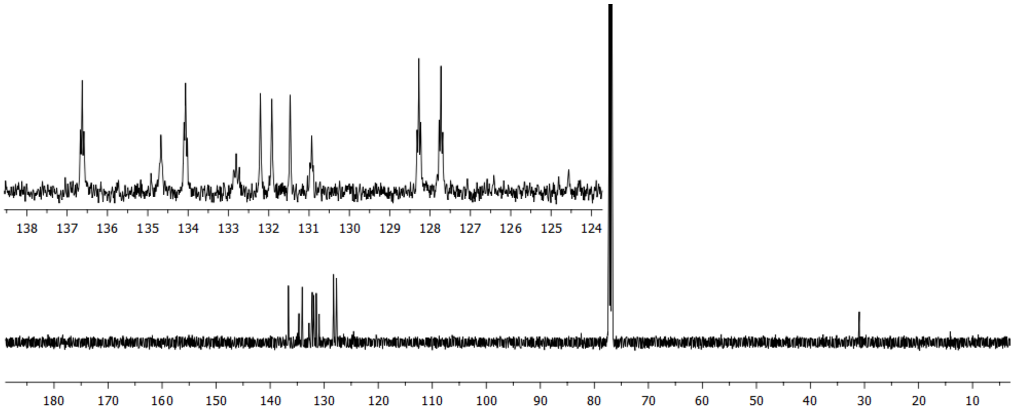

Figure 64. ^{13}C NMR of [ClGePtCl$_3$ (*o*-dppp)$_2$], complex **55** in CDCl$_3$.

CHAPTER IV

INVESTIGATING GERMANIUM-CONTAINING PALLADIUM AND GOLD COMPLEXES

4.1 Introduction

Tetrahedral compounds of heavier group 14 elements E (E= Si, Ge, and Sn) are prone to accept nucleophiles through donor-acceptor interactions with organic Lewis bases[125, 153] leading to the formation of hypervalent compounds of trigonal bipyramidal or octahedral geometries. This behavior stems from their larger atomic radius compare to carbon (C: 0.76 Å, Si: 1.11 Å, Ge: 1.20 Å, Sn: 1.39 Å),[154] which leads to less steric repulsion among their substituents, and also their electropositive properties allow them to interact with polarizable bases.[155]

Saturated group 14 molecules forming a σ- complexes with transition metals are classified into three categories[41, 156, 157] as illustrated in Figure 65. Complexes of type **A** feature a ligand→metal donation from a filled σ(E–H) orbital of the ligand to an empty d orbital of the metal. Complexes of type **B** feature a metal→ligand back-donation from a filled d orbital of the metal to an empty σ*(E–E) orbital of the ligand. Saturated heavier group 14 complexes of type **C** with a donation of an electron from an occupied d orbital at the metal to a low-lying vacant σ* orbital centered at E, are gaining more attention.[41, 52, 61, 155]

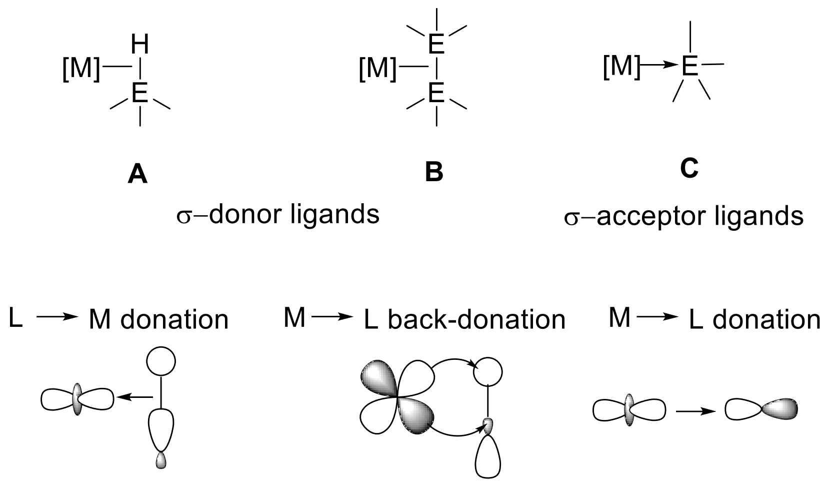

Figure 65. Complexes A–C featuring Group 14 saturated molecules coordinated to transition metals (E=Si, Ge, and Sn).

Metallosilatranes and metallostannatranes with buttressing bridges consisting of –XCH_2PMe_2 groups (X=O, CH_2),[158, 159] o-$(R_2P)C_6H_4$ groups (R=*i*Pr, Ph),[41, 61, 160, 161] methimazolyl,[162-165] pyridine-2-thionate,[166, 167] and azaindolyl[168] have been studied extensively. However, investigations of the germanium analogs are limited.[61, 158, 159]

4.2 Research objectives

The objective of this study is to investigate germanium containing complexes of palladium and gold with the o-$(Ph_2P)C_6H_4$ buttress. The target complexes will be designed to possess M→Ge interaction (M = Pd, Au). The properties and reactivities of the products will be compared to their silatrane, stannatrane, and platinum analogs.

4.3 Results and discussion

4.3.1 Complexes containing germanium and palladium

4.3.1.1 Reaction of compound **52** as a ligand with $PdCl_2$(cod)

Reaction of compound **52** with $PdCl_2$(cod) (cod = 1,8-cyclooctadiene) in CH_2Cl_2 afforded [$Cl_2GePdCl_2$(*o*-dppp)$_2$] (complex **56**, *o*-dppp = *o*-(Ph_2P)C_6H_4) as a result of fast Cl_2 reductive elimination to produce [ClGePdCl(*o*-dppp)$_2$], complex **57**, and along with undefined decomposition products.(see Figure 66)

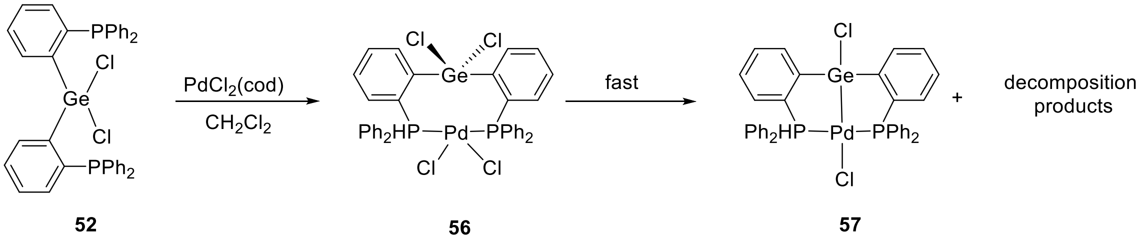

Figure 66. A scheme of the reaction of compound **52** as a ligand with $PdCl_2$(cod).

Upon mixing the ligand and $PdCl_2$(cod), the solution turned orange and showed a ^{31}P NMR resonance at δ= 23.9 ppm. Upon stirring for another hour, the color turned from orange to yellow. Following the reaction in an NMR tube by ^{31}P NMR, indicated that the color change is accompanied by the disappearance of the peak at δ= 23.9 and the appearance of a peak at δ= 56.3 ppm, which are respectively assigned to complexes **56** and **57**. Besides the peak at δ= 56.3 ppm, resonances between δ = 22 ppm and δ = 45 ppm were observed, and those were assigned to decomposition products resulting from oxidation of the ligand by the released chlorine equivalent (Figure 67). Complex **57** was also formed by the reaction of compound **52** with $Pd(PPh_3)_4$ in toluene, as confirmed by ^{31}P NMR spectroscopy analysis of an NMR scale reaction.

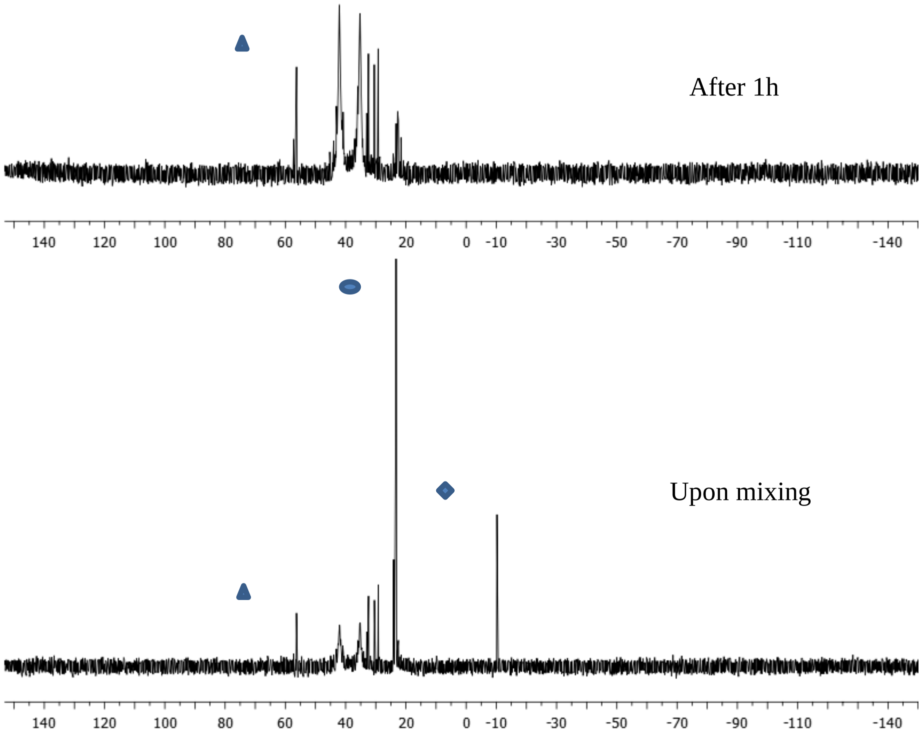

Figure 67. ^{31}P NMR monitoring of the reaction of compound **52** and PdCl$_2$(cod) in CH$_2$Cl$_2$. The resonances are marked as follows, ♦ compound **52**; ● compound **56**; ▲ compound **57**. All other resonances correspond to undefined decomposition products.

Based on the fact that the platinum complex **53** ([Cl$_2$GePtCl$_2$(*o*-dppp)$_2$]) displays a ^{31}P NMR signal at δ = 22.5 ppm, the peak at δ = 23.9 ppm was attributed to [Cl$_2$GePdCl$_2$(*o*-dppp)$_2$], complex **56**. The structure of complex **56** was later confirmed by X-ray diffraction analysis. With the hope that complex **56** show the same insolubility in toluene as complex **53**, single crystals appropriate for X-ray measurement were obtained by solvent diffusion of a cold solution of PdCl$_2$(cod) in CH$_2$Cl$_2$ to a cold solution of *o*-(dppp)$_2$GeCl$_2$ in toluene. According to the structure shown in Figure 68, the palladium center adopts a square planar geometry with the *cis*-coordination of the two phosphino arms of the ligand to the palladium center. A noticeable feature of this structure is the Pd-Ge-Cl1 angle which approaches linearity (162.990(51)°). The Ge–Pd bond distance of 3.3591(8) Å is beyond the sum of the covalent radii of germanium and palladium (2.61 Å), but it is shorter than the sum of van der Waals radii (3.74 Å) with a covalent bond ratio (*r)* of 0.90. The geometry around the germanium center is trigonal bipyramidal with the C1-Ge-Cl2, C1-Ge-C2, and C2-Ge-Cl2 angles equal to 116.485(202)°, 117.423(269)°, and 112.784(199)° respectively. The palladium atom appears to be positioned to engage the germanium center in a Pd→Ge interaction. In agreement with this view, the Ge–Cl1 bond (2.1721(17) Å) is longer than the Ge–Cl2 bond (2.1456(17) Å). Furthermore, NBO calculations confirm the donation of a palladium d-orbital lone pair into the σ* orbital of the Ge-Cl1 bond. This donation is weak, as indicated by the second-order perturbation energy of 1.04 Kcal/mol.

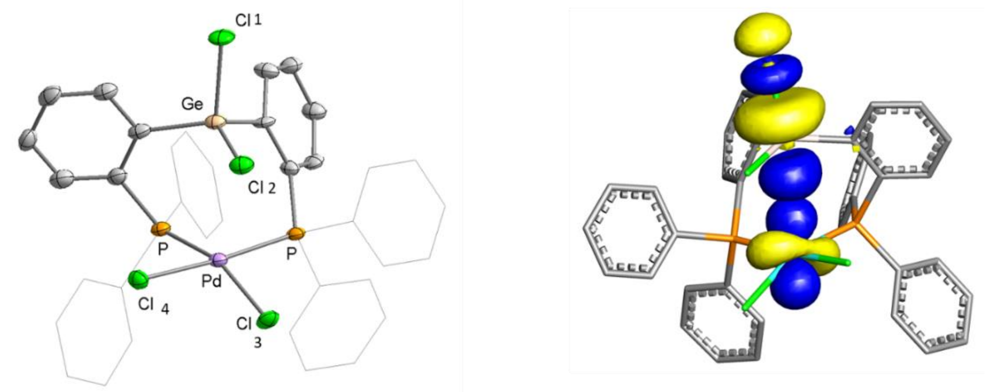

lp Pd → σ^* (Ge-Cl1)

Figure 68. Left: Solid state structure of complex **56**. Thermal ellipsoids are drawn at the 50% probability level. Phenyl groups are drawn in wireframe. Hydrogen atoms are omitted for clarity. Selected bonds and angles: Ge−Cl1 2.1721(17) Å, Ge−Cl2 2.1456(17) Å, Pd−Cl3: 2.3605(15) Å; Pd−Cl4: 2.3702(15) Å, ∠Cl3−Pd−Cl4, 91.163(59)°; ∠Cl1−Ge−Cl2, 99.104(66). Right: NBO plot (isovalue = 0.05) showing the lp(Pd) → σ^* (Ge–Cl1)) donor-acceptor interaction E(2) = 1.04 Kcal/mol.

Structural and spectroscopic comparison of complex **56** and the platinum analog, complex **53**, show similarities and differences. They have a similar ^{31}P NMR chemical shift. Both complexes, due to the presence of an M→Ge interaction, adopt similar structures, with the metal in a square planar geometry and the germanium center, in a trigonal bipyramidal geometry. The platinum analog complex **53** is an air-stable white solid with partial solubility in chlorinated solvents which undergoes reductive elimination of chlorine upon irradiation with UV light. However, complex **56** is not stable. It quickly decomposes to form **57** as the product of Cl_2 elimination along with many decomposition products.

4.3.1.2 Reaction of ligand **52** with $[PdCl(C_3H_5)]_2$

In pursuit of a cleaner reaction, $[PdCl(C_3H_5)]_2$ was allowed to react with ligand **52** in toluene (Figure 69). This reaction proceeded quickly to afford **57** and allyl chloride, as indicated by ^{1}H NMR (Figure 71).

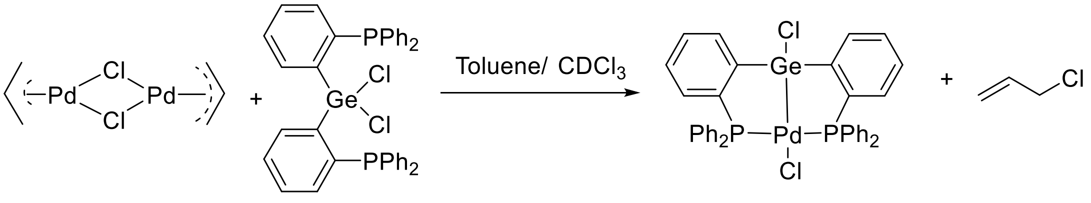

52 **57**

Figure 69. The reaction of $[PdCl(C_3H_5)]_2$ with ligand **52** producing complex **57**.

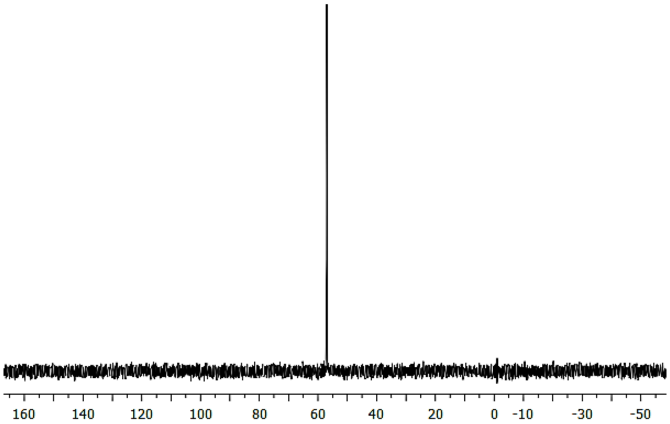

Figure 70. ^{31}PNMR of [ClGePdCl(*o*-dppp)$_2$], complex **57**, in toluene.

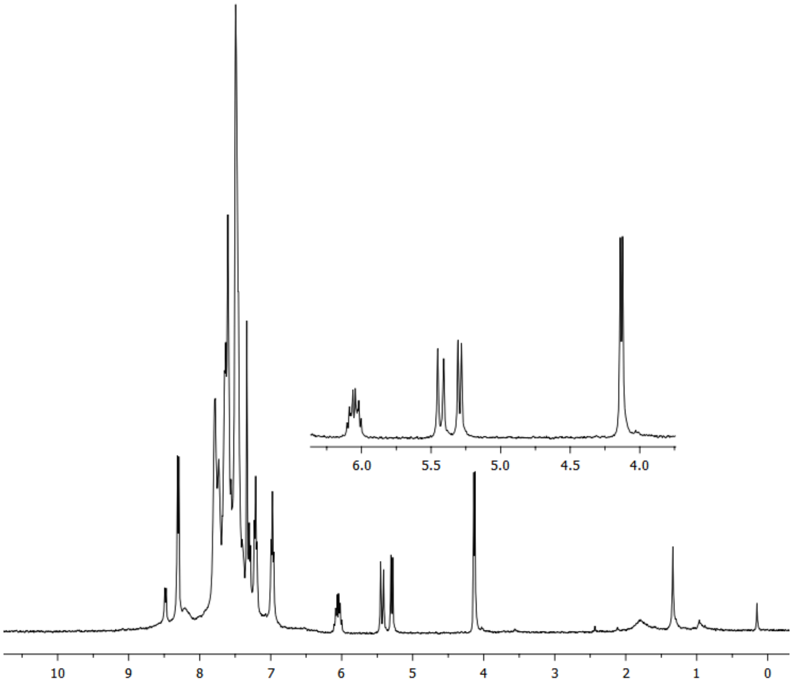

Figure 71. Formation of allylchloride during the reaction of compound **52** and $[PdCl(C_3H_5)]_2$ in $CDCl_3$. The inset is showing peaks related to the eliminated allylchloride.

The formation of complex **57** was confirmed by X-ray crystallography (Figure 72). According to the crystal structure, complex **57** displays a similar structure as the platinum analog, complex **54**. The palladium center adopts a square planar geometry. In this complex, the germanium and palladium centers form a short bond of 2.3185(5) Å corresponding to a covalent bond ratio of 0.90. An NBO analysis of the optimized structure of complex **57**, shows that the two central atoms are connected by an lp(Pd)→p(Ge) interaction associated with second-order perturbation energy of E(2) = 39.96 Kcal/mol. It is interesting to note that the NBO method describes the Pt–Ge bond in complex **54** as covalent and that in complex **57** as donor-acceptor. This discrepancy shows a limitation of the NBO method, which is not well adapted to analyze bonding in these complexes.

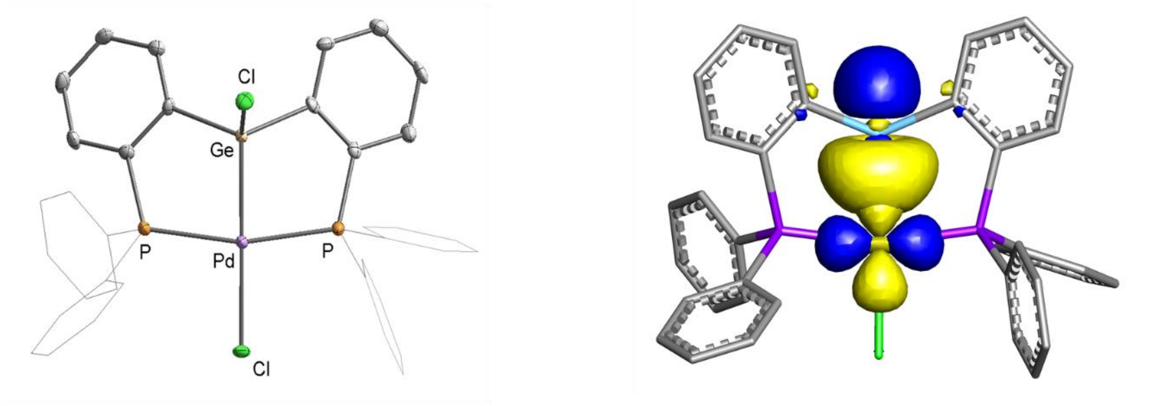

lp (Pd) → P(Ge)

Figure 72. Left: Solid state structure of complex **57**. Thermal ellipsoids are drawn at the 50% probability level. Phenyl groups are drawn in wireframe. Hydrogen atoms are omitted for clarity. Selected bonds and angles: Ge-Pd. 2.3185(5) Å, Ge−Cl 2.2097(12) Å, Pd−Cl: 2.33835(11) Å; ∠Ge−Pd−Cl, 178.16(3)°; ∠Cl−Ge−Pd 111.73(4). Right: NBO plot (isovalue = 0.05) showing the lp(Pd)→p(Ge) donor-acceptor interaction E(2) = 39.96 Kcal/mol

Inspired by the reductive elimination of allylchloride in the reaction of ligand **52** and $[PdCl(C_3H_5)]_2$, and on the other hand, the difficulty of reductive elimination of halobenzenes (chlorobenzene and fluorobenzene) from transition metals, the probability of reductive elimination of chlorobenzene from the palladium center using the germanium ligand **52** was examined. With this idea in mind, ligand **52** was allowed to react with *trans*-$Pd(PPh_3)_2PhCl$ in d_6-benzene. No reaction was observed at room temperature. The reaction was followed by ^{31}P NMR and ^{1}H NMR in d_6-benzene at 80°C to track any sign of formation of chlorobenzene. In ^{1}H NMR, no trace of formation of PhCl was observed.

4.3.2 Germanium gold complex

Herein, the synthesis and characterization of the gold complex formed by the reaction of compound **52** with a gold(I) precursor are described. Reaction of **52** with Au(AsPh$_3$)Cl in CH_2Cl_2 afforded [ClGeAuCl(*o*-dppp)$_2$]Cl (complex **58**, *o*-dppp = *o*-(Ph$_2$P)C$_6$H$_4$) as an air-stable white solid (Figure 73).

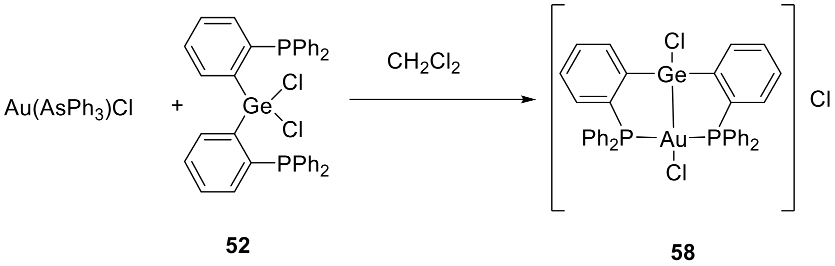

Figure 73. The reaction of compound **20** with Au(AsPh$_3$)Cl producing complex **58**.

This new complex has been characterized by ^{31}P NMR spectroscopy and X-ray diffraction. Complex **58** displays a ^{31}P NMR resonance at $\delta = 58.5$ ppm. The platinum and palladium analogs, complexes **54** and **57**, also show ^{31}P NMR signals in the same region. The solid state structure of **58** has been determined experimentally. According to the X-ray diffraction (Figure 74), complex **58** adopts an ionic structure with a Cl^- as a counterion. The geometry around the gold center is square planar with the P-Au-P and Ge−Au−Cl angles being respectively equal to 164.506(58)° and 178.405(42)°. The germanium-gold bond of 2.3941(8) Å is quite short, as indicated by the covalent bond ratio of 0.93, which is smaller than unity. The geometry around the germanium is best described as a distorted tetrahedral.

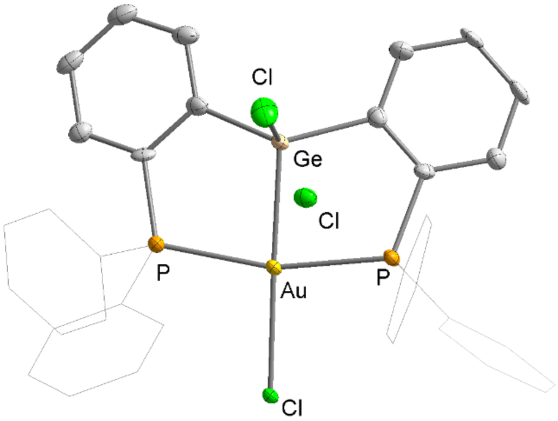

Figure 74. Solid state structure of complex **58**. Thermal ellipsoids are drawn at the 50% probability level. Phenyl groups are drawn in wireframe. Hydrogen atoms are omitted for clarity. Selected bonds and angles: Ge−Au: 2.3941(8) Å, Ge−Cl: 2.1960(19) Å, Au−Cl: 2.4535(15) Å; ∠Ge−Au−Cl, 178.405(42)°; ∠Cl−Ge−Au, 106.512(59)

Complex **58** was compared with the previously reported[41] silatrane and stannatrane gold complexes, complexes **59 – 61** shown in Figure 75. The ^{31}P NMR resonance of complex **59** appears at $\delta = 57.1$ ppm and falls in the same region as for complex **58**, while the ^{31}P NMR resonance for the tin-gold complexes **60** and **61** appears further downfield at $\delta = 79.1$ ppm and $\delta = 74.5$ ppm respectively.

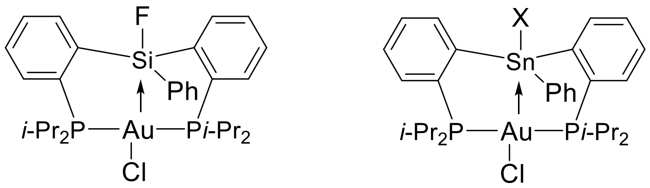

59

X = F **60**
X = Cl **61**

Figure 75. Gold silane and stannane complexes of the type [$o\{(i\mathrm{Pr}_2\mathrm{P})\mathrm{C}_6\ \mathrm{H}_4\}_2\mathrm{E(Ph)XAuCl}$].

In complex **59**, the Au–Si distance (3.090(2) Å) is longer than the sum of the covalent radii of gold and silicon (2.47 Å, r = 1.25), but significantly shorter than the sum of their van der Waals radii (4.20 Å). The Au–Sn distance in **60** (2.891(1) Å) is shorter than the Au–Si distance in **59**, despite the larger covalent radius of tin (r_{cov} (Sn) = 1.39 Å; r_{cov} (Si) = 1.11 Å). With an r factor of 0.93, the Au–Ge bond in complex **58** is comparatively a lot shorter and thus slightly stronger. As a result, formation of this bond can be seen as the result of an S_N2 reaction in which the gold atom acts as the nucleophile and induces the dissociation of a Ge–Cl bond with the chloride being the leaving group.

4.4 Experimental

Materials and methods: All chemicals were purchased from commercial sources and were used without any further purification. The solvents were purified by distillation. $PdCl_2(COD)$[169] (COD = 1,5- Cyclooctadiene) and o-$(Ph_2P)C_6H_4)_2GeCl_2$[52] were prepared by following previously published procedures. NMR spectra were recorded on a Varian Unity Inova 500 FT NMR spectrometer or Varian Inova 400 MHz or Bruker 400 MHz. Chemical shifts (δ) are given in ppm and are calibrated against residual solvent signals for ^1H and an external H_3PO_4 (85%) standard (assigned as 0 ppm) for ^{31}P.

Computational Details: Density functional theory (DFT) structural optimizations were performed using the Gaussian 09 suite of programs[106] with effective core potentials on all heavy atoms (functional: BP86;[107, 108] mixed basis set: Ge, Pd, Au: cc–pVTZ–PP;[109] P/Cl: 6–311g+(d,p);[110, 111] C, H: 6–31g.[112] Frequency calculations were also performed on the optimized geometry, showing no imaginary frequencies. The optimized structures were subjected to an NBO analysis, using the NBO 6.0 program.[148] The resulting NBOs and Natural Localized Molecular Orbitals (NLMOs) were visualized and plotted using the Jimp2 program.[149, 150]

Crystallographic Measurements: All reflections were measured at 110(2) K using a Bruker APEX-II CCD area detector diffractometer with Mo-Kα radiation (λ = 0.71073 Å). A specimen of suitable size and quality was selected and mounted onto a nylon loop/glass wool. The semi-empirical method SADABS was applied for absorption correction. The structure was solved by direct methods, which successfully located most of the non- hydrogen atoms. Subsequent refinement on F^2 using the SHELXTL/PC package (version 6.1)[151] and Olex2[152] allowed the location of the remaining non-hydrogen atoms. All H-atoms were geometrically placed and refined using a standard riding model.

[$Cl_2GePdCl_2$(*o*-dppp)$_2$], 56

To a solution of $PdCl_2$(cod) (5.1 mg, 0.018 mmol) in CH_2Cl_2 (0.6ml) in an NMR tube was added (*o*-(Ph_2P)C_6H_4)$_2GeCl_2$ (11.9 mg, 0.018 mmol). Single crystals appropriate for X-ray measurement were obtained by slow diffusion of a cold solution of $PdCl_2$(cod) in CH_2Cl_2 into a cold solution of *o*-(Ph_2P)C_6H_4)$_2GeCl_2$ in toluene.

[ClGePdCl(*o*-dppp)$_2$], 57

To a solution of (*o*-(Ph_2P)C_6H_4)$_2GeCl_2$, compound **52**, (50.0 mg, 0.075mmol) in toluene (5 ml) was added [$PdCl(C_3H_5)$]$_2$ (20.6 mg, 0.056 mmol) and the mixture was stirred overnight at 60

°C. After filtration, the solution was evaporated, and the residue was washed with Et_2O. Crystals were obtained by diffusion of hexanes into a CH_2Cl_2 solution of the compound. $^{31}P\{^1H\}$ NMR (202.2 MHz; CH_2Cl_2): 57.3 ppm.

[(*o*-dppp)$_2$Ge ClAuCl]Cl, 58

To a solution of $Au(AsPh_3)Cl$ (50 mg, 0.093 mmol) in CH_2Cl_2 (2 ml) was added (*o*-$(Ph_2P)C_6H_4)_2GeCl_2$, compound **52**, (61.8 mg, 0.093mmol). The mixture was stirred for 1 hour. The solvent was removed and washed with hexane. The residue was recrystallized from CH_2Cl_2/Hexanes. Yield: 75.1 mg (90.1%). Crystals suitable for X-ray crystallography were obtained by solvent diffusion of hexanes in a $CDCl_3$ solution of the compound. $^{31}P\{^1H\}$ NMR (202.2 MHz; CH_2Cl_2): 58.5 ppm.

CHAPTER V

BIMETALLIC GOLD COMPLEXES AS CATALYSTS FOR THE CARBOPHILIC ACTIVATION OF ALKYNES

5.1 Introduction

In the past few decades, homogeneous gold catalysis has gained widespread attention. Its peculiar π-acidity and high functional group tolerance have made gold a coveted catalytic metal for many organic transformations.[170-172] Most of the reactions catalyzed by gold are classified as the nucleophilic addition to unsaturated carbon multiple bonds (Figure 76).[173] The soft Lewis acidic gold center[174] is prone to the electrophilic activation of multiple bonds.[175] Gold(I) and gold(III) containing complexes show catalyze nucleophilic addition to alkenes and alkynes. Moreover, the +I and +III oxidation states that gold can adopt, allows to access a different level of hardness at the metal center, providing control over the properties of the catalysts containing this metal.[176-178] Most gold complexes used in catalysis are mononuclear derivatives of general formula of [LAu][X] or LAuCl/AgX (L=

ancillary ligand, X= non-coordinating anion).[173] Some common gold (I) catalysts used in organic transformations are shown in Figure 77.

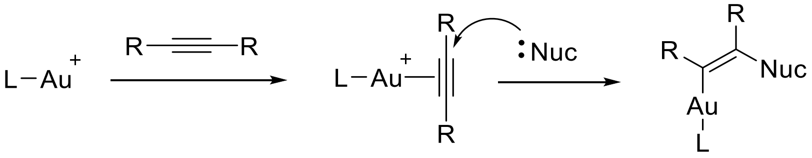

Figure 76. Schematic illustration of nucleophilic addition to unsaturated carbon multiple bonds activated electrophilically by gold complexes.

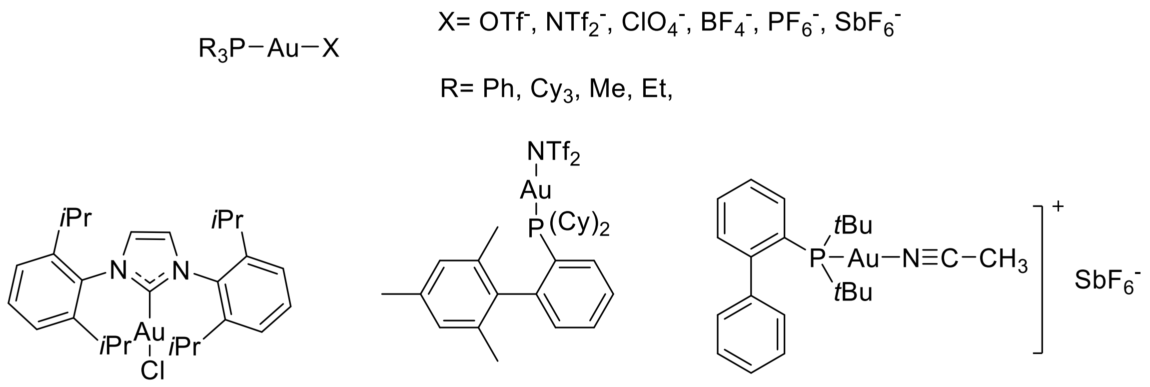

Figure 77. Examples of conventional catalysts and precatalysts used in homogenous gold catalysis.

Mechanistic studies show that the mono-ligated $[LAu]^+$ moiety is an active component in these systems, while species of general formula $[LAuL]^+$ are usually inactive. Recently, Mukai[71]*et al.* argued that $[LAuL]^+$ complexes such as **62** – **66** can be activated by introduction of a Lewis acidic borane in the ligand backbone. This group supported this proposal by demonstrating that these complexes catalyze enyne cyclization reactions. Later, the Gabbaï[179] group introduced the trifluorostiborane gold complex **67** and showed that this complex catalyzes hydroamination reactions (Complex **67**, Figure 79). A thorough literature survey showed that even small gold clusters with significant metal-metal interactions are active in catalysis. It has also been proposed that mono-ligated gold(I) complexes in the presence of a substrate will undergo a small amount of cluster formation and that those clusters might be responsible for catalytic reactivity.[180] These results combined show that polynuclear complexes hold promise in the area of gold catalysis.

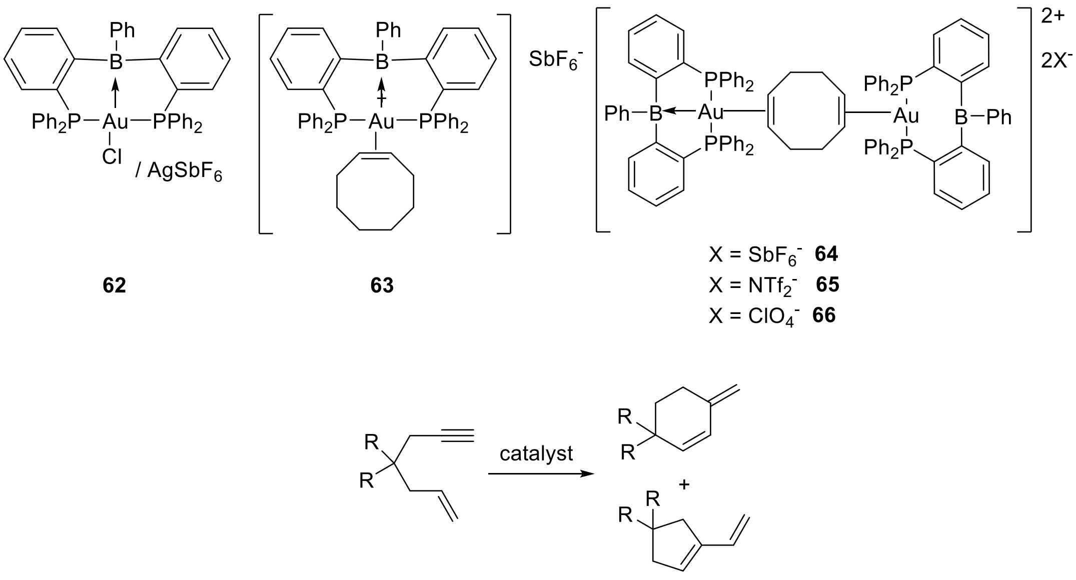

62

63

X = SbF_6^- **64**

X = NTf_2^- **65**

X = ClO_4^- **66**

Figure 78. Recently reported borane-gold catalysts used in Enyne cyclization.

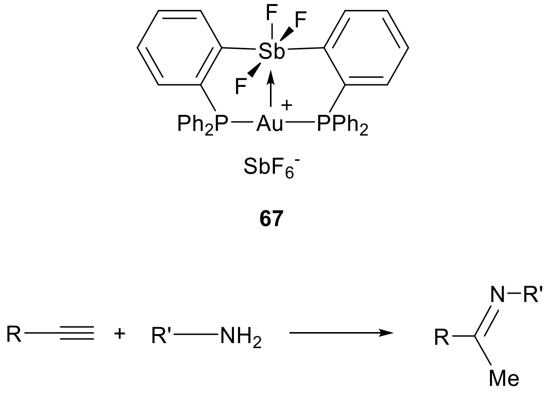

67

Figure 79. Trifluorostiborane gold complex as a catalyst for hydroamination reaction.

Utilizing bridging ligands is a common way to hold two gold nuclei in close proximity, which usually results in the formation of dimeric compounds, although chain formation is also possible.[181] Dithiocarbamate (dtc),[182] 1,1-bis(diphenylphosphino)methane (dppm),[183] (2-pyridyl)dimethylphosphine,[184] methylenethiophosphinate (mtp)[185] and phosphorus bis(ylides) [186, 187] illustrated in Figure 80 are common bridging ligands used to access dinuclear gold species.

Asymmetric dimers obtained by ligand exchange reactions between two symmetrical dimers lead to a variety of dimers with versatile electronic and steric properties.

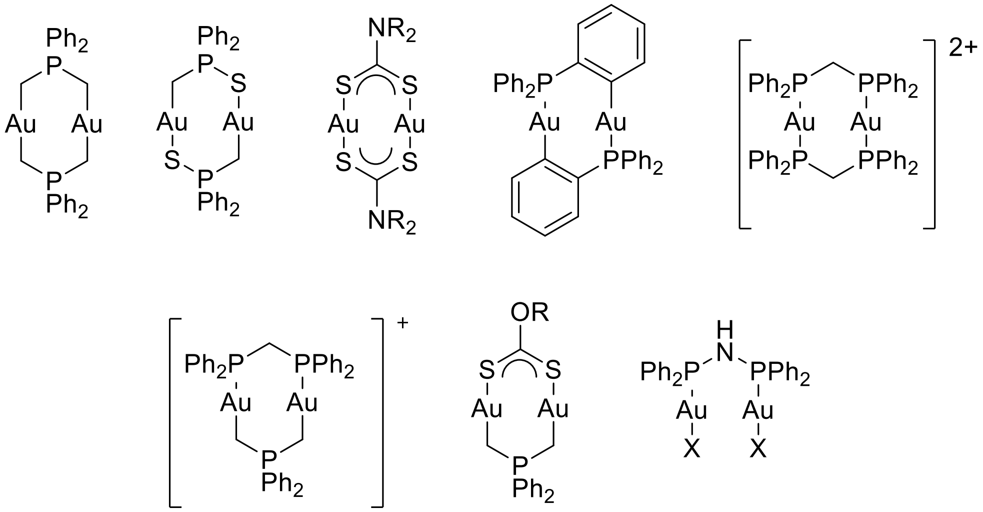

Figure 80.Examples of dinuclear gold(I) complexes.

There are extensive studies on the structural and luminescence properties of gold dimers[188-190] but their potential catalytic reactivity has been neglected. There are a handful of reports using gold of general formula of $[Au_2(L\text{-}L')]^{2+}(2X^-)$ as catalysts (complexes **68-71**, Figure 81). [191-195] Recently, Wade[174] reported an example of the doubly bridged gold dimer complex **72**, as a Lewis acid catalyst for Mukaiyama addition and alkyne hydroamination reactions (Figure 82).

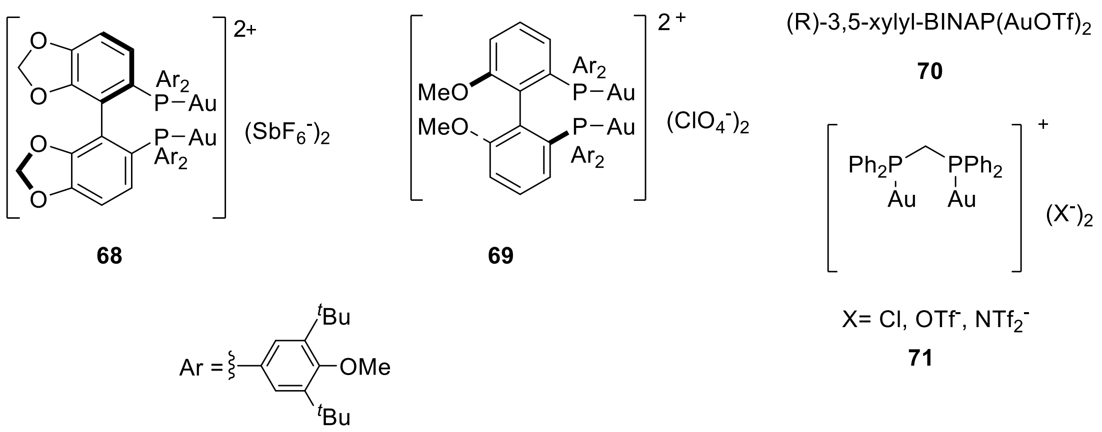

68 **69** **70** **71**

Figure 81. Examples of singly bridged gold dimers used in catalysis.

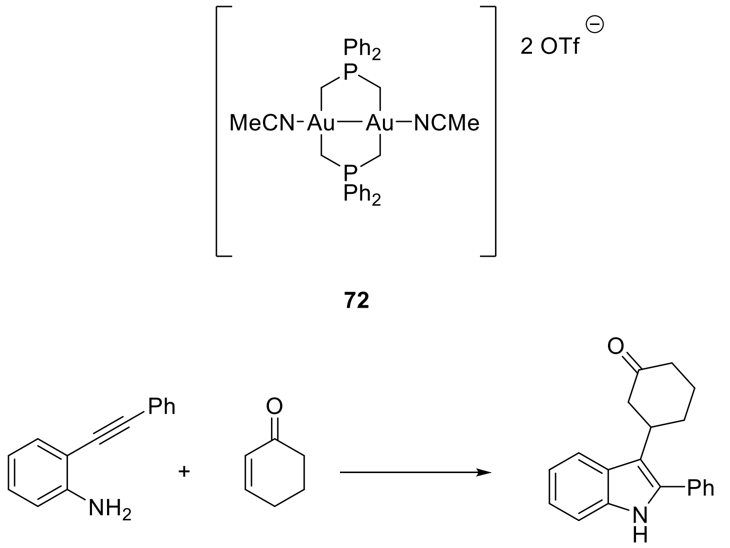

72

Figure 82. Doubly bridged dinuclear gold complex used as a Lewis acid catalyst for Mukaiyama addition and alkyne hydroamination reactions.

The cycloisomerization of *N*-propargyl carboxamides, which are highly functionalized compounds, is a favorable reaction to test the activity of gold catalysts. The compatibility of gold catalysts with mild reaction conditions[172, 196-198] is another favorable attribute when compared to the other pathways[199] or other metal centers[200] requiring harsh conditions. Hashmi[201-204] studied the cyclization of propargylic amides with a variety of gold (I) and gold (III) complexes. Different isomers of oxazoles were obtained[205] depending on the catalyst or the substrate being used (Figure 83).

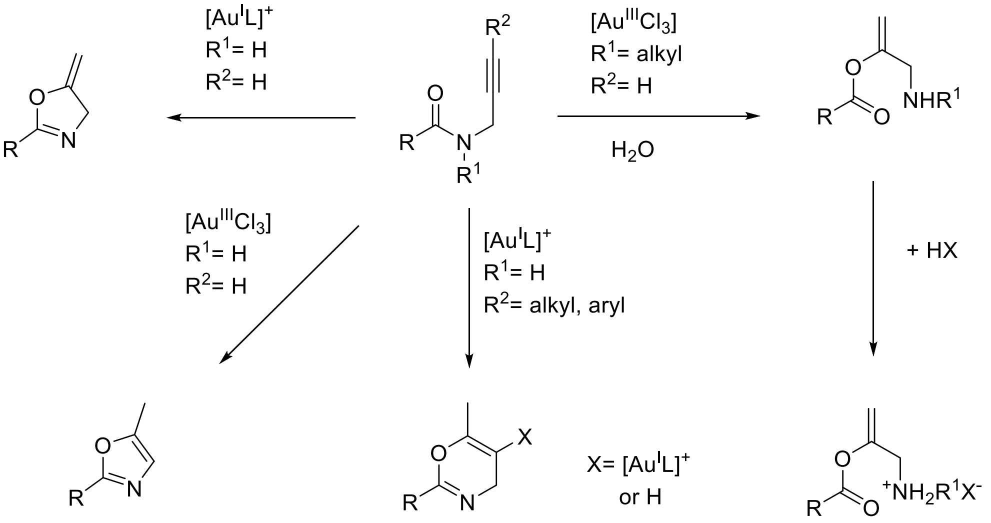

Figure 83. Illustration of the different outcomes observed in *N*-propargyl carboxamide cyclization reactions.

5.2 Research objective

The above mentioned work of Wade (Figure 82) which appeared while our work was in progress indicate that metal-metal bonded Au(II) species display carbophilic reactivity. The objective of this chapter is to test whether other supporting ligands can be used in such Au(II) catalysts.

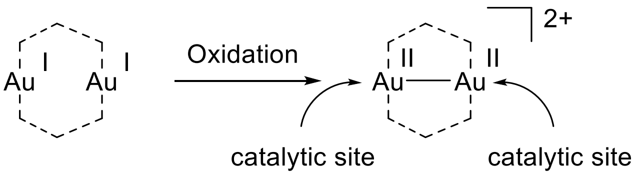

Figure 84. Au(II) catalyst targeted in this study.

5.3 Results and discussion

Herein, a series of symmetric and asymmetric gold (I) and gold (II) dimers (Figure 85) were synthesized, and their catalytic reactivity has been investigated. The cyclization of N-propargyl carboximide[197] (Figure 86) was utilized as a probe reaction to test catalytic reactivity.

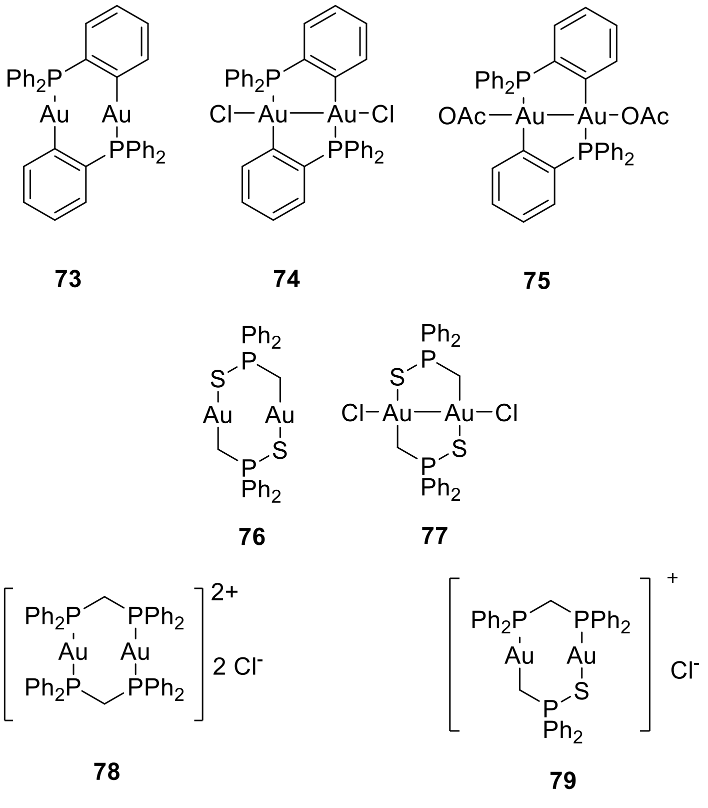
73 **74** **75** **76** **77** **78** **79**

Figure 85. Gold complexes synthesized and tested for catalytic reactivity in this project.

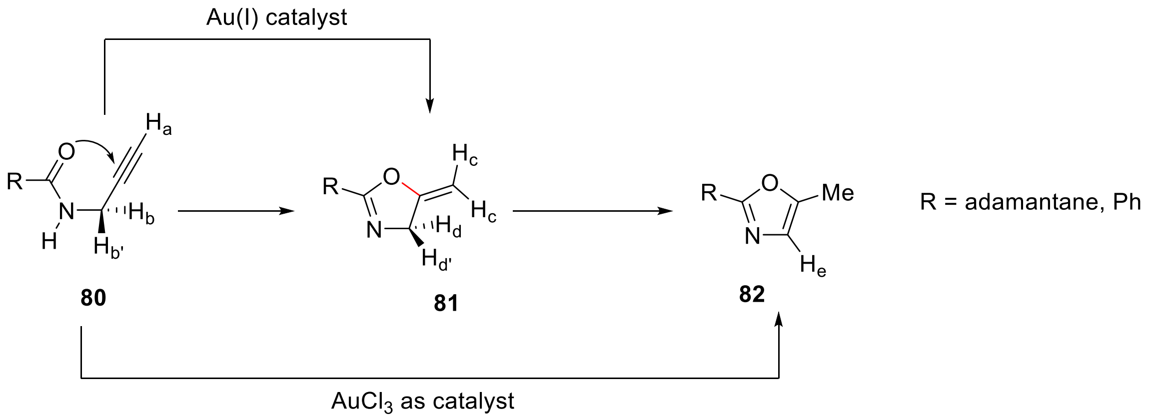

Figure 86. Cyclization of *N*-propargyl carboxamide

5.3.1 Synthesis and catalytic reactivity of complexes **73-75**

Complex **73**[206] was synthesized as a bench-stable compound with some modifications to the reported procedure (Figure 87). The reported method uses the air and moisture sensitive compound $[o\text{-}LiC_6H_4PPh_2]$. This compound can be converted into the more stable and easily handled compound, $[o\text{-}Me_3SnC_6H_4PPh_2]$[207], compound **83**, as a bench-stable compound. Compound **83** was reacted later with the Au(tht)Cl to produce complex **73**.

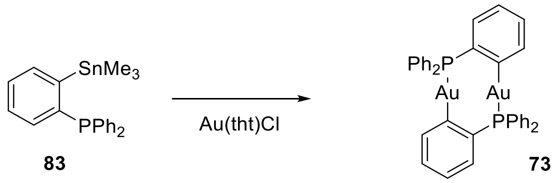

Figure 87. Modified synthetic pathway for making complex **73**.

Gold(II) dimers and their corresponding dications have been targeted for catalytic studies as well. Complex **74**[208] was obtained by oxidizing complex **73** with $PhICl_2$. Conversion of **74** into a gold (II) dications was first attempted by the addition of AgSbF$_6$. This reaction failed and afforded the hexameric gold cluster **84** first reported by Echavarren (Figure 88).[209]

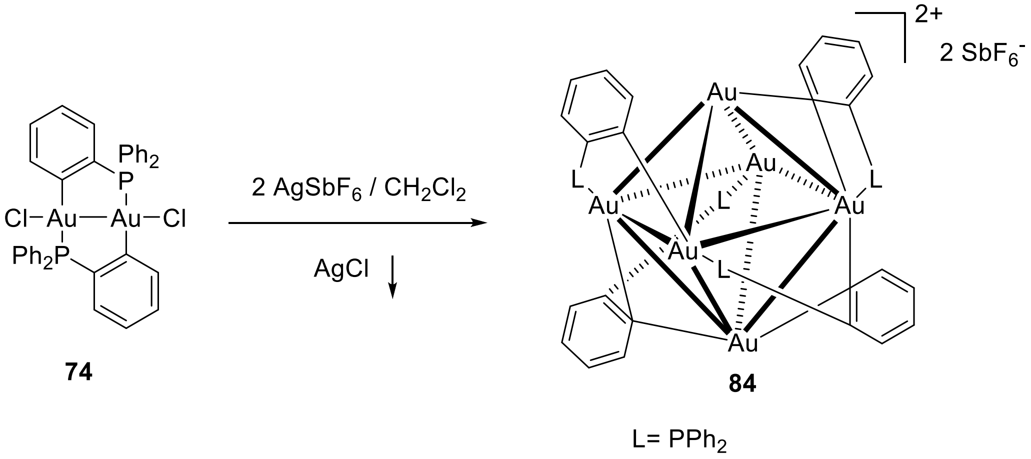

74

84

Figure 88. Gold hexamer formation.

The use of AgOAc as a halide abstractor afforded compound **75** as a stable compound characterized by a ^{31}P NMR signal at $\delta = 4.5$ ppm. The ^{1}H NMR spectra showed a resonance at $\delta = 1.4$ ppm corresponding to the CH$_3$ groups of the acetate anion. Complex **75** could be obtained from direct oxidation of complex **73** with PhI(OAC)$_2$. The structure of complex **75** was verified by X-ray crystallography (Figure 89). The crystal structure confirmed that the acetate anion is coordinated to the gold centers through an Au–O bond distance of 2.093(5) Å. The gold centers in this complex adopt a square planar geometry. Complex **75** features a short covalent Au–Au bond of 2.5539(6) Å.

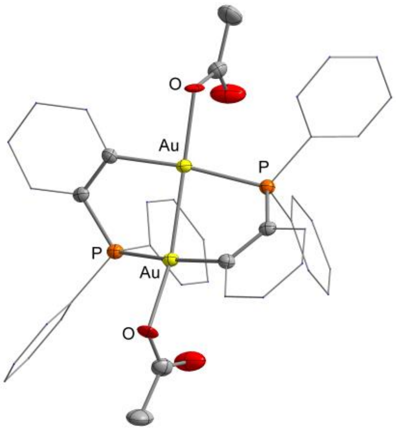

Figure 89. Crystal structure of complex **75**. Thermal ellipsoids are drawn at the 50% probability level. Phenyl groups are drawn in wireframe. Hydrogen atoms are omitted for clarity. Selected bonds: Au–Au: 2.5539(6)Å, Au–O: 2.093(5) Å.

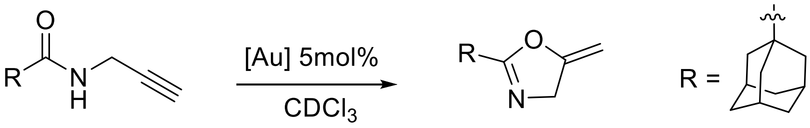

80

81

Figure 90. Catalytic reaction condition catalyzed by [Au] catalysts.

Next, all available complexes were tested in the reaction shown in Figure 90, with a 5% catalyst loading. The reaction can be followed by ^{1}H NMR spectroscopy, as the substrate, compound **80**, and the product, compound **81**, have characteristic resonances. Compound **80** has a distinct triplet at $\delta = 2.29$ ppm representing H_a hydrogen and two doublets very close to each other at $\delta = 4.02$ ppm as H_b and $H_{b'}$. The cyclization product, 5-methylene-4,5-dihydro oxazole, compound **81**, shows three sets of distinct peaks, two sets of doublets of doublets at $\delta = 4.2$ and 4.6 ppm for H_d and $H_{d'}$ and a triplet at $\delta = 4.4$ ppm depicting H_c. (See Figure 91).

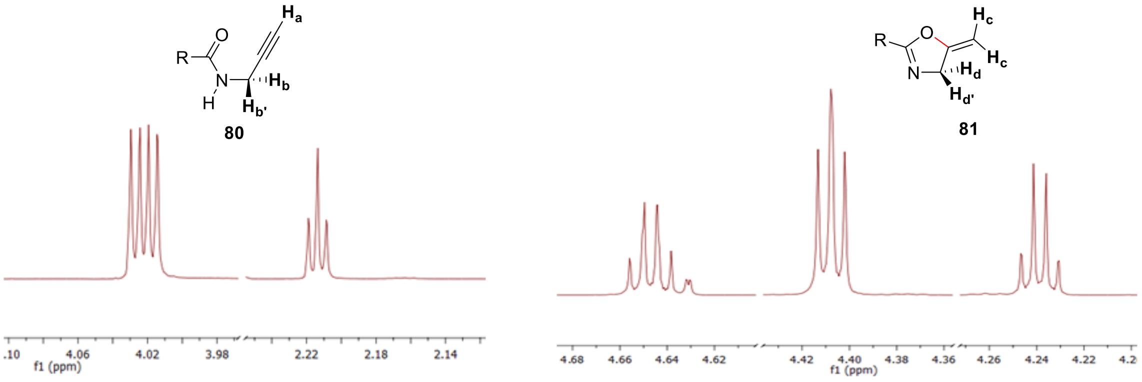

Figure 91. 1HNMR demonstration of compound **80** and **81.**

Complexes **73** and **74** showed no catalytic activity even at high temperatures, 50°C. Complex **74** is unstable while in solution and at temperatures higher than 60°C. The catalyst will undergo C-C coupling of phenyl rings to form the gold(I) complex **85**,[208, 210] making a study of its catalytic properties rather complicated (Figure 92). While some catalytic activity was observed when **74** was activated with Bi(OTf)$_3$ (Figure 93), ^{31}P NMR spectroscopy showed extensive decomposition of the catalyst such that little could be learned from this experiment.

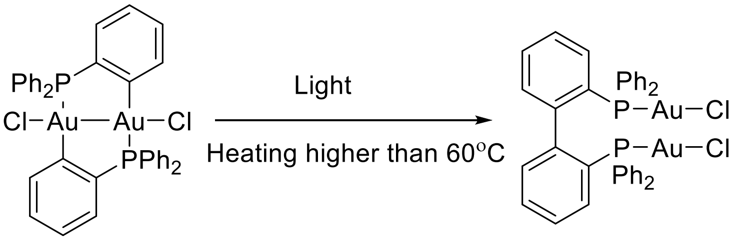

74

85

Figure 92. C-C coupling reaction of complex **74** in upon exposure to light or heat.

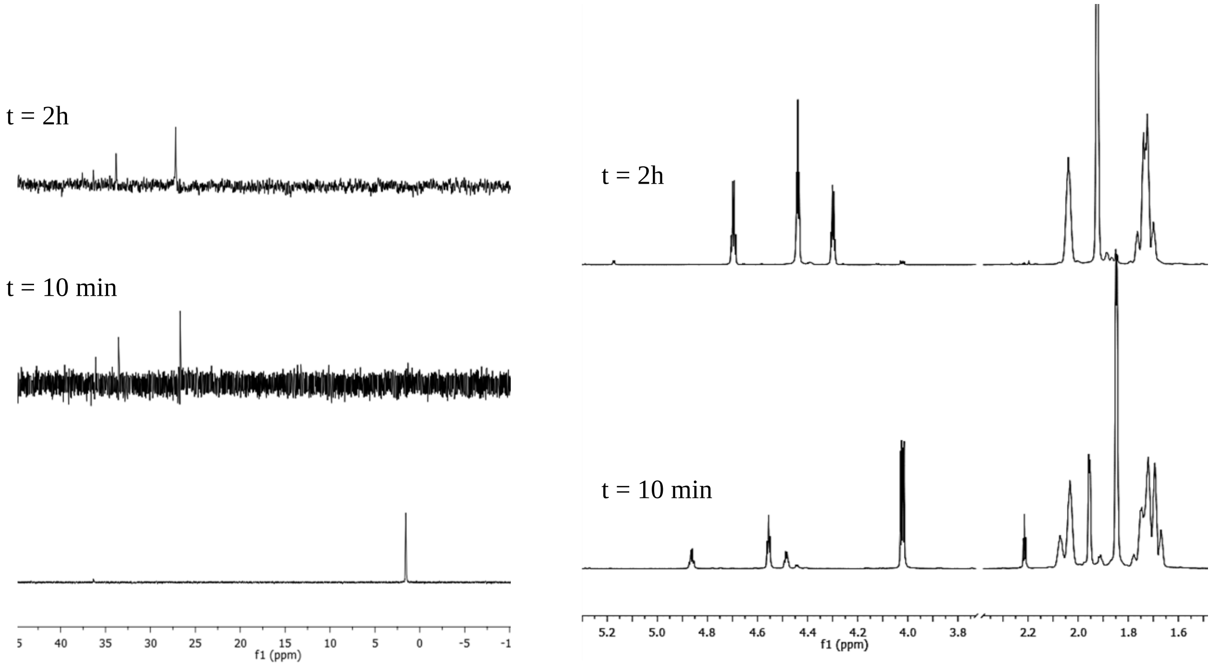

Figure 93. ^{31}P (left) and ^{1}H (right) NMR spectra recorded during the conversion of **80** into **81** catalyzed by **74** and Bi(OTf)$_3$.

Complex **75** showed weak to moderate reactivity at room temperature. Within the first 24 hours of the reaction, distinct progress was observed, but the reaction did not go to completion very fast and took 100 h to reach completion. The reactivity of complex **75** was notably enhanced at higher temperatures (40° C), and the reaction completed within 48 hours (Figure 94).

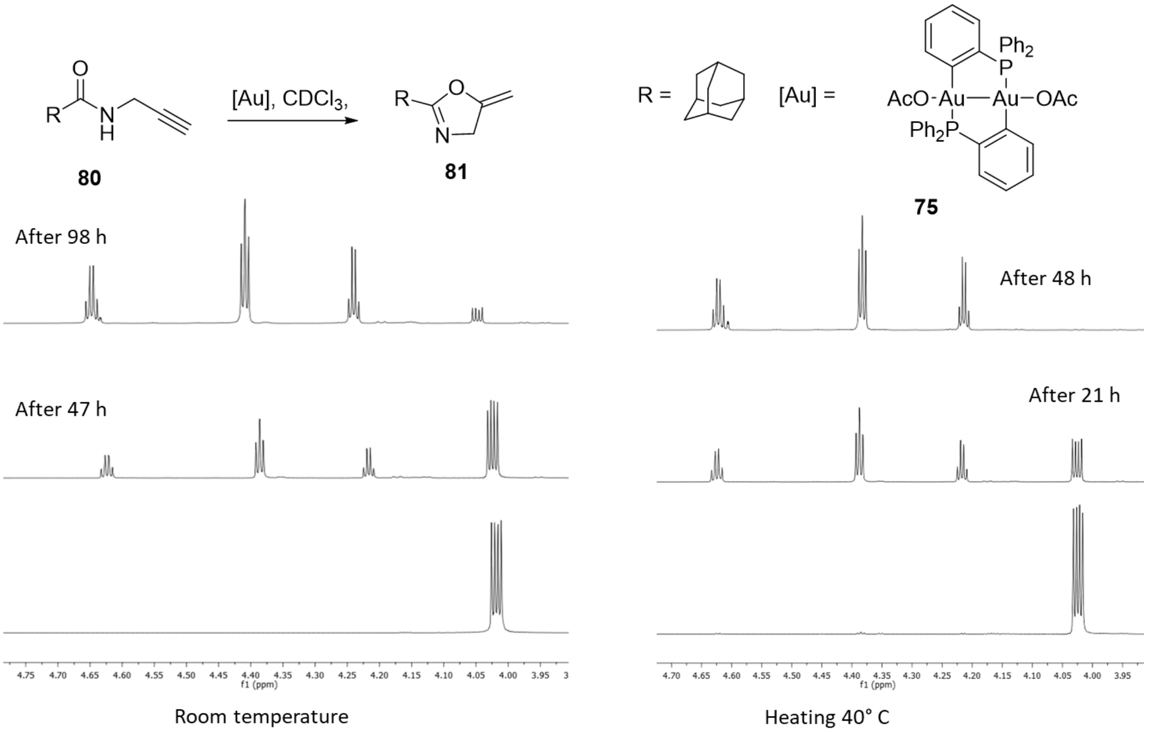

Figure 94. ^{1}HNMR spectra recorded during the conversion of **80** into **81** catalyzed by **75** at room temperature (left) and 40° C (right).

The ^{31}P NMR spectra during the reaction showed that by proceeding the reaction, the peak related to the catalyst at $\delta = 4.5$ ppm disappeared, and 3 peaks emerged at regions between $\delta = 35$ - 40 ppm. Complex **75** could be considered as a pre-catalyst, which in the presence of the substrate would be converted to the active catalyst (Figure 95).

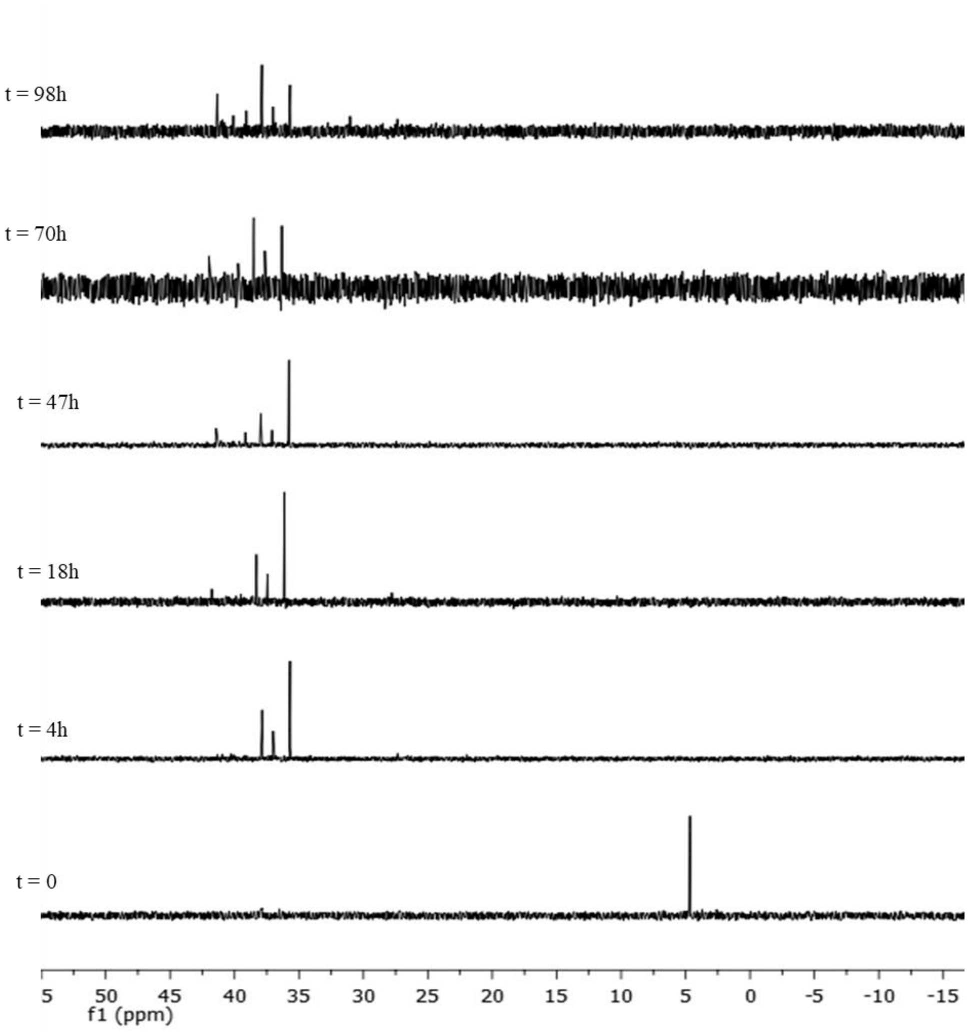

Figure 95. ^{31}P NMR spectra recorded during the conversion of **80** into **81** catalyzed by **75** at room temperature.

5.3.2 Synthesis and catalytic reactivity of complexes **76** and **77**

The second series of complexes studied in this research include **76** and **77**, which feature the mtp bridging ligand (mtp = methylenethiophosphinate). The mtp ligand provides a less crowded environment around the gold centers. Also, the presence of a phosphorus atom provides a convenient NMR spectroscopic handle. Complexes **76** and **77** were prepared by modification of the literature procedures.[211] The lithium salt $Ph_2P(S)CH_2Li$ was first converted to the bench stable compound $Ph_2P(S)CH_2SnMe_3$ (**86**) following similar literature procedure.[212] Further reaction of **86** with Au(tht)Cl yielded the corresponding dinuclear gold complex **76** (Figure 96).

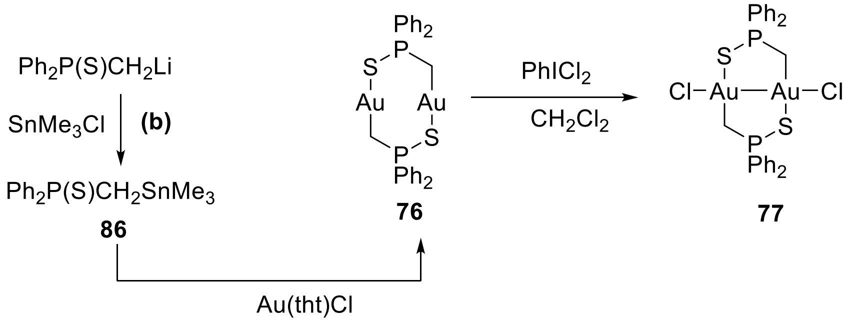

Figure 96. Synthetic pathways used to obtain complexes **76** and **77**.

Improved catalytic reactivity was observed for complexes **76** and **77**. Although complex **76** showed a weak reactivity at room temperature (10% progress), decent reactivity was observed at 50°C, and the reaction was completed within 20 hours to produce compound **81** (Figure 97, right). The ^{31}P NMR showed that the catalyst was intact in the course of the reaction (Figure 97, left).

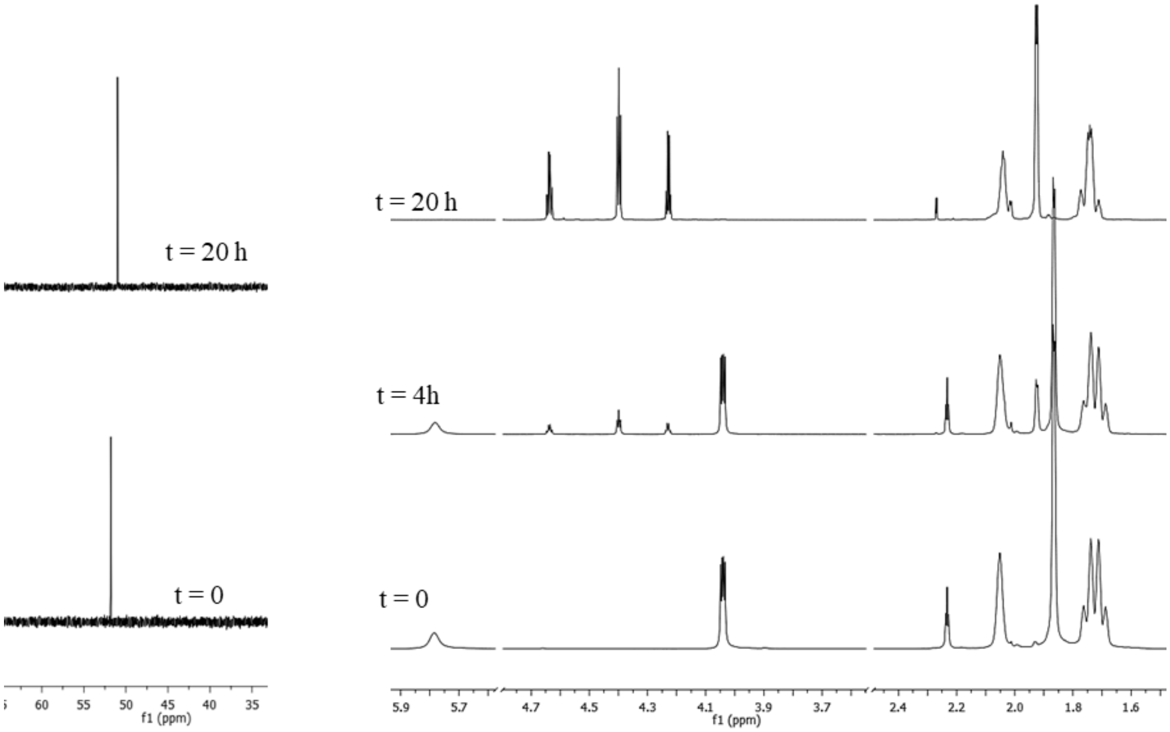

Figure 97. ^{31}P (left) and ^{1}H (right) NMR spectra recorded during the conversion of **80** into **81** catalyzed by **76**.

The gold (II) complex **77** showed catalytic reactivity at room temperature without any additive to produce compound **82** within 18-24 hours. The formation of compound **82** was confirmed by ^{1}H NMR with the characteristic resonances at $\delta = 2.42$ ppm as a doublet for the hydrogens of CH_3 group and a quartet at $\delta = 6.87$ ppm for H_e (Figure 98). It is noteworthy that compound **82** is usually formed in gold(III) mediated catalytic systems.

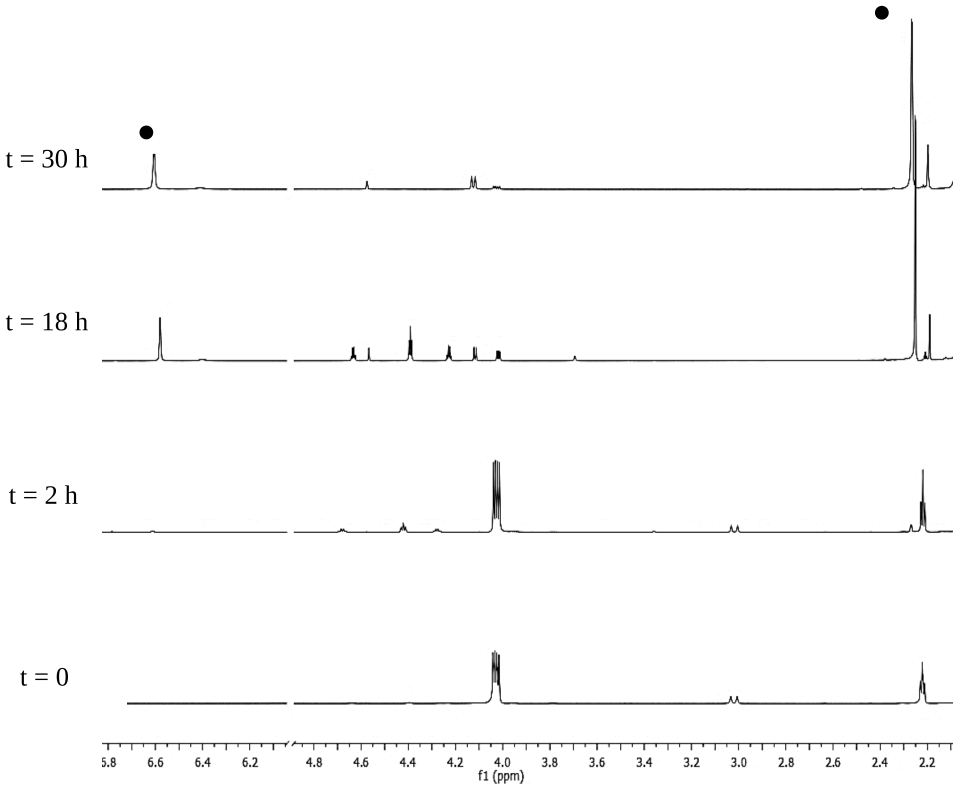

Figure 98. ^1H NMR spectra recorded during the conversion of **80** into **82** catalyzed by **77**. ● identifies characteristic peaks of **82**.

5.3.3 Synthesis and catalytic reactivity of complexes **78** and **79**

Complex **78** was synthesized as a cationic species by the reaction of diphenyl phosphino methane (dppm) ligand with Au(tht)Cl. No catalytic reactivity was observed for this complex. The catalytic reactivity silence could be attributed to the steric hindrance imposed by the PPh_2 groups around the gold centers, which would block the substrate from approaching the catalyst. It occurred to us that **78** could be used in ligand exchange reactions to access an asymmetric gold complex in which the presence of two ligands would provide additional opportunities for adjusting the electronic and steric properties of the complex. With this in mind, complex **78** and **76** were mixed in CH_2Cl_2, leading to the formation of complex **79** (Figure 99). A low-quality X-ray diffraction study suggested the proposed connectivity. The ^{31}P NMR spectrum show three individual resonances that display equal intensities. Two of these resonances, at δ = 36 ppm and δ = 38 ppm, are coupled to each other ($^2J_{PP}$ = 62 Hz) and are assigned to the phosphorus atom of the dppm ligand based on the observation. The third resonance at δ = 52 ppm corresponds to the mtp ligand. Complex **79** showed catalytic reactivity at 40°C resulting in the formation of isomer **81** within 48 hours as a product of catalysis. Following the reaction by ^{31}P NMR (Figure 100) showed that the three resonances assigned to complex **79** disappear over time, casting doubt about the nature of the catalytically active species.

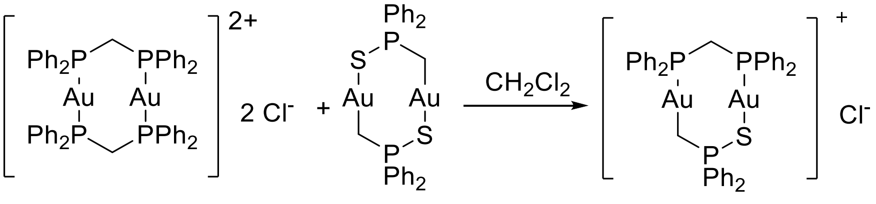

78 **76** **79**

Figure 99. Synthetic pathway for complex **79**.

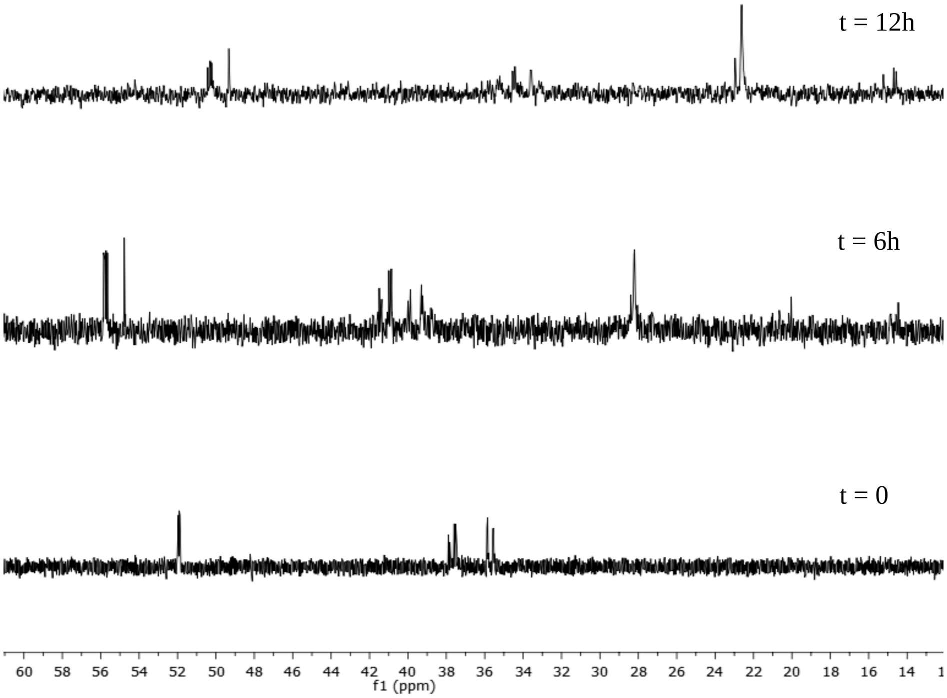

Figure 100. ^{31}P NMR spectra recorded during the conversion of **80** into **81** catalyzed by **79**.

5.4 Conclusion

The main conclusion of this section is that several of the dinuclear complexes investigated are indeed catalytically active. However, these complexes are not stable in solution making the assignment of structure-catalytic activity relationship impossible. The only exception might be complex **76** which remain intact throughout the reaction. However, the slow conversion observed raises the possibility of metallic impurities being responsible for the observed activity.

5.5 Experimental

Materials and methods: All chemicals were purchased from commercial sources and were used without any further purification. The solvents were purified by distillation. $PhICl_2$[147], Au(tht)Cl,[213] [o-$Me_3SnC_6H_4PPh_2$],[207] complexes **73**,[206] **74**,[206] **76**,[211] **77**,[211] and **78**[214] were prepared by following previously published procedures with some modifications in the case of **73** and **76**. NMR spectra were recorded on a Varian Unity Inova 500 FT NMR spectrometer or Varian Inova 400 MHz or Bruker 400 MHz. Chemical shifts (δ) are given in ppm and are calibrated against residual solvent signals for ^1H and an external H_3PO_4 (85%) standard (assigned as 0 ppm) for ^{31}P.

[Au$_2$(*o*-dppp)$_2$], 73

The reported procedure for the synthesis of complex **73** involves an air and moisture sensitive compound [*o*-$LiC_6H_4PPh_2$]. As a modification, [*o*-$Me_3SnC_6H_4PPh_2$][207] as a bench stable compound was prepared and was reacted with the gold precursor Au(tht)Cl (tht = tetrahydrothiophene) or Au($AsPh_3$)Cl to produce complex **73**.

[Au$_2$(*o*-dppp)$_2$(OAc)$_2$], 75

Complex **75** was synthesized by two different pathways. Path one: to a solution of complex **74** (61.3 mg, 0.062 mmol) in THF was added Ag(OAc) (20.72 mg, 0.124 mmol) as a halid2 abstractor. After stirring overnight, the mixture was filtered, and the solution was evaporated. The residue was washed with hexane and dried under vacuum. Yield (58.9 mg, 91.7%). Path two: to a solution of **73** (51 mg, 0.056 mmol) in CH_2Cl_2 was added PhI$(OAc)_2$ (26.8 mg, 0.083 mmol) and mixture was stirred overnight to yield complex **75**. The solvent was evaporated on rotavap. The residue was dissolved in a small amount of CH_2Cl_2 and precipitated with ether. Yield (45 mg, 78.17%). ^{1} H NMR (499.7; $CDCl_3$): 1.4 (s, CH_3 of acetate), 6.78 (q), 7.20 (t), 7.34-7.52 (m),
7.78 (q). ^{31}P {^1H} NMR (161.70 MHz; $CDCl_3$): 4.5 (s).

[Au(dppm)(Ph$_2$P(S)CH$_2$)]Cl, 79

The asymmetric gold complex **79** was synthesized by mixing complex **76** (41.8 mg, 0.049 mmol) and complex **78** (60.2 mg, 0.049 mmol) in CH_2Cl_2. The solution was concentrated at the solvent was precipitated with hexanes. (Yield: 102 mg, 99%). ^{1} H NMR (499.7; $CDCl_3$): 2.26 (dd), 4.56 (t, $^{2}J_{HP}$ = 12.7 Hz), 7.10-7.25 (m), 7.50-7.56 (m), 7.60 (m), 7.75-7.90 (m), 7.96 (dd). ^{31}P {^{1}H} NMR (161.70 MHz; CDCl$_3$): 36 (dd, $^{2}J_{p\text{-}p}$ = 62 Hz, $^{3}J_{p\text{-}p}$ =8.2), 38 (dd, $^{2}J_{p\text{-}p}$ = 62 Hz, $^{3}J_{p\text{-}p}$ = 15.7 Hz), 52 (dd, $^{3}J_{p\text{-}p}$ = 15.7 Hz and $^{3}J_{p\text{-}p}$ =8.2).

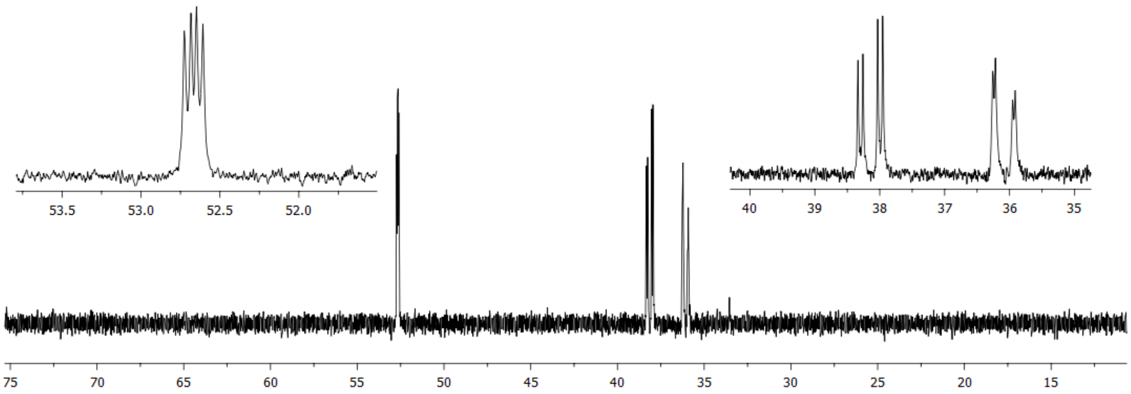

Figure 101. ^{31}P NMR of complex **79**

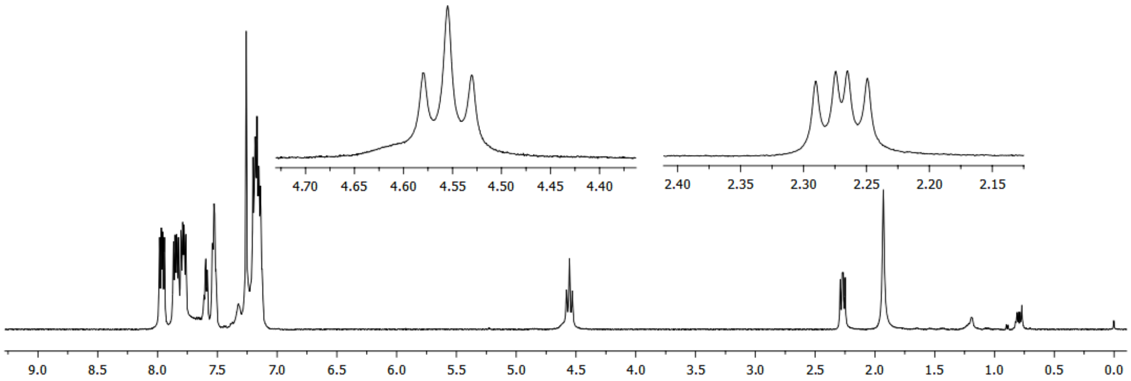

Figure 102. 1H NMR of complex **79**.

CHAPTER VI

CONCLUSION

The main focus of this thesis has been the study of complexes containing a Lewis acidic germanium-based Z-type ligand. The investigation of these complexes was stimulated by computational results presented in chapter 2 that show that germanium(IV) fluoride are effective *in silico* Z-type ligands for low valent platinum species. These computational efforts explored the reaction shown in Figure 103 and the properties of the resulting complexes.

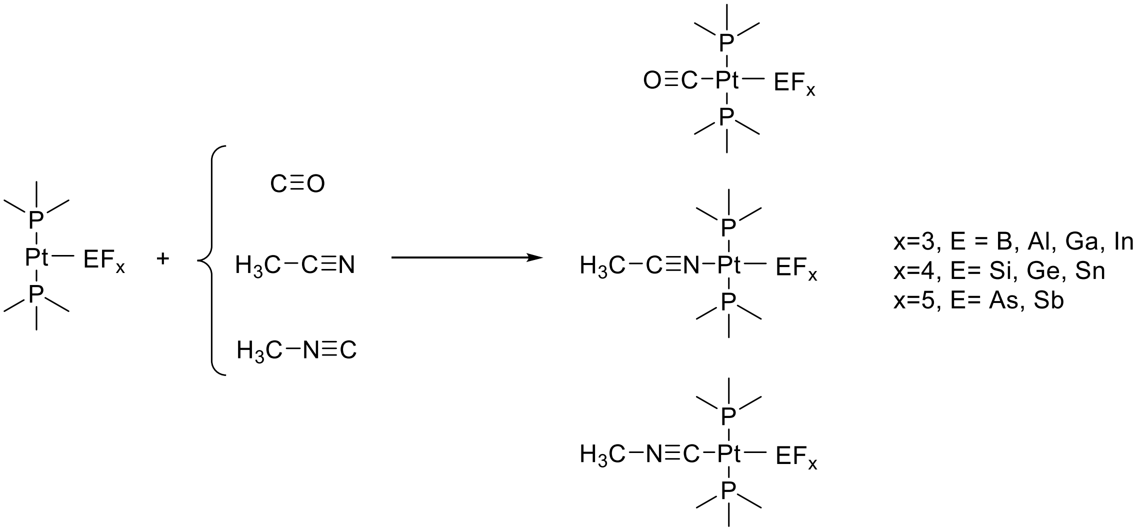

Figure 103. Interaction of metallobase adducts and the reporter fragments.

The Lewis acidity of the main group fluorides in these model complexes have been correlated to the computed energies of ν(CO), ν(CN), and ν(NC) and the enthalpy associated with the coordination of the reporter ligand. The stretching frequencies of the reporter ligand reflect the electron density on the metal center. Stronger Z-type ligands will make the Pt center more electron-poor, leading to stronger coordination of the reporter ligand, thereby increasing the corresponding stretching frequencies. The data obtained in this study divulge that going down the group, the Lewis acidity increases, and In(III), Ge(IV), Sn(IV), As(V), and Sb(V) fluorides appear to be the most Lewis acidic.

Table 16. The computed energies of ν(CO), ν(CN), and ν(NC) and the enthalpy associated with the coordination of the reporter ligand.

	CO		**CH_3CN**		**CH_3NC**	
EF_X	**ν(C≡O) (cm^{-1})**	**ΔH (Kcal/mol)**	**ν(C≡N) (cm^{-1})**	**ΔH (Kcal/mol)**	**ν(C≡N) (cm^{-1})**	**ΔH (Kcal/mol)**
BF_3	1797.28	-22.475	2190.12	-1.268	2071.64	-16.949
AlF_3	1832.99	-24.783	-	-	2107.15	-21.557
GaF_3	1865.43	-29.043	2214.68	-9.117	2129.67	-28.217
InF_3	1891.50	-31.645	2215.09	-12.042	2136.38	-31.913
SiF_4	-	-	2213.11	-7.7484	2124.33	-25.315
GeF_4	1885.53	-32.661	2220.31	-13.235	2139.66	-32.155
SnF_4	1899.16	-34.205	2222.03	-14.82	2144.54	-35.059
AsF_5	1873.78	-30.068	2226.25	-11.332	2151.31	-30.149
SbF_5	1885.82	-30.643	2228.78	-12.091	2153.56	-31.873

Drawing on the conclusion of the above computational survey, Pt(II), Pd(II), and Au(I) were used as a metallobase and a germanium (IV) moiety as a Z-type ligand. These efforts have resulted in the characterization of complex **53,** which possess a weak Pt(II)→Ge(IV) interaction. The structure of this complex, its spectroscopy, and computational analysis confirmed the existence of the dative interaction. Remarkably, this complex can be photoreduced cleanly in the presence of a sacrificial reducing agent to afford the corresponding Pt(I)-Ge(III), complex **54** as a result of chlorine elimination. Reoxidizing complex **54** led to the formation of complex **55** as a structural isomer of complex **53,** which can go under photoreduction reaction to produce complex **54**.

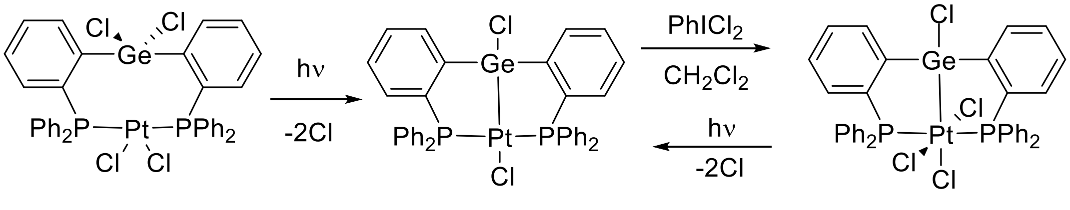

53 **54** **55**

Figure 104. Photoreductive elimination of complex **53** to complex **54** and reoxidation to complex **55** as a structural isomer.

To test the generality of these findings, the synthesis of related Pd-Ge complex **56** and **57** and Au-Ge complex **58** have been explored. It was observed that in the case of palladium, the reductive process described above for platinum takes place thermally, without the need for UV irradiation. Complex **56** is not stable upon formation in CH_2Cl_2. It undergoes fast reductive elimination leading to the corresponding Pd(I)-Ge(III) complex **57**. Characterization of complex **56** was possible via X-ray diffraction thanks to its insolubility in Toluene.

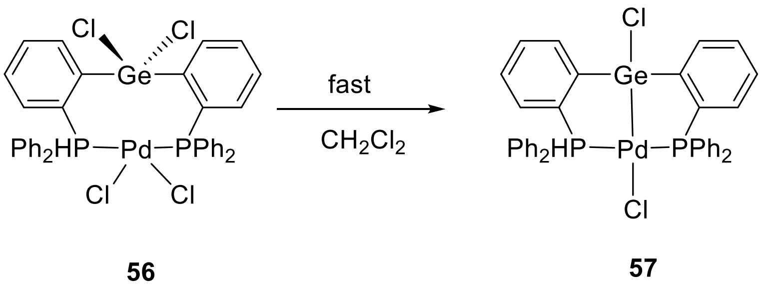

Figure 105. Fast reductive elimination of chlorine from complex **56** in CH_2Cl_2.

In the gold-containing complex **58**, strong Au→Ge interaction was observed, leading to the formation of a covalent Au–Ge bond. The establishment of this bond can be seen as the result of an S_N2 reaction in which the gold acts as the nucleophile and induces the dissociation of a Ge–Cl bond, with the chloride being the leaving group.

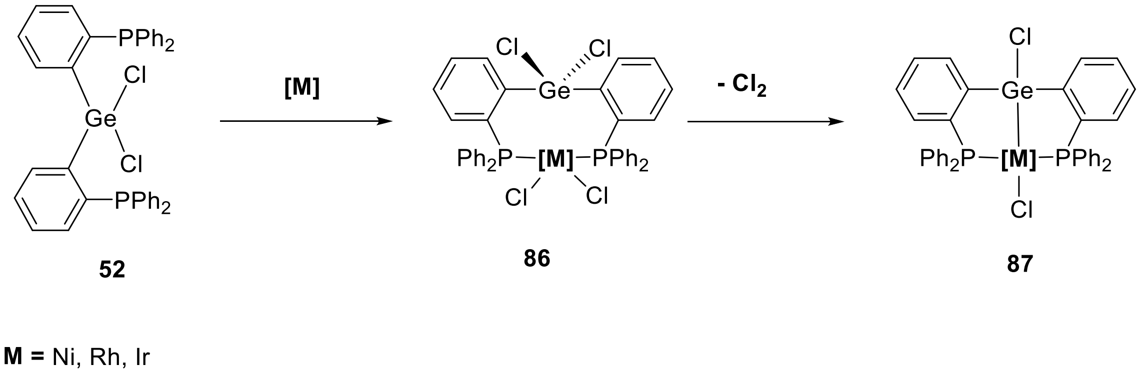

Figure 106. The reaction of compound **52** with different transition metal precursors.

As for future directions, there are stimulating possibilities. For example, using *o*-(dppp)$_2$GeF$_2$ (**88**) as a ligand could provide complexes that either resists photoreductive elimination or that eliminate high energy molecules such as XF as illustrated in Figure 107. If X is an alkyl or aryl group, such reactions could provide a path for C-F bond formation.

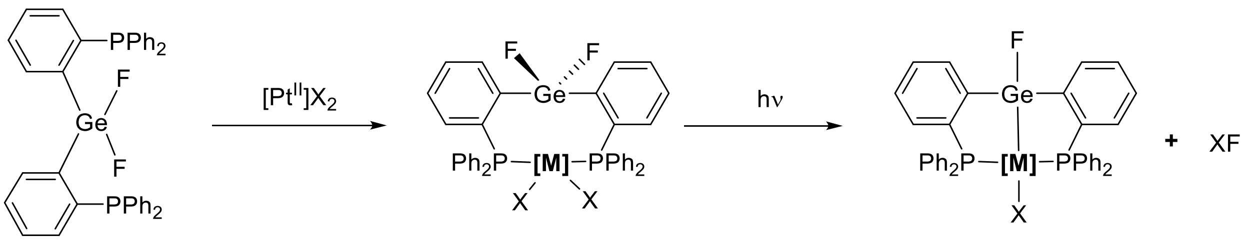

88 **89** **90**

X = F, Cl, Ph

Figure 107. Schematic reaction of *o*-(dppp)$_2$GeF$_2$ (**88)** with [Pt^{II}]X$_2$ (X = F, Cl, alkyl or aryl) as metallobase.

Last but not least, the germanium-containing gold complexes describe in chapter 3 deserve additional investigation. The gold complex **58** being cationic is set to provide an interesting platform for carbophilic catalysis that fellow group members are currently investigating.

REFERENCES

1. Le Quéré, C.; Andrew, R. M.; Friedlingstein, P.; Sitch, S.; Hauck, J.; Pongratz, J.; Pickers, P. A.; Korsbakken, J. I.; Peters, G. P.; Canadell, J. G.; Arneth, A.; Arora, V. K.; Barbero, L.; Bastos, A.; Bopp, L.; Chevallier, F.; Chini, L. P.; Ciais, P.; Doney, S. C.; Gkritzalis, T.; Goll, D. S.; Harris, I.; Haverd, V.; Hoffman, F. M.; Hoppema, M.; Houghton, R. A.; Hurtt, G.; Ilyina, T.; Jain, A. K.; Johannessen, T.; Jones, C. D.; Kato, E.; Keeling, R. F.; Goldewijk, K. K.; Landschützer, P.; Lefèvre, N.; Lienert, S.; Liu, Z.; Lombardozzi, D.; Metzl, N.; Munro, D. R.; Nabel, J. E. M. S.; Nakaoka, S. I.; Neill, C.; Olsen, A.; Ono, T.; Patra, P.; Peregon, A.; Peters, W.; Peylin, P.; Pfeil, B.; Pierrot, D.; Poulter, B.; Rehder, G.; Resplandy, L.; Robertson, E.; Rocher, M.; Rödenbeck, C.; Schuster, U.; Schwinger, J.; Séférian, R.; Skjelvan, I.; Steinhoff, T.; Sutton, A.; Tans, P. P.; Tian, H.; Tilbrook, B.; Tubiello, F. N.; van der Laan-Luijkx, I. T.; van der Werf, G. R.; Viovy, N.; Walker, A. P.; Wiltshire, A. J.; Wright, R.; Zaehle, S.; Zheng, B., *Earth Syst. Sci. Data* **2018,** *10* (4), 2141-2194.

2. Cook, T. R.; Dogutan, D. K.; Reece, S. Y.; Surendranath, Y.; Teets, T. S.; Nocera, D. G., *Chem. Rev.* **2010,** *110* (11), 6474-6502.

3. Bard, A. J.; Fox, M. A., *Acc. Chem. Res.* **1995,** *28* (3), 141-145.

4. Esswein, A. J.; Nocera, D. G., *Chem. Rev.* **2007,** *107* (10), 4022-4047.

5. Teets, T. S.; Nocera, D. G., *Chem. Commun.* **2011,** *47* (33), 9268-9274.

6. Troian-Gautier, L.; Turlington, M. D.; Wehlin, S. A. M.; Maurer, A. B.; Brady, M. D.; Swords, W. B.; Meyer, G. J., *Chem. Rev.* **2019,** *119* (7), 4628-4683.

7. Odom, A. L.; Heyduk, A. F.; Nocera, D. G., *Inorg. Chim. Acta* **2000,** *297* (1), 330-337.

8. Heyduk, A. F.; Macintosh, A. M.; Nocera, D. G., *J. Am. Chem. Soc.* **1999,** *121* (21), 5023-5032.

9. Heyduk, A. F.; Nocera, D. G., *Science* **2001,** *293* (5535), 1639.

10. Esswein, A. J.; Veige, A. S.; Nocera, D. G., *J. Am. Chem. Soc.* **2005,** *127* (47), 16641-16651.

11. Raphael Karikachery, A.; Lee, H. B.; Masjedi, M.; Ross, A.; Moody, M. A.; Cai, X.; Chui, M.; Hoff, C. D.; Sharp, P. R., *Inorg. Chem.* **2013,** *52* (7), 4113-4119.

12. Teets, T. S.; Nocera, D. G., *J. Am. Chem. Soc.* **2009,** *131* (21), 7411-7420.

13. Ovens, J. S.; Leznoff, D. B., *Dalton Transactions* **2011,** *40* (16), 4140-4146.

14. Cook, T. R.; Esswein, A. J.; Nocera, D. G., *J. Am. Chem. Soc.* **2007,** *129* (33), 10094-10095.

15. Bellachioma, G.; Cardaci, G.; Macchioni, A.; Venturi, C.; Zuccaccia, C., *J. Organomet. Chem.* **2006,** *691* (18), 3881-3888.

16. Cook, T. R.; McCarthy, B. D.; Lutterman, D. A.; Nocera, D. G., *Inorg. Chem.* **2012,** *51* (9), 5152-5163.

17. Teets, T. S.; Lutterman, D. A.; Nocera, D. G., *Inorg. Chem.* **2010,** *49* (6), 3035-3043.

18. Cook, T. R.; Surendranath, Y.; Nocera, D. G., *J. Am. Chem. Soc.* **2009,** *131* (1), 28-29.

19. Perera, T. A.; Masjedi, M.; Sharp, P. R., *Inorg. Chem.* **2014,** *53* (14), 7608-7621.

20. Li, P.-F.; Carrera, E. I.; Seferos, D. S., *ChemPlusChem* **2016,** *81* (9), 917-921.

21. Carrera, E. I.; Lanterna, A. E.; Lough, A. J.; Scaiano, J. C.; Seferos, D. S., *J. Am. Chem. Soc.* **2016,** *138* (8), 2678-2689.

22. Carrera, E. I.; Seferos, D. S., *Dalton Transactions* **2015,** *44* (5), 2092-2096.

23. Carrera, E. I.; McCormick, T. M.; Kapp, M. J.; Lough, A. J.; Seferos, D. S., *Inorg. Chem.* **2013,** *52* (23), 13779-13790.

24. Lemon, C. M.; Hwang, S. J.; Maher, A. G.; Powers, D. C.; Nocera, D. G., *Inorg. Chem.* **2018,** *57* (9), 5333-5342.

25. Lin, T.-P.; Gabbaï, F. P., *J. Am. Chem. Soc.* **2012,** *134* (29), 12230-12238.

26. Yang, H.; Gabbaï, F. P., *J. Am. Chem. Soc.* **2014,** *136* (31), 10866-10869.

27. Sahu, S.; Gabbaï, F. P., *J. Am. Chem. Soc.* **2017,** *139* (14), 5035-5038.

28. Khusnutdinova, J. R.; Rath, N. P.; Mirica, L. M., *J. Am. Chem. Soc.* **2010,** *132* (21), 7303-7305.

29. Fageria, P.; Uppala, S.; Nazir, R.; Gangopadhyay, S.; Chang, C.-H.; Basu, M.; Pande, S., *Langmuir* **2016,** *32* (39), 10054-10064.

30. Vinayan, B. P.; Nagar, R.; Ramaprabhu, S., *Journal of Materials Chemistry A* **2013,** *1* (37), 11192-11199.

31. Szabo, K. J.; Wendt, O. F., *Pincer and pincer-type complexes: applications in organic synthesis and catalysis*. John Wiley & Sons: 2014.

32. Selander, N.; Szabó, K. J., *Chem. Rev.* **2011,** *111* (3), 2048-2076.

33. Dupont, J.; Consorti, C. S.; Spencer, J., *Chem. Rev.* **2005,** *105* (6), 2527-2572.

34. Iwasawa, J. T. a. N., Heavier Group 14 Elements-Based Pincer Complexes in Catalytic Synthetic Transformations of Unsaturated Hydrocarbons. In *Pincer and Pincer-Type Complexes*.

35. Kameo, H.; Ishii, S.; Nakazawa, H., *Dalton Transactions* **2012,** *41* (37), 11386-11392.

36. Weinert, C. S., Germanium: Organometallic Chemistry. In *Encyclopedia of Inorganic and Bioinorganic Chemistry, Online*, John Wiley & Sons, Ltd: 2015; pp 2-18.

37. Glockling, F.; Wilbey, M. D., *Journal of the Chemical Society A: Inorganic, Physical, Theoretical* **1968,** (0), 2168-2171.

38. Howard, J.; Knox, S. A. R.; Stone, F. G. A.; Woodward, P., *Journal of the Chemical Society D: Chemical Communications* **1970,** (22), 1477-1478.

39. Sagawa, T.; Tanaka, R.; Ozawa, F., *Bull. Chem. Soc. Jpn.* **2004,** *77* (7), 1287-1295.

40. White, C. P.; Braddock-Wilking, J.; Corey, J. Y.; Xu, H.; Redekop, E.; Sedinkin, S.; Rath, N. P., *Organometallics* **2007,** *26* (8), 1996-2004.

41. Gualco, P.; Lin, T.-P.; Sircoglou, M.; Mercy, M.; Ladeira, S.; Buhadir, G.; Pérez, L. M.; Amgoune, A.; Maron, L.; Gabbaï, F. P.; Bourissou, D., *Angew. Chem. Int. Ed.* **2009,** *48* (52), 9892-9895.

42. Wang, W. Y.; Inoue, S.; Irran, E.; Driess, M., *Angew Chem Int Edit* **2012,** *51* (15), 3691-3694.

43. Gallego, D.; Bruck, A.; Irran, E.; Meier, F.; Kaupp, M.; Driess, M.; Hartwig, J. F., *J. Am. Chem. Soc.* **2013,** *135* (41), 15617-15626.

44. Bruck, A.; Gallego, D.; Wang, W. Y.; Irran, E.; Driess, M.; Hartwig, J. F., *Angew Chem Int Edit* **2012,** *51* (46), 11478-11482.

45. Gallego, D.; Inoue, S.; Blom, B.; Driess, M., *Organometallics* **2014,** *33* (23), 6885-6897.

46. Metsänen, T. T.; Gallego, D.; Szilvási, T.; Driess, M.; Oestreich, M., *Chemical Science* **2015,** *6* (12), 7143-7149.

47. Ren, H. L.; Zhou, Y. P.; Bai, Y. P.; Cui, C. M.; Driess, M., *Chem-Eur J* **2017,** *23* (24), 5663-5667.

48. Álvarez-Rodríguez, L.; Brugos, J.; Cabeza, J. A.; García-Álvarez, P.; Pérez-Carreño, E.; Polo, D., *Chem. Commun.* **2017,** *53* (5), 893-896.

49. Álvarez-Rodríguez, L.; Brugos, J.; Cabeza, J. A.; García-Álvarez, P.; Pérez-Carreño, E., *Chemistry – A European Journal* **2017,** *23* (60), 15107-15115.

50. Bestgen, S.; Rees, N. H.; Goicoechea, J. M., *Organometallics* **2018,** *37* (21), 4147-4155.

51. Cabeza, J. A.; Fernández, I.; Fernández-Colinas, J. M.; García-Álvarez, P.; Laglera-Gándara, C. J., *Chemistry – A European Journal* **2019,** *25* (53), 12423-12430.

52. Kameo, H.; Ikeda, K.; Sakaki, S.; Takemoto, S.; Nakazawa, H.; Matsuzaka, H., *Dalton Transactions* **2016,** *45* (18), 7570-7580.

53. Kameo, H.; Ikeda, K.; Bourissou, D.; Sakaki, S.; Takemoto, S.; Nakazawa, H.; Matsuzaka, H., *Organometallics* **2016,** *35* (5), 713-719.

54. Zhu, C.; Takaya, J.; Iwasawa, N., *Org. Lett.* **2015,** *17* (7), 1814-1817.

55. Takaya, J.; Nakamura, S.; Iwasawa, N., *Chem. Lett.* **2012,** *41* (9), 967-969.

56. Lv, X.; Huang, F.; Wu, Y.-B.; Lu, G., *Catalysis Science & Technology* **2018,** *8* (11), 2835-2840.

57. Takaya, J.; Iwasawa, N., *Eur. J. Inorg. Chem.* **2018,** *2018* (46), 5012-5018.

58. Kameo, H.; Ishii, S.; Nakazawa, H., *Dalton Transactions* **2012,** *41* (27), 8290-8296.

59. Kameo, H.; Ishii, S.; Nakazawa, H., *Organometallics* **2012,** *31* (6), 2212-2218.

60. Herrmann, R.; Wittwer, P.; Braun, T., *Eur. J. Inorg. Chem.* **2016,** *2016* (30), 4898-4905.

61. Kameo, H.; Kawamoto, T.; Bourissou, D.; Sakaki, S.; Nakazawa, H., *Organometallics* **2015,** *34* (8), 1440-1448.

62. Shriver, D. F., *Acc. Chem. Res.* **1970,** *3* (7), 231-238.

63. Hieber, W.; Schulten, H., *Z. Anorg. Allg. Chem.* **1937,** *232* (1), 29-38.

64. Hieber, W.; Schulten, H., *Z. Anorg. Allg. Chem.* **1937,** *232* (1), 17-28.

65. Hieber, W., *Angew. Chem.* **1936,** *49* (28), 463-464.

66. Davison, A.; McFarlane, W.; Pratt, L.; Wilkinson, G., *Journal of the Chemical Society (Resumed)* **1962,** (0), 3653-3666.

67. Piper, T. S.; Wilkinson, G., *J. Inorg. Nucl. Chem.* **1956,** *3* (2), 104-124.

68. You, D.; Yang, H.; Sen, S.; Gabbaï, F. P., *J. Am. Chem. Soc.* **2018,** *140* (30), 9644-9651.

69. Wächtler, E.; Gericke, R.; Brendler, E.; Gerke, B.; Langer, T.; Pöttgen, R.; Zhechkov, L.; Heine, T.; Wagler, J., *Dalton Transactions* **2016,** *45* (36), 14252-14264.

70. Liberman-Martin, A. L.; Levine, D. S.; Ziegler, M. S.; Bergman, R. G.; Tilley, T. D., *Chem. Commun.* **2016,** *52* (43), 7039-7042.

71. Inagaki, F.; Matsumoto, C.; Okada, Y.; Maruyama, N.; Mukai, C., *Angewandte Chemie (International ed. in English)* **2015,** *54* (3), 818-22.

72. Barnett, B. R.; Moore, C. E.; Chandrasekaran, P.; Sproules, S.; Rheingold, A. L.; DeBeer, S.; Figueroa, J. S., *Chemical Science* **2015,** *6* (12), 7169-7178.

73. Braunschweig, H.; Dewhurst, R. D., *Dalton Transactions* **2011,** *40* (3), 549-558.

74. Amgoune, A.; Bourissou, D., *Chem. Commun.* **2011,** *47* (3), 859-871.

75. Green, M. L. H., *J. Organomet. Chem.* **1995,** *500* (1), 127-148.

76. King, R. B., Coordination Number, Electronic Configuration, and Ionic Charge as Discrete Variables in Coordination Chemistry. In *Werner Centennial*, American Chemical Society: 1967; Vol. 62, pp 203-220.

77. Beckett, M. A.; Strickland, G. C.; Holland, J. R.; Sukumar Varma, K., *Polymer* **1996,** *37* (20), 4629-4631.

78. Mayer, U.; Gutmann, V.; Gerger, W., *Monatshefte für Chemie / Chemical Monthly* **1975,** *106* (6), 1235-1257.

79. R. F. Childs, D. L. M., A. Nixon, *Can. J. Chem.* **1982,** *60*, 809– 812.

80. Lappert, M. F., *Journal of the Chemical Society (Resumed)* **1962,** (0), 542-548.

81. Mallouk, T. E.; Rosenthal, G. L.; Mueller, G.; Brusasco, R.; Bartlett, N., *Inorg. Chem.* **1984,** *23* (20), 3167-3173.

82. Müller, L. O.; Himmel, D.; Stauffer, J.; Steinfeld, G.; Slattery, J.; Santiso-Quiñones, G.; Brecht, V.; Krossing, I., *Angew. Chem. Int. Ed.* **2008,** *47* (40), 7659-7663.

83. Haartz, J. C.; McDaniel, D. H., *J. Am. Chem. Soc.* **1973,** *95* (26), 8562-8565.

84. Frenking, G.; Fau, S.; Marchand, C. M.; Grützmacher, H., *J. Am. Chem. Soc.* **1997,** *119* (28), 6648-6655.

85. Huggett, P. G.; Manning, K.; Wade, K., *J. Inorg. Nucl. Chem.* **1980,** *42* (5), 665-673.

86. Abel, E. W.; Stone, F. G. A., *Quarterly Reviews, Chemical Society* **1969,** *23* (3), 325-371.

87. Greb, L., *Chemistry – A European Journal* **2018,** *24* (68), 17881-17896.

88. Braunschweig, H.; Brunecker, C.; Dewhurst, R. D.; Schneider, C.; Wennemann, B., *Chemistry – A European Journal* **2015,** *21* (52), 19195-19201.

89. Bertermann, R.; Böhnke, J.; Braunschweig, H.; Dewhurst, R. D.; Kupfer, T.; Muessig, J. H.; Pentecost, L.; Radacki, K.; Sen, S. S.; Vargas, A., *J. Am. Chem. Soc.* **2016,** *138* (49), 16140-16147.

90. Arnold, N.; Braunschweig, H.; Dewhurst, R. D.; Ewing, W. C., *J. Am. Chem. Soc.* **2016,** *138* (1), 76-79.

91. Braunschweig, H.; Dewhurst, R. D.; Hupp, F.; Wolf, J., *Chemistry – A European Journal* **2015,** *21* (5), 1860-1862.

92. Bertsch, S.; Brand, J.; Braunschweig, H.; Hupp, F.; Radacki, K., *Chemistry – A European Journal* **2015,** *21* (16), 6278-6285.

93. Brand, J.; Braunschweig, H.; Sen, S. S., *Acc. Chem. Res.* **2014,** *47* (1), 180-191.

94. Braunschweig, H.; Ye, Q.; Damme, A.; Radacki, K., *Chem. Commun.* **2013,** *49* (69), 7593-7595.

95. Braunschweig, H.; Damme, A.; Dewhurst, R. D.; Hupp, F.; Jimenez-Halla, J. O. C.; Radacki, K., *Chem. Commun.* **2012,** *48* (84), 10410-10412.

96. Bertsch, S.; Braunschweig, H.; Forster, M.; Gruss, K.; Radacki, K., *Inorg. Chem.* **2011,** *50* (5), 1816-1819.

97. Braunschweig, H.; Radacki, K.; Schwab, K., *Chem. Commun.* **2010,** *46* (6), 913-915.

98. Braunschweig, H.; Brenner, P.; Cogswell, P.; Kraft, K.; Schwab, K., *Chem. Commun.* **2010,** *46* (42), 7894-7896.

99. Bauer, J.; Braunschweig, H.; Brenner, P.; Kraft, K.; Radacki, K.; Schwab, K., *Chemistry – A European Journal* **2010,** *16* (39), 11985-11992.

100. Braunschweig, H.; Gruss, K.; Radacki, K., *Angew. Chem. Int. Ed.* **2009,** *48* (23), 4239-4241.

101. Braunschweig, H.; Radacki, K.; Uttinger, K., *Chemistry – A European Journal* **2008,** *14* (26), 7858-7866.

102. Braunschweig, H.; Gruss, K.; Radacki, K., *Inorg. Chem.* **2008,** *47* (19), 8595-8597.

103. .Braunschweig, H.; Radacki, K.; Uttinger, K., *Inorg. Chem.* **2007,** *46* (21), 8796-8800.

104. Braunschweig, H.; Gruss, K.; Radacki, K., *Angew. Chem. Int. Ed.* **2007,** *46* (41), 7782-7784.

105. Muessig, J. H.; Stennett, T. E.; Schmidt, U.; Dewhurst, R. D.; Mailänder, L.; Braunschweig, H., *Dalton Transactions* **2019,** *48* (11), 3547-3550.

106. M. J. Frisch, G. W. T., H. B. Schlegel, G. E. Scuseria, M. A. Robb, J. R. Cheeseman, G. Scalmani, V. Barone, B. Mennucci, G. A. Petersson, H. Nakatsuji, M. Caricato, X. Li, H. P. Hratchian, A. F. Izmaylov, J. Bloino, G. Zheng, J. L. Sonnenberg, M. Hada, M. Ehara, K. Toyota, R. Fukuda, J. Hasegawa, M. Ishida, T. Nakajima, Y. Honda, O. Kitao, H. Nakai, T. Vreven, J. A. Montgomery, Jr., J. E. Peralta, F. Ogliaro, M. Bearpark, J. J. Heyd, E. Brothers, K. N. Kudin, V. N. Staroverov, R. Kobayashi, J. Normand, K. Raghavachari, A. Rendell, J. C. Burant, S. S. Iyengar, J. Tomasi, M. Cossi, N. Rega, J. M. Millam, M. Klene, J. E. Knox, J. B. Cross, V. Bakken, C. Adamo, J. Jaramillo, R. Gomperts, R. E. Stratmann, O. Yazyev, A. J. Austin, R. Cammi, C. Pomelli, J. W. Ochterski, R. L. Martin, K. Morokuma, V. G. Zakrzewski, G. A. Voth, P. Salvador, J. J. Dannenberg, S. Dapprich, A. D. Daniels, Ö. Farkas, J. B. Foresman, J. V. Ortiz, J. Cioslowski, and D. J. Fox, Gaussian~ 09, Revision D.01. Gaussian, Inc.: Wallingford, CT, USA,, 2013.

107. Perdew, J. P., *Physical Review B* **1986,** *33* (12), 8822-8824.

108. Becke, A. D., *Physical Review A* **1988,** *38* (6), 3098-3100.

109. Dunning, T. H., *The Journal of Chemical Physics* **1989,** *90* (2), 1007-1023.

110. McLean, A. D.; Chandler, G. S., *The Journal of Chemical Physics* **1980,** *72* (10), 5639-5648.

111. Krishnan, R.; Binkley, J. S.; Seeger, R.; Pople, J. A., *The Journal of Chemical Physics* **1980,** *72* (1), 650-654.

112. Ditchfield, R.; Hehre, W. J.; Pople, J. A., *The Journal of Chemical Physics* **1971,** *54* (2), 724-728.

113. McNair, A. M.; Ault, B. S., *Inorg. Chem.* **1982,** *21* (5), 1762-1765.

114. Helminiak, H. M.; Knauf, R. R.; Danforth, S. J.; Phillips, J. A., *The Journal of Physical Chemistry A* **2014,** *118* (24), 4266-4277.

115. Starowieyski, K.; Pasynkiewicz, S.; Boleslawski, M., *J. Organomet. Chem.* **1967,** *10* (3), 393-400.

116. Jennings, J. R.; Wade, K., *Journal of the Chemical Society A: Inorganic, Physical, Theoretical* **1967,** (0), 1222-1226.

117. Timoshkin, A. Y.; Schaefer, H. F., *J. Am. Chem. Soc.* **2003,** *125* (33), 9998-10011.

118. Timoshkin, A. Y.; Suvorov, A. V.; Bettinger, H. F.; Schaefer, H. F., *J. Am. Chem. Soc.* **1999,** *121* (24), 5687-5699.

119. Timoshkin, A. Y.; Bodensteiner, M.; Sevastianova, T. N.; Lisovenko, A. S.; Davydova, E. I.; Scheer, M.; Graßl, C.; Butlak, A. V., *Inorg. Chem.* **2012,** *51* (21), 11602-11611.

120. Davydova, E. I.; Timoshkin, A. Y.; Sevastianova, T. N.; Suvorov, A. V.; Frenking, G., *Journal of Molecular Structure: THEOCHEM* **2006,** *767* (1), 103-111.

121. Frenking, G.; Fau, S.; Marchand, C. M.; Grutzmacher, H., *J. Am. Chem. Soc.* **1997,** *119* (28), 6648-6655.

122. Sevastianova, T. N.; Davydova, E. I.; Kazakov, I. V.; Timoshkin, A. Y., *Russ. Chem. Bull.* **2015,** *64* (11), 2523-2535.

123. Vollmer, M. V.; Xie, J.; Lu, C. C., *J. Am. Chem. Soc.* **2017,** *139* (19), 6570-6573.

124. Cammarota, R. C.; Lu, C. C., *J. Am. Chem. Soc.* **2015,** *137* (39), 12486-12489.

125. D. Kost, I. K., Hypervalent silicon compounds. In *The Chemistry ofOrganic Silicon Compounds*, Z. Rappoport, Y. A., Ed. Wiley: Chichester, 1998; Vol. 2, p 1339.

126. Jupp, A. R.; Johnstone, T. C.; Stephan, D. W., *Inorg. Chem.* **2018,** *57* (23), 14764-14771.

127. Yang, H.; Gabbaï, F. P., *J. Am. Chem. Soc.* **2015,** *137* (41), 13425-13432.

128. Yang, Z.; Zhang, J.; Kintner-Meyer, M. C. W.; Lu, X.; Choi, D.; Lemmon, J. P.; Liu, J., *Chem. Rev.* **2011,** *111* (5), 3577-3613.

129. Nocera, D. G., *Inorg. Chem.* **2009,** *48* (21), 10001-10017.

130. Mann, K. R.; Lewis, N. S.; Miskowski, V. M.; Erwin, D. K.; Hammond, G. S.; Gray, H. B., *J. Am. Chem. Soc.* **1977,** *99* (16), 5525-5526.

131. Maverick, A. W.; Gray, H. B., *Pure Appl. Chem.* **1980,** *52* (10), 2339-2348.

132. Gray, H. B.; Maverick, A. W., *Science* **1981,** *214* (4526), 1201-1205.

133. Powers, D. C.; Hwang, S. J.; Anderson, B. L.; Yang, H.; Zheng, S. L.; Chen, Y. S.; Cook, T. R.; Gabbai, F. P.; Nocera, D. G., *Inorg. Chem.* **2016,** *55* (22), 11815-11820.

134. Hwang, S. J.; Powers, D. C.; Maher, A. G.; Anderson, B. L.; Hadt, R. G.; Zheng, S. L.; Chen, Y. S.; Nocera, D. G., *J. Am. Chem. Soc.* **2015,** *137* (20), 6472-5.

135. Perera, T. A.; Masjedi, M.; Sharp, P. R., *Inorg. Chem.* **2014,** *53*, 7608–7621.

136. Powers, D. C.; Chambers, M. B.; Teets, T. S.; Elgrishi, N.; Anderson, B. L.; Nocera, D. G., *Chem. Sci.* **2013,** *4* (7), 2880-2885.

137. Karikachery, A. R.; Lee, H. B.; Masjedi, M.; Ross, A.; Moody, M. A.; Cai, X.; Chui, M.; Hoff, C. D.; Sharp, P. R., *Inorg. Chem.* **2013,** *52* (7), 4113-4119.

138. Cook, T. R.; Esswein, A. J.; Nocera, D. G., *J. Am. Chem. Soc.* **2007,** *129* (33), 10094-10095.

139. Carrera, E. I.; Lanterna, A. E.; Lough, A. J.; Scaiano, J. C.; Seferos, D. S., *J. Am. Chem. Soc.* **2016,** *138* (8), 2678-89.

140. Sahu, S.; Gabbaï, F. P., *J. Am. Chem. Soc.* **2017**.

141. Rigamonti, L.; Manassero, C.; Rusconi, M.; Manassero, M.; Pasini, A., *Dalton Trans* **2009,** (7), 1206-13.

142. Bontemps, S.; Bouhadir, G.; Gu, W.; Mercy, M.; Chen, C.-H.; Foxman, B. M.; Maron, L.; Ozerov, O. V.; Bourissou, D., *Angew. Chem. Int. Ed.* **2008,** *47* (8), 1481-1484.

143. Sircoglou, M.; Saffon, N.; Miqueu, K.; Bouhadir, G.; Bourissou, D., *Organometallics* **2013,** *32* (22), 6780-6784.

144. Sircoglou, M.; Mercy, M.; Saffon, N.; Coppel, Y.; Bouhadir, G.; Maron, L.; Bourissou, D., *Angew. Chem. Int. Ed.* **2009,** *48* (19), 3454-3457.

145. Derrah, E. J.; Sircoglou, M.; Mercy, M.; Ladeira, S.; Bouhadir, G.; Miqueu, K.; Maron, L.; Bourissou, D., *Organometallics* **2011,** *30*, 657-660.

146. Hill, G. S.; Irwin, M. J.; Levy, C. J.; Rendina, L. M.; Puddephatt, R. J., *Inorg. Synth.* **1998,** *32*, 149-153.

147. Zhao, X.-F.; Zhang, C., *Synthesis* **2007,** *2007* (04), 551-557.

148. Glendening, E. D.; Landis, C. R.; Weinhold, F., *J. Comput. Chem.* **2013,** *34* (16), 1429-1437.

149. Hall, M. B.; Fenske, R. F., *Inorg. Chem.* **1972,** *11* (4), 768-775.

150. Manson, J. W., C. E.; Pérez, L. M.; Hall, M. B. http://www.chem.tamu.edu/jimp2/index.html.

151. Sheldrick, G. M. *SHELXTL-2008/4Structure Determination Software Suite*, Bruker AXS: Madison, Wisconsin, USA, 2008, 2008.

152. Dolomanov, O. V.; Bourhis, L. J.; Gildea, R. J.; Howard, J. A. K.; Puschmann, H., *J. Appl. Crystallogr.* **2009,** *42* (2), 339-341.

153. Tandura, Y. I. B. a. S. N., Hypervalent compounds of organic germanium, tin and lead derivatives. In *The chemistry of organic germanium, tin and lead compounds*, Rappoport, Z., Ed. John Wiley & Sons, Inc.: 2002; Vol. 2.

154. Cordero, B.; Gómez, V.; Platero-Prats, A. E.; Revés, M.; Echeverría, J.; Cremades, E.; Barragán, F.; Alvarez, S., *Dalton Transactions* **2008,** (21), 2832-2838.

155. Kameo, H.; Nakazawa, H., *Chemical Record* **2017,** *17* (3), 268-286.

156. Crabtree, R. H., *Angewandte Chemie International Edition in English* **1993,** *32* (6), 789-805.

157. Bercaw, J. E.; Labinger, J. A., *Proceedings of the National Academy of Sciences* **2007,** *104* (17), 6899.

158. Grobe, J.; Wehmschulte, R.; Krebs, B.; Ĺuge, M., *Z. Anorg. Allg. Chem.* **1995,** *621* (4), 583-596.

159. Grobe, J.; Krummen, N.; Wehmschulte, R.; Krebs, B.; Läge, M., *Z. Anorg. Allg. Chem.* **1994,** *620* (9), 1645-1658.

160. Gualco, P.; Mercy, M.; Ladeira, S.; Coppel, Y.; Maron, L.; Amgoune, A.; Bourissou, D., *Chemistry – A European Journal* **2010,** *16* (35), 10808-10817.

161. Gualco, P.; Mallet-Ladeira, S.; Kameo, H.; Nakazawa, H.; Mercy, M.; Maron, L.; Amgoune, A.; Bourissou, D., *Organometallics* **2015,** *34* (8), 1449-1453.

162. Autschbach, J.; Sutter, K.; Truflandier, L. A.; Brendler, E.; Wagler, J., *Chemistry – A European Journal* **2012,** *18* (40), 12803-12813.

163. Truflandier, L. A.; Brendler, E.; Wagler, J.; Autschbach, J., *Angew. Chem. Int. Ed.* **2011,** *50* (1), 255-259.

164. Wagler, J.; Brendler, E., *Angew. Chem. Int. Ed.* **2010,** *49* (3), 624-627.

165. Wagler, J. Hill, A. F.; Heine, T., *Eur. J. Inorg. Chem.* **2008,** *2008* (27), 4225-4229.

166. Martincová, J.; Dostál, L.; Herres-Pawlis, S.; Růžička, A.; Jambor, R., *Chemistry – A European Journal* **2011,** *17* (27), 7423-7427.

167. Wächtler, E.; Gericke, R.; Zhechkov, L.; Heine, T.; Langer, T.; Gerke, B.; Pöttgen, R.; Wagler, J., *Chem. Commun.* **2014,** *50* (40), 5382-5384.

168. Wahlicht, S.; Brendler, E.; Heine, T.; Zhechkov, L.; Wagler, J., *Organometallics* **2014,** *33* (10), 2479-2488.

169. Drew, D.; Doyle, J. R., *Inorg. Synth.* **1990,** *28* (Reagents Transition Met. Complex Organomet. Synth.), 346-9.

170. Pflasterer, D.; Hashmi, A. S., *Chem. Soc. Rev.* **2016,** *45* (5), 1331-67.

171. Dorel, R.; Echavarren, A. M., *Chem. Rev.* **2015,** *115* (17), 9028-9072.

172. Hashmi, A. S. K.; Rudolph, M., *Chem.Soc.Rev.* **2008,** *37*, 1766-1775.

173. Biasiolo, L.; Del Zotto, A.; Zuccaccia, D., *Organometallics* **2015,** *34* (9), 1759-1765.

174. Reiner, B. R.; Bezpalko, M. W.; Foxman, B. M.; Wade, C. R., *Organometallics* **2016,** *35* (17), 2830-2835.

175. Hutchings, G., *J. Catal.* **1985,** *96* (1), 292-295.

176. Morita, N.; Yasuda, A.; Shibata, M.; Ban, S.; Hashimoto, Y.; Okamoto, I.; Tamura, O., *Org. Lett.* **2015,** *17* (11), 2668-2671.

177. Reetz, M. T.; Sommer, K., *Eur. J. Org. Chem.* **2003,** (18), 3485-3496.

178. Sromek, A. W.; Rubina, M.; Gevorgyan, V., *J. Am. Chem. Soc.* **2005,** *127* (30), 10500-10501.

179. Yang, H. F.; Gabbai, F. P., *J. Am. Chem. Soc.* **2015,** *137* (41), 13425-13432.

180. Oliver-Meseguer, J.; Cabrero-Antonino, J. R.; Domínguez, I.; Leyva-Pérez, A.; Corma, A., *Science (New York, N.Y.)* **2012,** *338* (6113), 1452-5.

181. Schmidbaur, H.; Schier, A., *Chem. Soc. Rev.* **2008,** *37* (9), 1931-1951.

182. Akerstrom, S., *Ark. Kemi* **1959,** *14*, 387-387.

183. Schmidbaur, H.; Wohlleben, A.; Schubert, U.; Frank, A.; Huttner, G., *Chem. Ber.* **1977,** *110* (8), 2751-2757.

184. Inoguchi, Y.; Milewski-Mahrla, B.; Schmidbaur, H., *Chem. Ber.* **1982,** *115* (9), 3085-3095.

185. Mazany, A. M.; Fackler, J. P., *J. Am. Chem. Soc.* **1984,** *106* (3), 801-802.

186. Grohmann, A.; Schmidbaur, H., In *Comprehensive Organometallic Chemistry II*, Abel, E. W.; Stone, F. G. A.; Wilkinson, G., Eds. Elsevier: Oxford, 1995; Vol 3, pp 1-56.

187. Schmidbaur, H.; Grohmann, A.; Olmos, M. E., In *Gold: Progress in Chemistry, Biochemistry and Technology,* Schmidbaur, H., Ed. John Wiley & Sons: Chichester, 1999; pp 647-746.

188. van Zyl, W. E.; López-de-Luzuriaga, J. M.; Fackler Jr, J. P., *J. Mol. Struct.* **2000,** *516* (1), 99-106.

189. Zhang, H. X.; Che, C. M., *Chemistry (Weinheim an der Bergstrasse, Germany)* **2001,** *7* (22), 4887-93.

190. van Zyl, W. E.; López-de-Luzuriaga, J. M.; Mohamed, A. a.; Staples, R. J.; Fackler, J. P., *Inorg. Chem.* **2002,** *41* (17), 4579-89.

191. Gorin, D. J.; Davis, N. R.; Toste, F. D., *J. Am. Chem. Soc.* **2005,** *127* (32), 11260-1.

192. Muñoz, M. P.; Adrio, J.; Carretero, J. C.; Echavarren, A. M., *Organometallics* **2005,** *24* (6), 1293-1300.

193. LaLonde, R. L.; Sherry, B. D.; Kang, E. J.; Toste, F. D., *J. Am. Chem. Soc.* **2007,** *129* (9), 2452-2453.

194. Tarselli, M. A.; Chianese, A. R.; Lee, S. J.; Gagné, M. R., *Angewandte Chemie (International ed. in English)* **2007,** *46* (35), 6670-3.

195. Zhang, Z.; Bender, C. F.; Widenhoefer, R. A., *Org. Lett.* **2007,** *9* (15), 2887-9.

196. Hashmi, A. S. K.; Blanco Jaimes, M. C.; Schuster, A. M.; Rominger, F., *J. Org. Chem.* **2012,** *77* (15), 6394-6408.

197. Weyrauch, J. P.; Hashmi, A. S. K.; Schuster, A.; Hengst, T.; Schetter, S.; Littmann, A.; Rudolph, M.; Hamzic, M.; Visus, J.; Rominger, F.; Frey, W.; Bats, J. W., *Chemistry - A European Journal* **2010,** *16* (3), 956-963.

198. Hashmi, A. S. K.; Weyrauch, J. P.; Frey, W.; Bats, J. W., *Org. Lett.* **2004,** *6* (23), 4391-4394.

199. Pan, Y. M.; Zheng, F. J.; Lin, H. X.; Zhan, Z. P., *J. Org. Chem.* **2009,** *74* (8), 3148-3151.

200. Beccalli, E. M.; Borsini, E.; Broggini, G.; Palmisano, G.; Sottocornola, S., *J. Org. Chem.* **2008,** *73* (12), 4746-4749.

201. Hashmi, A. S. K., *Angew. Chem. Int. Ed.* **2005,** *44* (43), 6990-6993.

202. Hashmi, A. S. K.; Rudolph, M.; Schymura, S.; Visus, J.; Frey, W., *Eur. J. Org. Chem.* **2006,** *2006* (21), 4905-4909.

203. Palmer, D. C.; Venkatraman, S., *The Chemistry of Heterocyclic Compounds, A Series of Monographs, Oxazoles: Synthesis, Reactions, and Spectroscopy, Part A.* John Wiley & Sons: Hoboken, 2003.

204. Rudolph, M.; Hashmi, a. S. K., *Chemical communications (Cambridge, England)* **2011,** *47* (23), 6536-6544.

205. Hashmi, A. S. K.; Molinari, L.; Rominger, F.; Oeser, T., *Eur. J. Org. Chem.* **2011,** *2011* (12), 2256-2264.

206. Bennett, M. A.; Bhargava, S. K.; Griffiths, K. D.; Robertson, G. B.; Wickramasinghe, W. A.; Willis, A. C., *Angewandte Chemie International Edition in English* **1987,** *26* (3), 258-260.

207. Privér, S. H.; Bennett, M. A.; Willis, A. C.; Pottabathula, S.; Lakshmi Kantam, M.; Bhargava, S. K., *Dalton transactions (Cambridge, England : 2003)* **2014,** *43* (31), 12000-12.

208. Bennett, M. A.; Bhargava, S. K.; Hockless, D. C. R.; Welling, L. L.; Willis, A. C., *J. Am. Chem. Soc.* **1996,** *118* (43), 10469-10478.

209. Smirnova, E. S.; Echavarren, A. M., *Angew. Chem. Int. Ed.* **2013,** *52* (34), 9023-9026.

210. Bennett, M. A.; Hockless, D. C. R.; Rae, A. D.; Welling, L. L.; Willis, A. C., *Organometallics* **2001,** *20* (1), 79-87.

211. Fackler, J.; Galarza, E.; Garzon, G.; Mazany, A.; Murray, H.; Omary, M. R.; Raptis, R.; Staples, R.; Van Zyl, W.; Wang, S., *Inorg. Synth.* **2002,** *33*, 171-180.

212. Fackler, J. P.; Garzon, G.; Kresinski, R. A.; Murray, H. H.; Raptis, R. G., *Polyhedron* **1994,** *13* (11), 1705-1713.

213. Uson, R.; Laguna, A.; Laguna, M.; Briggs, D.; Murray, H.; Fackler Jr, J., *Inorg. Synth.* **2007,** *26*, 85-91.

214. Che, C.-M.; Kwong, H.-L.; Poon, C.-K.; Yam, V. W.-W., *J. Chem. Soc., Dalton Trans.* **1990,** (11), 3215-3219.